Functional characterization of Ceroid Lipofuscinosis Neuronal 3 (CLN3) interactions

Dissertation

Zur Erlangung des akademischen Grades

des Doktors der Naturwissenschaften

des Fachbereichs Biologie

der Fakultät für Mathematik, Informatik und Naturwissenschaften

der Universität Hamburg

Vorgelegt von

Abuzar Kaleem

Aus Rahim Yar Khan, Pakistan

Hamburg, 2017

Erstgutachter: PD Dr. Guido Hermey

Zentrum für Molekulare Neurobiologie Hamburg (ZMNH)

Zweitgutachter: Prof. Dr. Christian Lohr

Universität Hamburg

Die Arbeit wurde im Zeitraum von Januar 2015 bis Dezember 2017 im Zentrum für Molekulare Neurobiologie Hamburg (ZMNH) unter der Anleitung von PD Dr. Guido Hermey angefertigt.

Tag der Disputation: 30.05.2018

EIDESSTATTLICHE VERSICHERUNG

Hiermit erkläre ich an Eides statt, dass ich die vorliegende Dissertationsschrift selbst verfasst und keine anderen als die angegebenen Quellen und Hilfsmittel benutzt habe.

Hamburg, den 15.12.2017

_____

Unterschrift

Table of contents

Figures

Tables

Abbreviations

4E-BP	-	Eukaryotic initiation factor 4E (eIF4E) binding protein
ADAM	-	A disintegrin and metalloproteinase,
AMPA	-	α-amino-3-hydroxy-5-methyl-4-isoxazolepropionic acid
AMPK	-	Adenosine monophosphate-activated protein kinase
ANCL	-	Adult NCL
AP 1-4	-	Adaptor proteins 1-4
AP-clathrin complex	-	Adaptor protein clathrin complex
APCs	-	Antigen presenting cells
APH-1	-	Anterior pharynx defective 1
APP	-	Amyloid precursor protein
APP-ICD	-	APP intracellular domain
ARSA	-	Arylsulfatase A
Atg	-	Autophagy-related gene
Aβ	-	Amyloid β
BACE 1	-	βAPP cleaving enzyme 1
CatD	-	Cathepsin D
CGN	-	Cis-Golgi network
CLN3	-	Ceroid Lipofuscinosis Neuronal 3
CMA	-	Chaperone-mediated autophagy
CONCL	-	Congenital NCL
COP-I	-	Coatomer protein complex-I
COP-II	-	Coatomer protein complex-II
CTF	-	C-terminal fragment
eIF4G	-	Eukaryotic initiation factor 4G
FAD	-	Familial form of Alzheimer's disease
FRET	-	Fluorescence resonance energy transfer
FTD	-	Frontotemporal dementia

GM2A	-	GM2 activator protein
gRNAs	-	guide RNAs
HR	-	Homologous recombination
INCL	-	Infantile NCL
JNCL	-	Juvenile Neuronal Ceroid Lipofuscinosis
LAMP2	-	Lysosome-associated membrane protein 2
LC3	-	Light chain 3
LIMP-2	-	Lysosome membrane protein 2
LINCL	-	Late infantile NCL
LMP	-	Lysosomal membrane permeabilization
LSDs	-	Lysosomal storage diseases
LTM	-	lysosomal targeting motifs
M6P	-	Mannose-6 phosphate
M6PRs	-	Mannose-6 phosphate receptors
MCS	-	Multiple cloning sites
mTOR	-	Mammalian target of rapamycin
NCL	-	Neuronal Ceroid Lipofuscinoses
NCT	-	Nicastrin
NICD	-	Notch intracellular domain
NLS	-	Nuclear localization sequence
NMDA	-	N-methyl-D-aspartate
NPC1 and 2	-	Niemann-Pick C 1 and 2
NTF	-	N-terminal fragment
PAS	-	Pre-autophagosomal structure
PE	-	Phosphatidylethanolamine
Pen2	-	Presenilin enhancer 2
PGRN	-	Progranulin
PM	-	Plasmamembrane
PS	-	Presenilin

pS6K	-	Phosphorylated S6 kinase
RT-PCR	-	Reverse transcription PCR
S6K	-	S6 kinase
SAD	-	Sporadic form of Alzheimer's disease
SDS-PAGE	-	Sodium dodecyl sulfate-polyacrylamide gel electrophoresis
SSA	-	Single-strand annealing
TAD	-	Transactivation domain
TDP43	-	Tar DNA binding protein 43
TGN	-	Trans-Golgi network
TPC2	-	Two-pore channel 2
TRPML-1	-	Transient receptor potential cation channel, mucolipin subfamily, member 1
UAS	-	Upstream activator sequence
ULK1	-	Unc51 like kinase
β-Hex A	-	β-hexosaminidase A

Summary

Juvenile Neuronal Ceroid Lipofuscinosis (JNCL) is an autosomal recessive neurodegenerative disease also known as Batten disease mainly affecting children. JNCL patients show accumulation of autofluorescent material in lysosomes. The disease affects several organs but the most drastically affected organ is the brain and neuronal dysfunctions characterize the disease. JNCL is caused by mutations in the gene CLN3. The encoded protein CLN3 is a six transmembrane protein and predominantly localized to late endosomal/lysosomal compartments. To date the function of a CLN3 is unknown. Pen2 has been previously identified as an interaction partner for CLN3. Pen2 is a subunit of the γ-secretase complex. Dysfunction of the γ-secretase is thought to underlie Alzheimer's disease. The suggested function of Pen2 is allowing full assembly, stabilization and proper trafficking of the γ-secretase complex.

In this thesis, co-localization and interaction of tagged versions of CLN3 and Pen2 were demonstrated in HeLa and COS-7 cells. Moreover, isogenic CLN3 and Pen2 knockout HeLa cells were generated by using the CRISPR/Cas9 system to investigate the cellular function of both proteins. The phenotypic characterization of both knockout cell lines in comparison to wild type cells included the activity of the γ-secretase. Processing of the well-known substrates amyloid precursor protein (APP) and Notch was analyzed. As expected, processing of both substrates was hampered in Pen2 knockout cell and this phenotype was rescued by overexpression of GFP-Pen2. In CLN3 knockout cells, processing of γ-secretase substrates was not altered and comparable to wild type cells. Further investigations comprised alterations in the lysosomal-autophagosomal system in both knockout cells as compared to wild type cells. Lysosomal enzymatic activities were analyzed and a reduced β-hexosaminidase A activity was observed in both knockout cell lines. Moreover, an increase in the level of autophagosomes was observed. To evaluate these changes, different steps of the autophagy pathway were challenged. To this end cells were treated with mTOR complex inhibitors, a disaccharide sugar, trehalose, that induces mTOR-independent autophagy and inhibitors of the autophagosomal-lysosomal fusion step. Inhibition of the mTOR-dependent pathway did not further induce autophagosomes accumulation in CLN3 and Pen2 knockout cells as compared to wild type cells. In contrast, CLN3 and Pen2 knockout cells clearly exhibited an increased level of autophagosomes after induction of the mTOR-independent

pathway by trehalose and after inhibition of autophagosomal-lysosomal fusion. In addition, both knockout cell lines displayed decreased autophagic flux.

In conclusion, the current data strongly suggests that CLN3 and Pen2 interaction has a γ-secretase independent function. In this thesis, it has been reported for the first time that Pen2 deletion cause changes in lysosomal and autophagosomal functions. In addition, the presented data is in agreement with previous reports suggesting a role for CLN3 in lysosomal function and in autophagy. Because of the shared phenotypes, the interaction of both proteins could be important for normal functioning of lysosomes. Disruption of this interaction is likely to cause alterations of lysosomal enzymatic activities and in the autophagy pathway. These effects may be involved in the development of both, childhood neurodegenerative diseases, such as JNCL and in adult neurodegenerative diseases such as Alzheimer's disease.

Zusammenfassung

Die Juvenile Neuronale Ceroid Lipofuscinose (JNCL), auch “Morbus Batten” genannt, ist eine autosomale rezessive neurodegenerative Erkrankung bei Kindern. Die Akkumulation von autofluoreszentem Material in Lysosomen kennzeichnet diese. Hierbei sind verschiedene Organe betroffen, aber das am drastischsten betroffene Organ ist das Gehirn und neuronale Dysfunktionen charakterisieren die Erkrankung. JNCL wird durch Mutationen im Gen CLN3 hervorgerufen. Das kodierte Protein, CLN3, hat sechs Transmembran-Domänen und ist prädominant in späten endosomalen/lysosomalen Kompartimenten lokalisiert. Bis heute ist die Funktion von CLN3 unbekannt. In vorherigen Studien wurde Pen2 als Interaktionspartner von CLN3 identifiziert. Pen2 ist eine Untereinheit des γ-Sekretase Komplexes. Es wird angenommen, dass eine Dysfunktion der γ-Sekretase die Entstehung von Morbus Alzheimer begünstigen kann. Pen2 spielt eine wichtige Rolle bei der Bildung, der Stabilisierung und dem intrazellulärem Transport des γ-Sekretase Komplexes.

In dieser Arbeit wurde die Co-Lokalisation und Interaktion von unterschiedlich markierten Versionen von CLN3 und Pen2 in HeLa und COS-7 Zellen demonstriert. Weiterhin wurden isogene CLN3 und Pen2 knockout HeLa Zellen mit Hilfe des CRISPR/Cas9 Systems generiert, um die zelluläre Funktion beider Proteine zu untersuchen. Die phänotypische Charakterisierung beider knockout Zelllinien im Vergleich zu wild typ Zellen beinhaltete die Aktivität der γ-Sekretase. Die Prozessierung der bereits beschriebenen Substrate Amyloid Precursor Protein (APP) und Notch wurden analysiert. Wie erwartet, war die Prozessierung beider Substrate in Pen2 knockout Zellen inhibiert und dieser Phänotyp konnte durch die Expression von GFP-Pen2 aufgehoben werden. In CLN3 knockout Zellen war die Prozessierung von γ-Sekretase Substraten im Vergleich zu wild typ Zellen nicht verändert. Weitere Untersuchungen umfassten Veränderungen im lysosomalen-autophagosomalen System in beiden knockout Zelllinien im Vergleich zu wild typ Zellen. Lysosomale enzymatische Aktivitäten wurden analysiert und eine reduzierte β-Hexosaminidase A Aktivität in beiden knockout Zelllinien beobachtet. Weiterhin wurde eine Zunahme von Autophagosomen gefunden. Um diese Veränderungen zu evaluieren, wurden unterschiedliche Schritte des Autophagie-Pfads experimentell betrachtet. Dabei wurden Zellen mit Inhibitoren des mTOR Komplexes behandelt, mit einem Disaccharid, Trehalose, welcher mTor unabhängige Autophagie induziert und mit Inhibitoren der Autophagosomen-

Lysosomen-Fusion. Die Inhibition des mTOR abhängigen Pfads führte zu keiner weiteren Akkumulation von Autophagosomen in CLN3 und Pen2 knockout Zellen. Im Kontrast dazu, zeigten CLN3 und Pen2 knockout Zellen einen eindeutigen Anstieg im Autophagosomen Level nach Induktion des mTOR unabhängigen Pfads durch Trehalose und nach Inhibition der Autophagosomen-Lysosomen-Fusion. Zusätzlich wurde in beiden knockout Zelllinien ein verringerter Autophagie-Flux nachgewiesen.

Die Resultate dieser Arbeit weisen sehr deutlich darauf hin, dass die CLN3 und Pen2 Interaktion einer von der γ-Sekretase unabhängige Funktion unterliegt. Weiterhin verdeutlichen die hier durchgeführten Analysen zum ersten Mal, dass die Deletion von Pen2 lysosomale und autophagosomale Funktionen verändert. Zusätzlich sind die Ergebnisse im Einklang mit früheren Studien, welche für CLN3 eine funktionale Rolle in Lysosomen und Autophagosomen nahegelegt haben. Aufgrund des gemeinsamen Phänotyps und ihrer Interaktion könnten beide Proteine wichtig für die lysosomale Funktionalität sein. Eine Aufhebung dieser Interaktion scheint Veränderungen in der lysosomalen enzymatischen Aktivität und im Autophagie Pfad zu bedingen. Diese Effekte spielen möglicherweise bei der Entstehung sowohl von neurodegenerativen Erkrankungen des Kindesalters, wie JNCL, als auch von neurodegenerativen Erkrankungen Erwachsener, wie Morbus Alzheimer, ein Rolle.

1 Introduction

1.1 Protein trafficking

Protein translation occurs at free ribosomes in the cytoplasm or at ribosomes associated to the endoplasmic reticulum (rough ER) (Figure 1). Proteins undergo modification steps during and after translation at the endoplasmic reticulum, such as specific proteolytic cleavage (Johnson et al., 2013; Snapp et al., 2017), chaperone mediated folding (Braakman and Hebert, 2013), formation of disulfide bonds (Bulleid, 2012), assembly of protein subunits (Gaut and Hendershot, 1993), and initiation of glycosylation (Breitling and Aebi, 2013). Proteins must go through the quality control examination to exit the endoplasmic reticulum. In the Golgi compartment, further modification takes place like the completion of glycosylation process (Stanley, 2011). Delivery of newly synthesized lysosomal hydrolases to lysosomes is depending on the mannose-6 phosphate (M6P) pathway. In the cis-Golgi network (CGN), mannose-6 phosphate (M6P) groups are added to the lysosomal hydrolases precursors. In the trans-Golgi network (TGN) mannose-6 phosphate receptors (M6PRs) bind specifically to the M6P residues of the modified lysosomal hydrolases in a basic environment. Clathrin-coated vesicles filled with lysosomal enzymes are bud off from TGN and fuse with late endosomes (Figure 1). In acidic pH, the lysosomal enzymes dissociate from the MP6Rs and the receptors are recycled back to the TGN for further functioning (Coutinho et al., 2012). Lysosomal transmembrane proteins contain sorting signals in their cytosolic domain. These signals comprise sorting motifs such as dileucine-based motifs or tyrosine-based motifs. Binding of these motifs by GGAs or adaptor proteins (AP1) targets the transmembrane proteins toward late endosomes/lysosomes (Braulke and Bonifacino, 2009). A number of soluble lysosomal proteins are transported to late endosomal/lysosomal compartments through other receptors such as sortilin and lysosomal integral-membrane protein 2 (LIMP-2) (Staudt et al., 2016). Newly synthesized secretory proteins are delivered to the plasmamembrane (Figure 1). Secretory vesicles are formed as well at the trans-Golgi network. The vesicles filled with proteins are fused with the plasmamembrane (PM) and secrete protein content out of the cell (Lippincott-Schwartz et al., 2000). Transport of proteins between the compartments is facilitated by the vesicular intermediates that bud off from one compartment and fuse with the next compartment. The fusion of vesicles is mediated by SNAREs, Rab GTPases and vesicle tethering complexes. Coatomer protein

complex-II (COP-II) mediates trafficking from the endoplasmic reticulum to the Golgi compartment. Coatomer protein complex-I (COP-I) is crucial for retrograde trafficking from the Golgi compartment to the endoplasmic reticulum. Adaptor protein clathrin complex (AP-clathrin complex) is important for trafficking from Golgi compartment to endosomes or plasmamembrane (Mellman and Nelson, 2008) (Figure 1).

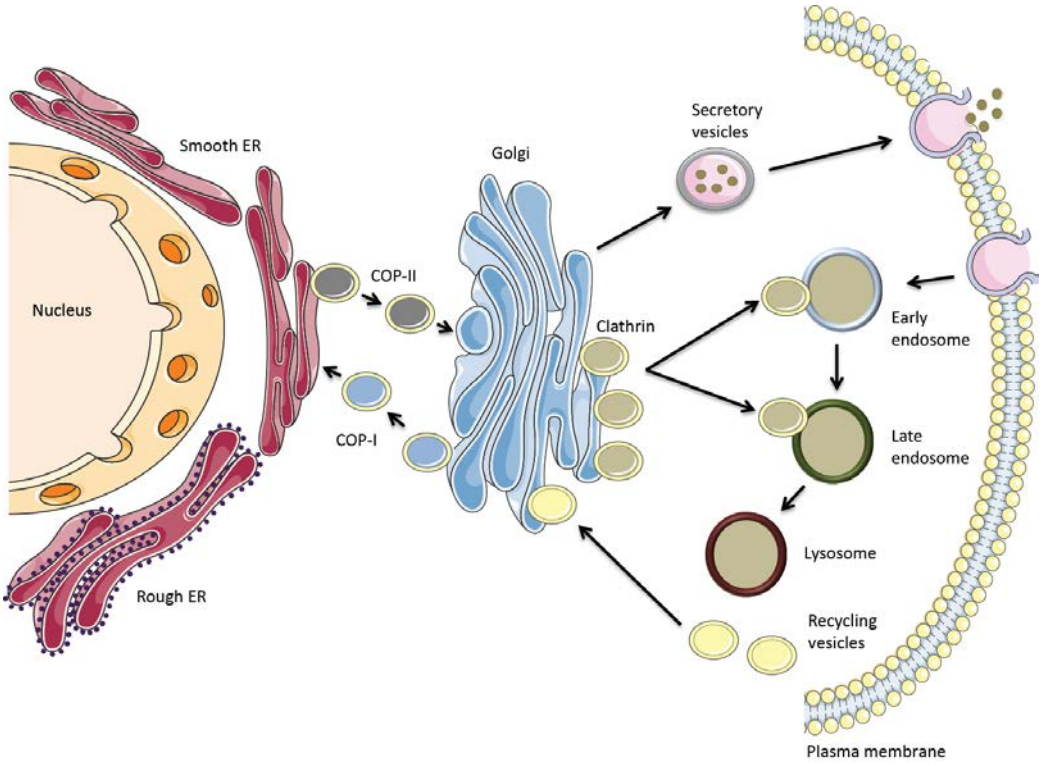

Figure 1: Illustration of the secretory and endocytic pathway. Newly synthesized proteins undergo modifications in the endoplasmic reticulum. These proteins are transported through COP-II coated vesicles to the Golgi for additional modifications. Defective proteins such as misfolded or unassembled proteins are retrogradely transported via COP-I coated vesicles back to the endoplasmic reticulum. Clathrin-coated vesicles are targeting lysosomal hydrolases, other lysosomal soluble proteins and transmembrane proteins to late endosomal/lysosomal compartments. Secretory vesicles filled with proteins are formed at the trans-Golgi network. These fuse with the plasmamembrane and secrete proteins out of the cells. The figure was prepared by using the medical art (http://smart.servier.com/).

1.2 Lysosomes

Lysosomes are intracellular organelles present in all eukaryotic cells. They contain different types of hydrolases. The luminal acidic pH (4.5 - 5) is required for optimal function of lysosomal hydrolases (Duve, 1975; Mindell, 2012). The size of lysosomes varies from 50nm to 500nm (Bandyopadhyay et al., 2014). These organelles receive and degrade intra- and extracellular material. Beside degradation, they are involved in many cellular processes such as plasmamembrane repair, cholesterol homeostasis and pathogen inactivation. The

extracellular material is taken up by endocytosis and delivered by maturation, vesicular, kiss and run or hybrid manner to lysosomes for degradation. The intracellular material is degraded through autophagy (Luzio et al., 2007; Saftig and Klumperman, 2009). The lysosomal membrane protects hydrolytic enzymes from the cytosolic environment. The vacuolar H^+ ATPase pump is maintaining the lysosomal acidic pH and ions homeostasis by pumping protons to lysosomes (Ishida et al., 2013; Oot et al., 2017). Well-known ion channels such as the transient receptor potential cation channel, mucolipin subfamily, member 1 (TRPML-1) and two-pore channel 2 (TPC2) are involved in maintaining lysosomal calcium homeostasis (Lee et al., 2015) (Figure 2).

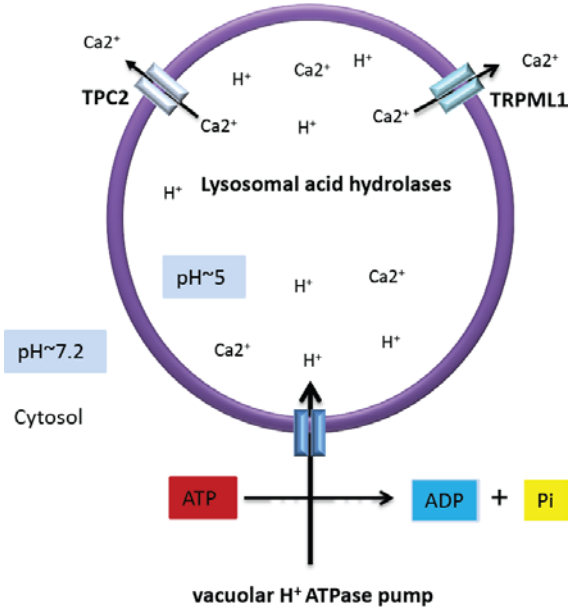

Figure 2: Lysosomal pH and calcium regulation. The vaculoar H^+ ATPase drives proton into the lumen to maintained lysosomal pH. TRPML1 and TPC2 ion channels are involved in maintaining lysosomal calcium homeostasis. Modified after (Lee et al., 2015).

1.2.1 Autophagy

Autophagy is an intracellular mechanism that delivers the cytoplasmic unnecessary and dysfunctional components such as mitochondria, protein aggregates and ribosomes to lysosomes for degradation and recycling which is important for cell survival (Boya et al., 2013). A defect in autophagy underlies many diseases for instance cancer, muscle, neurodegenerative, liver, cardiac, aging, immunity and inflammatory diseases (Levine and Kroemer, 2008).

Different types of autophagy have been described but three types have been widely studied. These are macroautophagy, microautophagy and chaperone-mediated autophagy (CMA) (Boya et al., 2013). Macroautophagy can be described as a four step process comprised of nucleation, expansion, fusion and degradation (Marzban et al., 2014). Glucose starvation or treatment with a natural disaccharide such as trehalose or sucrose (Chen et al., 2016) induces mammalian target of rapamycin (mTOR) independent autophagy. In this pathway, Unc51 like kinase (ULK1) is directly activated by phosphorylation through adenosine monophosphate-activated protein kinase (AMPK) (Kim et al., 2011; Yoon et al., 2017). Nutrient starvation or treatment with mTOR inhibitors such as rapamycin and torin1 (Zullo et al., 2014) induce mTOR dependent autophagy. In this pathway, mTOR activity is inhibited which leads to dephosphorylation of ULK1. As a result, the interaction of ULK1 with APMK is disrupted (Kim et al., 2011; Shang et al., 2011). Conversely, the availability of nutrients activates mTOR. This leads to phosphorylation of the eukaryotic initiation factor 4E (eIF4E) binding protein (4E-BP), eukaryotic initiation factor 4G (eIF4G) and S6 kinase (S6K). These activated factors are involved in transcription, translation, protein synthesis and cell survival. The Inhibition of mTOR complex reduces protein translation and others cellular mechanism (Kudchodkar et al., 2004; Magnuson et al., 2012) (Figure 3). The autophagy pathway starts by initiation of phagophores from the endoplasmic reticulum upon autophagy induction signaling (Hayashi-Nishino et al., 2009; Ylä-Anttila et al., 2014). The autophagy induction activates or dephosphorylates the ULK kinase, a part of a protein complex containing Atg13 and Fip2000 (Jung et al., 2009). Beclin-1 with other cofactors is activated by the ULK kinase (Kang et al., 2011) as a result other Atg (autophagy-related gene) proteins are recruiting to the growing phagophores (Xie and Klionsky, 2007). Full-length light chain 3 (LC3) is a cytosolic protein which is cleaved by Atg 4 and thereby converted into LC3-I. Subsequently, LC3-I is cleaved by Atg-3 and Atg-7 and then conjugates with phosphatidylethanolamine (PE) which generate active LC3-II. This is recruited to the growing phagophores by the Atg complex (Atg-5, Atg-12 and Atg-16). Autophagosomes are formed by fusion of both ends of the growing phagophore (Glick et al., 2010). The fusion of mature autophagosomes with lysosomes is creating autolysosomes. Cytoplasm derived materials are degraded by lysosomal hydrolyses in autolysosomes (Mizushima, 2007) (Figure 4).

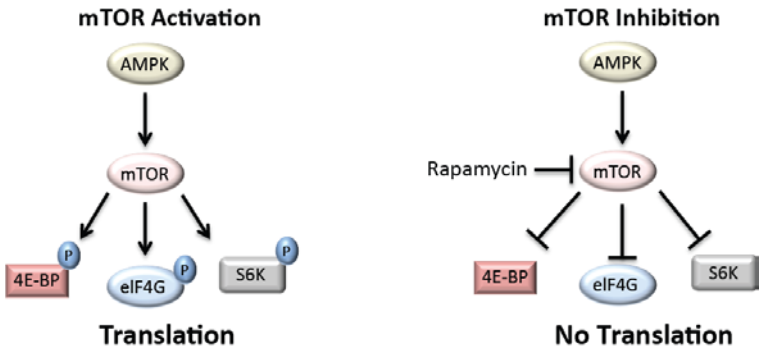

Figure 3: The role of the mTOR complex in the cellular process. Active mTOR phosphorylates 4E-BP, eIF4G and S6K. Activation of these factors is involved in protein translation and other cellular processes. The inhibition of mTOR hampers translation. Modified after (Kudchodkar et al., 2004).

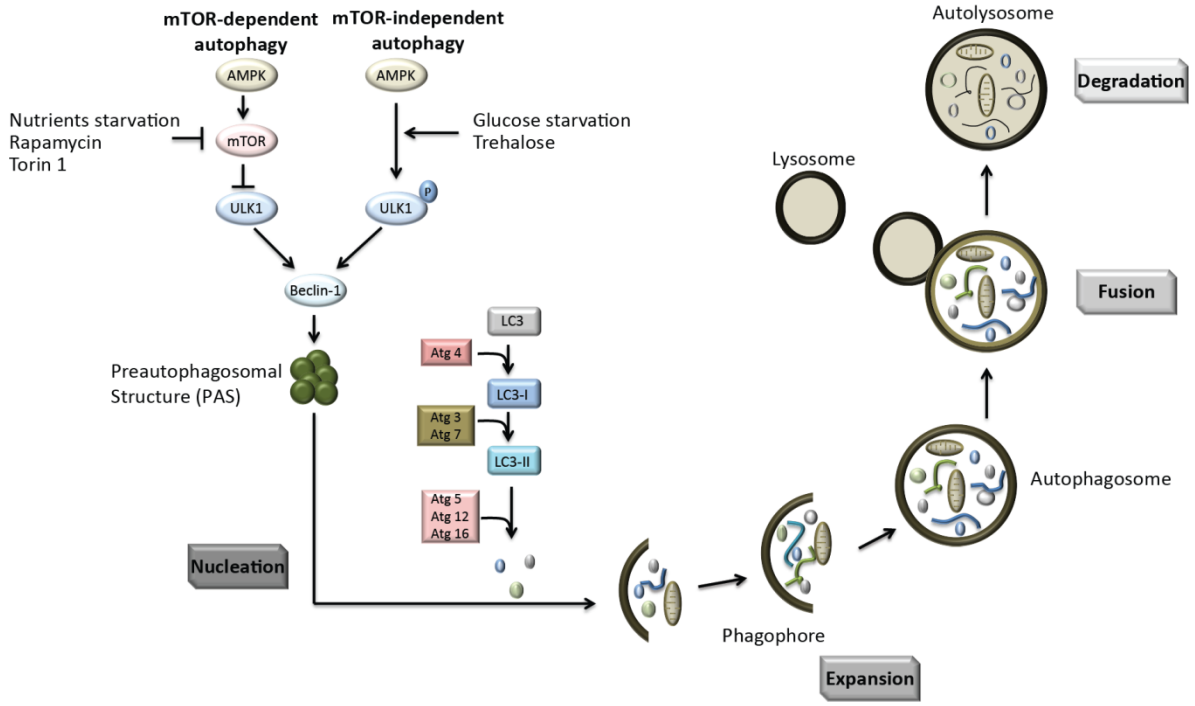

Figure 4: The macroautophagy pathway. Macroautophagy is induced by mTOR-dependent or mTOR-independent pathways. In the mTOR-dependent pathway, mTOR is inhibited by nutrient starvation, rapamycin or torin1 which dephosphorylate ULK1. In the mTOR-independent pathway, glucose starvation or disaccharides such as trehalose activate ULK1 by phosphorylation through AMPK. Dephosphorylation or phosphorylation of ULK1 activates Beclin-1 with others co-factors. Nucleation starts by formation of the pre-autophagosomal structure (PAS). During expansion, Atg activates LC3-II and it is recruited to growing phagophores. Autophagosomes are formed by the fusion of both ends of the growing phagophore. The fusion of mature autophagosomes with lysosomes is forming autolysosomes. Cytosolic materials are degraded in autolysosomes. Modified after (Marzban et al., 2014).

Modulation of autophagy induction through the mTOR-dependent or mTOR-independent pathway could be a potential therapeutic approach to treat a number of neurodegenerative diseases and cancer (Belzile et al., 2015; Levy et al., 2017; Nah et al., 2015; Sarkar et al., 2007; Zhang et al., 2014).

1.3 Lysosomal storage diseases

Lysosomal storage diseases (LSDs) are a group of about 50 genetic disorders. Defective lysosomes or lysosomal protein deficiency are the main cause for LSDs (Ballabio and Gieselmann, 2009). Due to these alterations, cellular material is accumulated in lysosomes (Onyenwoke and Brenman, 2015). Many factors can contribute to LSDs diseases such as, a defect in the autophagy pathway (Elrick and Lieberman, 2013; Lieberman et al., 2012), lysosomal pH imbalance due to impairment of vacuolar H^+ATPase pump (Colacurcio and Nixon, 2016), alterations in trafficking of lysosomal enzymes due to flaw in mannose-6-phosphate (M6P) molecule (Coutinho et al., 2012) or defects in lysosomal membrane permeabilization (LMP) (Appelqvist et al., 2011). A large number of lysosomal storage diseases have been described and for some the underlying dysfunctional protein has been identified. Examples are, Danon disease, Niemann-Pick C disease and Gaucher disease which are caused by defects in lysosome-associated membrane protein 2 (LAMP2), Niemann-Pick C 1 and 2 (NPC1 and 2) and β-Glucosidase proteins respectively (Futerman and van Meer, 2004).

1.3.1 Neuronal Ceroid Lipofuscinoses (NCL)

Neuronal Ceroid Lipofuscinoses (NCL) are a group of inherited autosomal recessive neurodegenerative diseases that affect children and adults. In NCL the lysosomal accumulation of autofluorescent material known as 'ceroid lipofuscin' affecting many cell types but most dramatically neuronal cells which leads to a neuronal loss (Haltia, 2003). The main symptoms of these diseases are seizures, dementia, retinopathy, mental disorder, motor deterioration and eventually premature death (Jalanko and Braulke, 2009).

Currently, 14 known genes (CLN-1 to CLN-14) have been associated with NCL. Mutations in each of these genes leads to a particular type of NCL such as infantile NCL (INCL), late infantile NCL (LINCL), juvenile NCL (JNCL), adult NCL (ANCL) and congenital NCL (CONCL) (Carcel-Trullols et al., 2015). NCL proteins are translated at the endoplasmic reticulum and most of them are transported to late endosomal/lysosomal compartments. NCL genes encode lysosomal enzymes (CLN1, CLN2, CLN10 and CLN13), soluble lysosomal proteins (CLN5), transmembrane proteins which localized to late endosomes/lysosomes (CLN3, CLN7 and CLN12) or endoplasmic reticulum (CLN6 and CLN8), cytoplasmic proteins that peripherally associate to vesicular membrane proteins (CLN4 and CLN14) and proteins in the

secretory pathway (CLN11) (Table 1). These proteins may directly or indirectly have an impact on the regulation of lysosomal function (Carcel-Trullols et al., 2015; Kollmann et al., 2013; Mole and Cotman, 2015) (Figure 5).

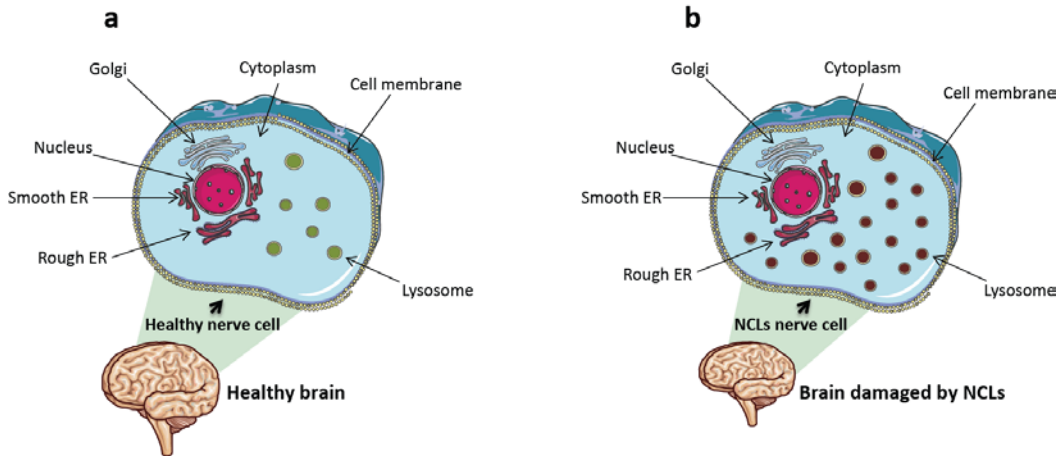

Figure 5: Comparison of a healthy brain and a brain damaged by NCL. (a) In a healthy brain, lysosomes perform its normal function. Lysosomes contain a variety of enzymes that are digesting many types of biomolecules. (b) In NCL, the brain size is decreased and lysosomes are defective due to mutations in NCL genes. Consequently, autofluorescent material accumulates in lysosomes. The figure was prepared by using the medical art (http://smart.servier.com/).

Table 1: NCL associated genes. Modified after (Carcel-Trullols et al., 2015).

Disease onset	Other disease name / Gene	Numbers of amino acid / type of Protein	Subcellular localization	Function
Infantile NCL	CLN1/*PPT1*	306 aa/soluble	Lysosomal matrix	Palmitoylthioesterase
Late infantile NCL	CLN2/*TPP1*	563 aa/soluble	Lysosomal matrix and ER	Serine protease
Juvenile NCL	CLN3/*CLN3*	438 aa/transmembrane	Late endosomes/lysosomes	Unknown
Adulthood NCL	CLN4/*DNAJC5*	198 aa/soluble membrane	Cytosolic, associated to vesicular	Hsc70 co-chaperone
Late infantile NCL	CLN5/*CLN5*	407 aa/soluble	Lysosomal matrix	Unknown
Late infantile NCL	CLN6/*CLN6*	311 aa/transmembrane	ER membrane	Lysosomal enzyme transporter
Late infantile NCL	CLN7/*MFSD8*	518 aa/transmembrane	Lysosomal membrane	Unknown
Late infantile NCL	CLN8/*CLN8*	286 aa/transmembrane	ER and ERGIC	Unknown

(Continued)

Disease onset	Other disease name / Gene	Numbers of amino acid / type of Protein	Subcellular localization	Function
Juvenile NCL	CLN9/*unknown*	Unknown	Unknown	Unknown
Congenital NCL	CLN10/*CTSD*	412 aa/soluble	Lysosomal matrix and extracellular	Aspartyl endopeptidase
Adulthood NCL	CLN11/*GRN*	593 aa/soluble	Extracellular	Unknown
Kufor-Rakeb syndrome	CLN12/*ATP13A2*	1180 aa/transmembrane	Lysosomal membrane and multivesicular bodies	Unknown
Adult kufs type	CLN13/*CTSF*	484 aa/soluble	Lysosomal matrix	Cysteine protease
Infancy, progressive myoclonus epilepsy 3	CLN14/*KCTD7*	289 aa/soluble	Cytosolic	Unknown

ER, endoplasmic reticulum; ERGIC, endoplasmic reticulum-Golgi intermediate compartment

NCL may be also linked to other neurodegenerative diseases. NCL disease patients show altered full-length amyloid precursor protein (APP) processing in brain tissue (Wisniewski et al., 1990a). Frontotemporal dementia (FTD) is caused by the heterozygous loss of function mutation in progranulin (GRN/CLN11) gene which leads to an accumulation of Tar DNA binding protein 43 (TDP43) in the brain. NCL identical storage material, retinal abnormalities and impaired lysosomal protease activity are observed in FTD affected patients (Hafler et al., 2014; Smith et al., 2012; Valdez et al., 2017; Ward et al., 2017). The homozygous loss of function mutation in GRN causes a lysosomal storage NCL like a disease. Notably, some patients with NCL disease show accumulation of phosphorylated TDP 43 within their brain (Gotzl et al., 2014; Holler et al., 2017; Zhou et al., 2015).

1.3.2 Juvenile Neuronal Ceroid Lipofuscinosis (JNCL)

Juvenile Neuronal Ceroid Lipofuscinosis (JNCL) is an autosomal recessive neurodegenerative disease also known as Batten disease mainly affecting children. The main feature of this disease is an accumulation of autofluorescent material including the “mitochondrial ATP subunit C” in lysosomes (Ding et al., 2011). The accumulation occurs in many organs such as gastrointestinal, glandular/secretory tissues (Chattopadhyay and Pearce, 2000) but the most affected organ is the brain (Ding et al., 2011; Prasad and Pullarkat, 1996). The main

symptoms of this disease are an impaired vision, cognitive disorder, motor decline, dementia, seizures and eventually death in the second or third decade of life (Cotman and Staropoli, 2012). However, one study suggests that in JNCL myoclonus seizures are uncommon (Augustine et al., 2015) additionally JNCL patients show sleep alteration (Kirveskari et al., 2000). Among genders, females get the disease later than males, show low functional competency, low quality of life and die earlier (Cialone et al., 2012; Nielsen and Ostergaard, 2013).

The Ceroid Lipofuscinosis Neuronal 3 (CLN3) gene is localized on chromosome 16p12 (Callen et al., 1991; Yan et al., 1993) and mutations in this gene are responsible for a Juvenile form of NCL. Around 15% of the JNCL patients carry missense, nonsense and indel mutations while 85% comprise 1kb deletion of exon 7/8 ($CLN3^{\Delta ex7/8}$) which leads to a formation of truncated CLN3 protein (Chan et al., 2008; Greene et al., 1999; Rothberg et al., 2004) (Figure 6).

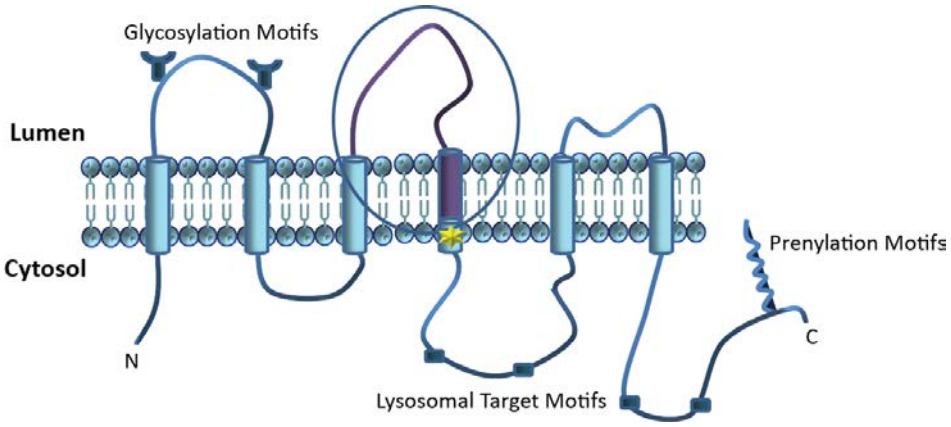

Figure 6: Ceroid Lipofuscinosis Neuronal 3 (CLN3) protein topology and mutation. The CLN3 protein consists of 6 transmembrane domains in which N- and C-termini are facing the cytosol (Ratajczak et al., 2014). Lysosomal targeting motifs, prenylation motifs and glycosylation motifs are indicated. The 1kb deletion of $CLN3^{\Delta ex7/8}$ leads to a premature stop codon and forms a truncated protein (circle). Modified after (Cotman and Staropoli, 2012).

The primary function of the CLN3 protein is still elusive however, some studies suggest that CLN3 is involved in neuronal survival, lipid homeostasis and protein folding/sorting in the endoplasmic reticulum (Scifo et al., 2013). Interaction of CLN3 with the other NCL genes like CLN5 (Lyly et al., 2009) may play a role in neuronal cell formation, survival and also in subunit C protein turnover. CLN3 is transported from the endoplasmic reticulum to the TGN and finally to late endosomal/lysosomal compartments (Haskell et al., 1999). It has been demonstrated that adaptor protein 1 and 3 (AP 1 and 3) bind the cytosolic lysosomal

targeting motifs of CLN3 and convey its targeting from the TGN to late endosomes/lysosomes (Kyttala et al., 2005; Mao et al., 2003). However, another study suggests that CLN3 traffics to late endosomal/lysosomal compartments without interacting with adaptor proteins (Storch et al., 2004). The identified interaction of the microtubule binding protein Hook1 with CLN3 and the small GTPases Rab7, Rab9 and Rab11 indicate other regulators in endosomal trafficking of CLN3 (Luiro et al., 2004). In neurons, CLN3 is transported through vesicles positive for to the late endosomal/lysosomal marker Rab7 (Oetjen et al., 2016). A CLN3 construct corresponding to the most common disease causing mutant form of CLN3 ($CLN3^{\Delta ex7/8}$) is ceased in the endoplasmic reticulum (Oetjen et al., 2016).

In JNCL many organs are affected but the most dramatically damaged organ is the brain. Several studies have demonstrated the effect of CLN3 mutations in JNCL patients and in addition, a large number of animal models have been generated for example in Mouse, Yeast and Drosophila. The affected brain of JNCL patients and other CLN3 mutant animal models show altered phenotype in different parts of the brain such as neurodevelopmental delay (Osorio et al., 2009), changed neuronal activity in synaptic and non-synaptic cells (Burkovetskaya et al., 2017), decreased gray and white matter in the dorsomedial part of thalamus and corona radiata respectively (Autti et al., 2007), decreased hippocampal volume as well as the whole brain volume (Tokola et al., 2014), Defect in cerebellum maturation (Weimer et al., 2009), α-amino-3-hydroxy-5-methyl-4-isoxazolepropionic acid (AMPA) and *N*-methyl-D-aspartate (NMDA) glutamate receptor alteration in cerebellar granule cells (CGCs) (Finn et al., 2011; Kovacs et al., 2015; Kovacs et al., 2006) and dopamine alteration (J. O. Rinne et al., 2002; Weimer et al., 2007). In JNCL non-neuronal cells such as astrocytes and microglia are functionally compromised (Pontikis et al., 2004; Pontikis et al., 2005) as a result chemokines, cytokines, mitogen, calcium and glutamate secretion are altered (Parviainen et al., 2017; Xiong and Kielian, 2013). The disease causes abnormalities in the immune system such as alterations in antigen presenting cells (APCs) (Hersrud et al., 2016). Due to this defect autoantibodies are increased which leads to an inflammation response in brain (Lim et al., 2007).

The loss of CLN3 imbalance lysosomal pH (Holopainen et al., 2001; Pearce et al., 1999) altered cathepsin D (CTSD) enzymatic activity (Carcel-Trullols et al., 2017) and effect arginine

homeostasis (Chan et al., 2009; Vitiello et al., 2007). Intracellular processing of CTSD and amyloid β protein precursor are changed due to the disturbance of lysosomal acidification (Golabek et al., 2000). CLN3 mutations altered macroautophagy which is the reason for a decreased protein degradation, impaired autophagosomes maturation and increased lysosomal pH (Vidal-Donet et al., 2013). Additionally, the autophagic flux (Chandrachud et al., 2015) and the TORC pathway (Bond et al., 2015) are disrupted. The CLN3 mutations also cause cardiac muscle (Ostergaard et al., 2011) and retinal (Volz et al., 2014; Weimer et al., 2006) dysfunction.

There is no specific treatment available for the NCL excluding the late infantile form (LINCL). A Food and Drug Administration (FDA) approved enzyme replacement therapy for late infantile neuronal ceroid lipofuscinosis (CLN2) is available. Patients are treated by administration of Brineura (cerliponase alfa) into the cerebrospinal fluid (www.FDA.gov). For JNCL some therapeutic approaches have been reported as helpful to slow down the disease by decreasing lysosomal storage pathology, improving motor function (Cooper, 2008; Kovacs et al., 2012; Kovacs et al., 2011), decreasing neuronal and axonal loss, retinal thinning and brain shrinking (Groh et al., 2017) and controlling seizure (Aberg et al., 2000; Larsen and Ostergaard, 2014). Other approaches such as enzyme replacement therapy, stem cell treatment, gene therapy, immune therapy and other pharmacological drugs could be helpful to treat JNCL and other NCL (Kohan et al., 2011).

1.3.3 Interaction partners of CLN3

Several studies aimed at identifying interaction partners of CLN3. Some of these have highlighted links of CLN3 with other NCL genes such as CLN5 (Lyly et al., 2009). The interaction of CLN3 with adaptor proteins 1 and 3 (AP 1 and 3) (Kyttala et al., 2005; Mao et al., 2003)and with cytoskeleton-associated proteins such as HooK1 (Luiro et al., 2004) may play a role in trafficking of CLN3. However, another study has presented the adaptor proteins independent trafficking of CLN3 protein (Storch et al., 2004). However, although, several studies identified interaction partners of CLN3, their possible role in the molecular mechanism underlying JNCL are still not conclusive.

In a TAP-tag screen Pen2 has been identified as a new interaction partner of CLN3. Pen2 is an important subunit of the γ-secretase complex. It has been suggested that Pen2 is involved

in assembly, stabilization and trafficking of the γ-secretase complex (Holmes et al., 2014). CLN3 is localized to late endosomal/lysosomal compartments (Oetjen et al., 2016). Previous findings demonstrated co-localization of CLN3 and Pen2 to late endosomes/lysosomes. Furthermore, in-situ hybridization and co-immunoprecipitation validated the interaction of both proteins (Sandra Oetjen; Ph.D. Thesis). More studies were needed for the functional characterization of this interaction and to find the functional role of CLN3 in JNCL pathology.

1.4 γ-secretase complex

Alzheimer's disease (AD) is a neurodegenerative disorder which starts between the fourth to sixth decades of life. Mutations in presenilin and amyloid precursor protein (APP) are mainly responsible for the familial form of Alzheimer's disease (FAD) (Goate et al., 1991; Haass and De Strooper, 1999). Many genetic and environmental factors contribute to the development of the sporadic form of Alzheimer's disease (SAD) (Stozicka et al., 2007). The main feature of Alzheimer's disease is the accumulation of amyloid β (Aβ) plaques particularly Aβ40/Aβ42 in the brain. APP is first cleaved by β-secretase (βAPP cleaving enzyme 1, BACE 1) and subsequently, cleaved by γ-secretase within the transmembrane domain. As a result toxic Aβ is produced, which aggregates in amyloid plaques. Accumulation of Aβ is thought as the main cause leading to neurodegeneration (Chami and Checler, 2012; Greenfield et al., 2000).

Formation and stability of the γ-secretase complex depends on four subunits which are Presenilin (PS), anterior pharynx defective 1 (APH-1), nicastrin (NCT) and presenilin enhancer 2 (Pen2) (De Strooper, 2003). The two homologous genes presenilin 1 (PS1) and presenilin 2 (PS2) are localized on chromosome 14 and chromosome 1 respectively. PS is a nine transmembrane protein in which the N- and C-terminus faces the cytosol and lumenal site respectively. As these four γ-secretase subunits interact and make up the functional γ-secretase complex, PS goes through the endoproteolytic cleavage between transmembrane 6 (TM6) and transmembrane 7 (TM7) as a result N-terminal fragment (NTF) and C-terminal fragment (CTF) are produced in neuronal and non-neuronal cells. The fragments bind and make an active and stable PS heterodimer (Podlisny et al., 1997; Thinakaran et al., 1996). Most AD-causing mutations have been found in PS1. The trafficking of βAPP to the cell surface is altered due to mutations in PS1 which increase the generation of Aβ plaques (Cai et al., 2003; Vetrivel et al., 2006). Nicastrin is a type 1 transmembrane protein which is involved in stability of the γ-secretase complex. Mature glycosylated nicastrin assembled

into the γ-secretase complex by its binding to presenilins (Yang et al., 2002). APH-1 is a seven transmembrane protein in which the N-terminus faces the lumen and C-terminus faces the cytosol. APH-1 has 3 homologous APH1-a, APH1-b and APH1-c. APH1-a has two splice variants APH1-aL and APH1-aS (Hebert et al., 2004; Meckler and Checler, 2016). Pen2 is a two transmembrane protein in which the N- and C-termini face the lumenal site (Crystal et al., 2003) (Figure 7). However, another recent study shows that the N-terminus faces the cytosol and N-terminus faces the lumen (Zhang et al., 2015).

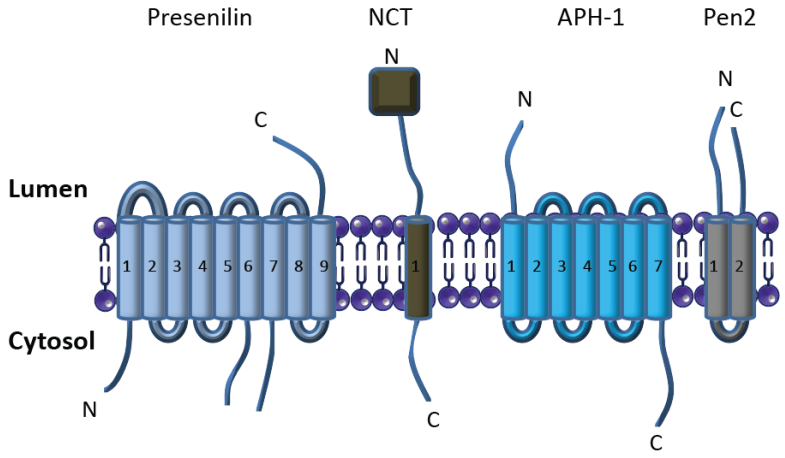

Figure 7: γ-secretase complex. Illustration of the γ-secretase complex which consists of four subunits: presenilin (PS), nicastrin (NCT), anterior pharynx defective 1 (APH-1) and presenilin enhancer 2 (Pen2). Assembly of all four subunits is important for stability and proper function of the γ-secretase complex. Modified after (Boulton et al., 2008).

Deficiency of one of the four subunits alters the γ-secretase function. Due to mutations in PS1, Pen2 is retained in the endoplasmic reticulum and trafficking of nicastrin to the Golgi is altered (Leem et al., 2002; Wang et al., 2004). Pen2 mutations lead to an accumulation of full-length PS1 and hampers PS1 endoproteolytic activation (Luo et al., 2003). Mutations in nicastrin and APH-1 decrease the stability and activity of the γ-secretase complex (Ma et al., 2005).

The γ-secretase complex formation starts in the endoplasmic reticulum with the interaction of APH-1 with nicastrin (LaVoie et al., 2003). Presenilin binds the stable intermediate by interacting with its C-terminus with nicastrin (Kaether et al., 2004). Subsequently, Pen2 interacts with the transmembrane domain 4 of presenilin (Watanabe et al., 2005). After the formation of the complete γ-secretase complex PS1 undergoes endoproteolysis and this results in an active γ-secretase complex (Fukumori et al., 2010). The binding of Pen2 allows the γ-secretase complex to leave the endoplasmic reticulum, to enter the Golgi (Holmes et

al., 2014; Kaether et al., 2007) and to traffic to the plasmamembrane or to late endosomal/lysosomal compartments depending on PS1 or PS2 respectively (Meckler and Checler, 2016).

γ-secretase is the key enzyme in regulated intramembrane proteolysis of type-1 transmembrane proteins such as amyloid precursor protein (APP) and Notch (De Strooper et al., 1999; De Strooper et al., 1998). Notch and APP signaling play a vital role during development and is involved in cell proliferation, survival and differentiation (Kopan and Ilagan, 2009; Muller and Zheng, 2012).

Notch is first cleaved in the TGN by furin (S1 cleavage) and binds to the type-1 transmembrane protein Delta of neighbor cells which is exposed at the plasmamembrane. Notch undergoes the second cleavage by α-secretase (a disintegrin and metalloproteinase, ADAM) (S2 cleavage). Finally, the γ-secretase mediated cleavage (S3 cleavage) within the transmembrane domain releases the Notch intracellular domain (NICD) which enters the nucleus and is involved in gene regulation (Bray, 2016; Guruharsha et al., 2012; Kopan et al., 1996) (Figure 8). Mutations in PS (Donoviel et al., 1999), Nicastrin (Li et al., 2003), APH-1 (Ma et al., 2005) and Pen2 (Francis et al., 2002) are embryonic lethal probably mainly due to a defect in notch signaling. Additionally, some studies show that Pen2 mutations cause familial AD (Sala Frigerio et al., 2005), skin diseases such as familial comedones syndrome (Panmontha et al., 2015) and acne inversa (Ralser et al., 2017).

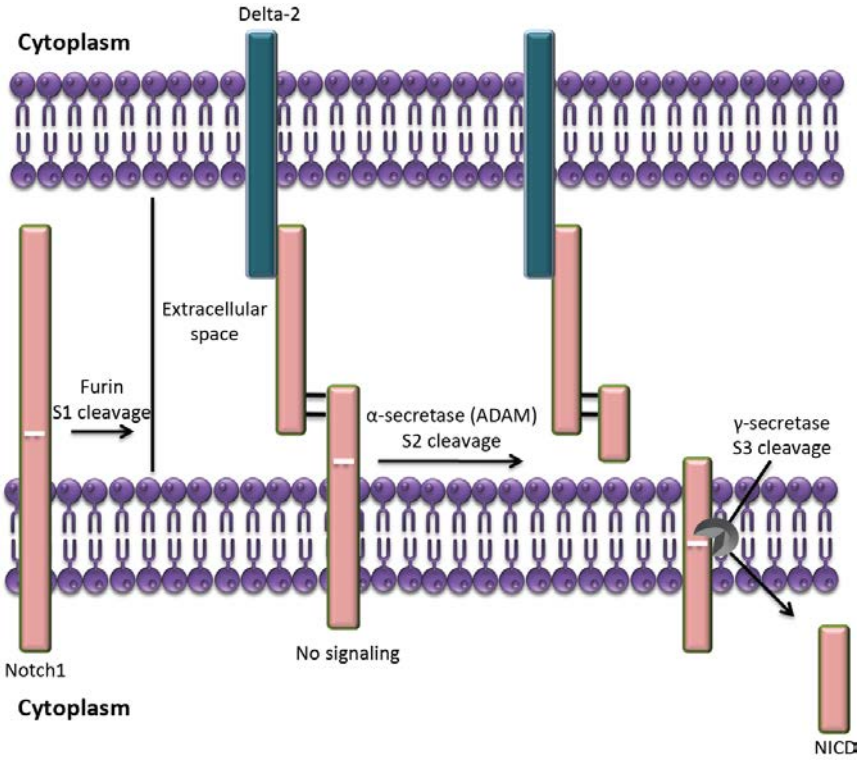

Figure 8: Proteolytic processing of the Notch. Notch is first cleaved by furin in the trans-Golgi network during maturation. The cleaved heterodimer binds Delta at the cell surface of neighboring cells. Cleavage by α-secretase generated a small transmembrane fragment. Subsequently, cleavage by γ-secretase releases the Notch intracellular domain (NICD) which enters the nucleus. There it is involved in cell fates specification during development. Modified after (Steiner and Haass, 2000).

The APP is first cleaved by the α-secretase (ADAM10 or ADAM17) within the Aβ domain or by β-secretase (BACE) which generates soluble APP αCTF and APP βCTF respectively. The γ-secretase cleavage within the transmembrane domain of APP αCTF and APP βCTF generate nontoxic P83 and neurotoxic Aβ plaques particularly Aβ40/Aβ42 respectively (Proctor et al., 2012; Zhang et al., 2011). APP cleavages produce APP intracellular domain (APP-ICD) which enters the nucleus and is involved in transcriptional activation process (von Rotz et al., 2004; Zhang et al., 2007) (Figure 9).

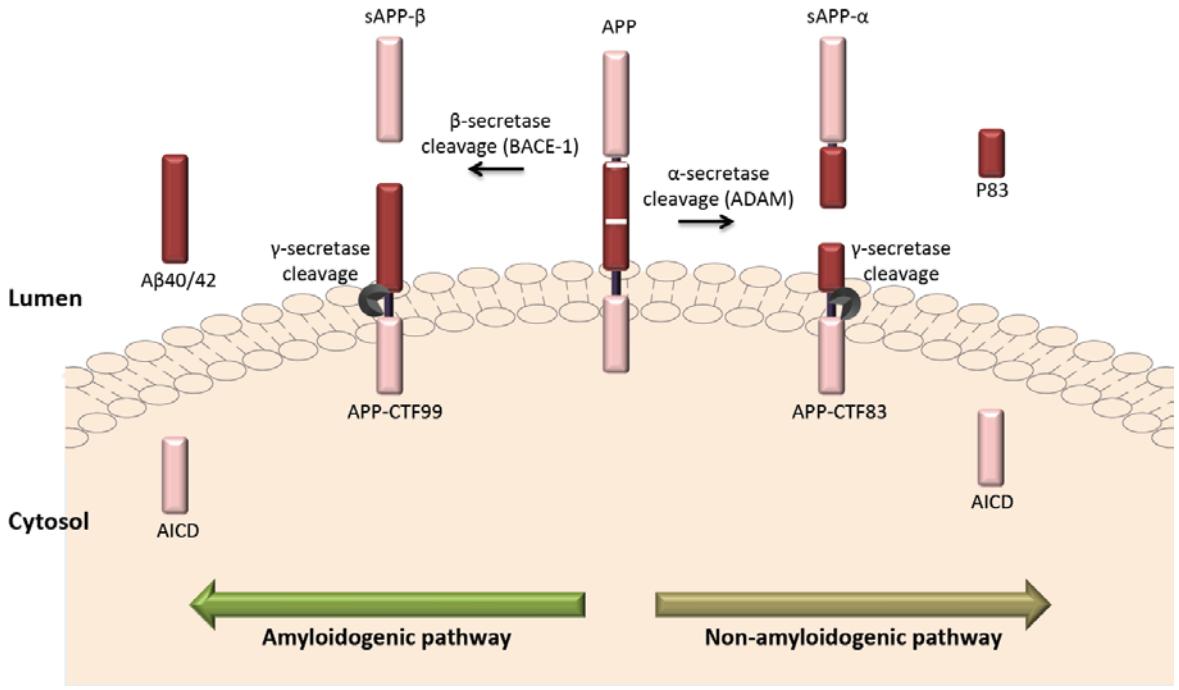

Figure 9: Proteolytic processing of the amyloid precursor protein (APP). In the non-amyloidogenic pathway, the type-I transmembrane full-length amyloid precursor protein (APP) is cleaved within the amyloid-β (Aβ) domain by α-secretase which generated the sAPP-α fragment. Then cleavage of the APP-CTF83 fragment by γ-secretase produces soluble p83 and APP intracellular domain (AICD) fragments. APP-ICD enters the nucleus and is involved in transcriptional activation processes. In the amyloidogenic pathway, β-secretase cleavage generates sAPP-β and APP-CTF99 fragments. Subsequently, cleavage of the small transmembrane fragment by γ-secretase produces Aβ40/42 plaques and AICD fragments. Modified after (Pajak et al., 2016).

2 Aims of the study

To date the function of the protein Ceroid Lipofuscinosis Neuronal 3 (CLN3) is unknown. CLN3 is predominantly localized to late endosomal/lysosomal compartments. This suggests the possible role of CLN3 in protein trafficking, autophagy and lysosomal homeostasis. Pen2 has been identified as an interaction partner of CLN3. The main aim of this project is a functional characterization of the Pen2-CLN3 interaction. This characterization should be supportive to understand the possible role of CLN3 in the molecular mechanism underlying Juvenile Neuronal Ceroid Lipofuscinosis (JNCL). Furthermore, it could be helpful to find therapeutic approaches to cure the disease.

Specific aims are:

Aim 1: Analyze co-localization of CLN3 with Pen2 in secondary cell lines.

Aim 2: Generate isogenic CLN3 and Pen2 knockout HeLa cells by using the CRISPR/Cas9 system.

Aim 3: Examine the lysosomal enzymatic activities in CLN3 and Pen2 knockout cell lines.

Aim 4: Investigate the autophagy pathway in CLN3 and Pen2 knockout cell lines.

3 Materials

3.1 Chemicals and reagents for cell culture

Earle's Balanced Salt Solution (EBSS) medium	Thermo Fisher Scientific, 24010-043
Lipofectamine 2000	Invitrogen, 11668-019
OptiMEM medium	Gibco, 11058-021
Penicillin Streptomycin (PS)	Thermo Fisher Scientific, 15140-122
Trypsin	Thermo Fisher Scientific, 25300-054
Zeocin	Invitrogen, ant-zn-1p

3.2 Chemicals and reagents for molecular biology

Agarose	Serva, 11406.03
Ammonium chloride (NH_4Cl)	Sigma, A9434
Bright-Glo^{TM} luciferase substrate	Promega, E2620
D-(+)-Trehalosedihydrate	Sigma , T9531
Deoxynucleotide (dNTPs)	GENEON, 110-012
Diethyl pyrocarbonate (DEPC)	Applichem, A0881.0100
Dimethyl sulfoxide (DMSO)	Sigma, D5879
DNA ladder, 1kb plus	Thermo Fisher Scientific, SM1331
DreamTaq enzyme	Thermo Fisher Scientific, EP0703
Dual-Glo luciferase substrate	Promega, E2920
Dual-Glo stop substrate	Promega, E2920
E-64d protease inhibitor	Sigma, E8640
Ethidium bromide	Roth, 7870.1
Iso-propanol	Chemsolute, 1136.1000
Lysozyme	Applichem, A3711.0010
Pepstatin A	Applichem, A2205,0010
Proteinase K	GeneON, 405-010
Pwo Master mix	Roche, 03789403001

Rapamycin	Selleckchem, S1039
Torin1	Selleckchem, 52827
TRIzol Reagent	Thermo Fisher Scientific, 15596018

3.3 Kits

BCA™ protein assay	Thermo-scientific, JJ125810
ECL-solution (SuperSignal® West Pico)	Thermo-scientific, 34580
ECL-solution (SuperSignal® West Femto)	Thermo-scientific, 34094
Gateway LR clonase-II enzyme mix	Invitrogen, K1820-00
Gateway LR Clonase-II	Invitrogen, 12538-120
NucleoBond® Xtra Midi	Macherey- Nagel, 740410.50
PCR Cleanup	Macherey- Nagel, 740609.250
Superscript™ II RT	GIBCO BRL, 18064-022
Transcriptor High Fidelity cDNA Synthesis	Roche, 05081866001

3.4 Solutions and buffers

Ohrlochpuffer (50ml)

Tris pH 8.5, 2M, (ROTH, 5429.2)	2.5ml
Ethylene-Diamine-Tetra-Acetic acid (EDTA), 0.5M, (Sigma, E6758)	0.5ml
Sodium Dodecyl Sulfate (SDS), 10%, (ROTH, 4360.2)	1.0ml
Sodium Chloride (NaCl), 5M, (ROTH, 9265.2)	2.0ml
Distilled water	44ml

Classical lysis buffer (10ml)

Triton X-100, 10%, (ROTH, 3051.2)	1ml
Tris-HCL PH 8, 1M, (ROTH, 5429.2)	0.2ml
Ethylene-Diamine-Tetra-Acetic acid (EDTA) pH 8, 0.5M, (Sigma, E6758)	0.2ml
Protease inhibitor (25X), (Roche, 04693132001)	0.4ml
Distilled water	8.2ml

Phosphate buffer saline (PBS)

Sodium chloride (NaCl), (ROTH, 9265.2)	1.73M
Potassium chloride (KCl), (Sigma, P9333)	27mM
di-Sodium hydrogen phosphate dehydrate ($Na_2HPO_2 . 2H_2O$), (ROTH, 4984.1)	81mM
Potassium dihydrogen phosphate (KH_2PO_4), (MERCK, 1.04873.1000)	14.7mM

Stacking gel

Acrylamide/Bis Solution, (Serva, P130190)	4%
Tris-HCL, pH 6.8, (ROTH, 5429.2)	125mM
Sodium Dodecyl Sulfate (SDS), (ROTH, 4360.2)	0.1%
Ammonium persulfate (APS), (AppliChem, A2941.0100)	0.05%
Tetramethylethylenediamine (TEMED), (AppliChem, A1148.0100)	0.05%

Running gel

Acrylamide/Bis Solution, (Serva, P130190)	10-12%
Tris-HCL, pH 8.8, (ROTH, 5429.2)	380mM
Sodium Dodecyl Sulfate (SDS), (ROTH, 4360.2)	0.1%
Ammonium persulfate (APS), (AppliChem, A2941.0100)	0.05%
Tetramethylethylenediamine (TEMED), (AppliChem, A1148.0100)	0.05%

Running buffer

Tris-Base, (ROTH, 5429.2)	250mM
Glycine, (ROTH, 3908.3)	1.92M
Sodium Dodecyl Sulfate (SDS), (ROTH, 4360.2)	1%

Blotting buffer

Tris-Base, (ROTH, 5429.2)	25mM
Glycine, (ROTH, 3908.3)	192mM
Methanol, (Chemsolute, 23.1411003)	10%

Super optimal broth (SOC) medium (1L)

SOB, (AppliChem, A0980.0500G)	25.5g
Distilled water	980ml
Autoclaved and cool it down at around 60°C	
Magnesium chloride ($MgCl_2$), 1M, (Sigma, M2670)	10ml
Glucose, 1M, (Sigma, G-7021)	10ml

After sterile filtration add $MgCl_2$ and Glucose to the SOB medium at around 60°C.

β-hexosaminidase A (β-Hex A) substrate (2.5ml)

4-nitrophenyl-N-acetyl-β-D-glucosaminide, 14.6mM, (Sigma , N9376)	1712µl
Sodium citrate, pH 4.6, 1M, (ROTH, 3580.3)	250µl
Triton X-100, 10%, (ROTH, 3051.2)	50µl
Distilled water	488µl

Arysulfatase A (ARSA) substrate (2.5ml)

4-Nitrocatechol sulfate dipotassium salt, 32.1mM, (Sigma, N7251)	779µl
Sodium citrate, pH 4.6, 1M, (ROTH, 3580.3)	250µl
Triton X-100, 10%, (ROTH, 3051.2)	50µl
Distilled water	1421µl

Stop buffer (50ml)

Glycine, 0.2M, (ROTH, 3908.3)	12.5ml
Sodium hydroxide (NaOH), 0.2M, (ROTH, 6771.3)	9.65ml
pH10.4	
Distilled water	27.85ml

Freezing medium (10ml)

Dulbecco's modified eagle medium (DMEM), (Biochrom, FG0435)	7ml
Fetal calf serum (FCS), (PAN, 1506-P131304)	2ml
Dimethyl sulfoxide (DMSO), (Sigma, D5879)	1ml

Saponin (50ml)

Saponin, 5%, (Sigma, S7900)	5ml
Fetal calf serum (FCS), (PAN, 1506-P131304)	5ml
PBS, 10x	5ml
Distilled water	35ml

Tris-EDTA (TE) buffer (100x)

Tris, 1M, (ROTH, 5429.2)	60.57g
Ethylenediaminetetraacetic acid (EDTA) di-sodium salt, (AppliChem, A1104,1000)	1.85g
Distilled water	500ml

STET lysis buffer (100ml)

Sucrose, 8% (w/v), (ROTH, 4621.1)	8g
Triton X-100, 0.1%, (ROTH, 3051.2)	0.1g
Ethylene-Diamine-Tetra-Acetic acid (EDTA), pH 8, 50mM (Sigma, E6758)	10ml
Tris-HCL, pH 8, 50mM, (ROTH, 5429.2)	5ml
Distilled water	100ml

Hexade Cetyl trimethyl ammonium bromide (CTAB) (100ml)

CTAB, (Sigma, H5882)	5g
Sodium chloride (NaCl), 0.5M, (ROTH, 9265.2)	100ml

DNA loading buffer (10x)

Tris-HCl, pH 7.6, (ROTH, 5429.2)	10mM
Glycine, (ROTH, 3908.3)	50%
Ethylene-Diamine-Tetra-Acetic acid (EDTA), pH 8, (Sigma, E6758)	60mM
Bromphenolblue, (Sigma, B8026)	0.25%
Xylenecyanole, (IBI, 72120)	0.25%

Paraformaldehyde (PFA) fixation solution

Phosphate buffer saline (PBS)	1x
Paraformaldehyde (PFA), (ROTH, 0335.3)	4%
Sucrose, (ROTH, 4621.1)	4%

Tris-acetate-EDTA (TAE) buffer (50x)

Tris-base, (ROTH, 5429.2)	96.8g
Sodium acetate (NaAc) H_2O free, (Merck, 1.06268.1000)	16.4g
EDTA.$2H_2O$, (AppliChem, A1104.1000)	7.4g

Adjust pH 7.8

3.5 Primers

3.5.1 PCR Primers

For: Forward, Rev: Reverse

Primers	Sequence
E^{242}EE>AAA	**For:** TCCGCTAGCATCTCATCAGGCCTTGGGGAG
	Rev: GGCTGCGCTCTCTGCTGCTGCTGCCCC
L^{253}I>AA	**For:** AGCGCAGCCCGGCAGCCCGCAGCAAGA
	Rev: GCGGGTACCAGCGGTATTGCTGAGCGTGAC
M^{409}>A	**For:** CGTGGTACCAGATGCTGTACCAGGCTGGCG
	Rev: AGAGATGCAGGTGGCCGCTGCTGCAAACTC
G^{419}>A	**For:** ACCTGCATCTCTGACACACTGGCAATCTCC
	Rev: TGCGGATCCGTTATCACCACTTTGTACAAG
U6	**For:** ACGATACAAGGCTGTTAGAGAGA
Pen2	**For:** TTGTTCTAATAGGGGCGTGG
	Rev: CCTCCTCTGTGCTCTAGACT
Pen2 CRISPR	**For:** TGCTTTCAGCAAACCGACCT
	Rev: TCCTCATTCCTCAGGACCCA
HPen2 EGxxFP	**For:** TATGCTAGCTTGTTCTAATAGGGGCGTGG
	Rev: CATGAATTCCCTCCTCTGTGCTCTAGACT
hPen2 RT	**For:** TAGATGAACCTGGAGCGAGTGTCCA
	Rev: ATATCAGGGGGTGCCCAGAGGTATG
CLN3	**For:** CCAGCCCCTCCCTTTTTCACG
	Rev: TGGGGCAAACCAGTGGATTCAG
HCLN3 EGxxFP	**For:** TTAGGATCCAGCTTCCTTGATGGATC
	Rev: ATAGAATTCCGGTCACTTCCCTCTTC
hCLN3 RT	**For:** ATGGGAGGCTGTGCAGGCTC
	Rev: AGCACAGCAGCCGTAGAGAC
Pen2 gRNA 1	**For:** CACCGCCAGGTAGTACTTCCGGCAC
	Rev: AAACGTGCCGGAAGTACTACCTGGC
Pen2 gRNA 2	**For:** CACCGCCTGTGCCGGAAGTACTACC
	Rev: AAACGGTAGTACTTCCGGCACAGGC
Pen2 gRNA 3	**For:** CACCGCCTCATTGGACACTCGCTCC
	Rev: AAACGGAGCGAGTGTCCAATGAGGC
Pen2 gRNA 4	**For:** CACCGCCTGGAGCGAGTGTCCAATG
	Rev: AAACCATTGGACACTCGCTCCAGGC
CLN3 gRNA 1	**For:** CACCGCGGCGCTTTTCGGATTCCGA
	Rev: AAACTCGGAATCCGAAAAGCGCCGC
CLN3 gRNA 2	**For:** CACCGAGGCTCGCGGCGGCGCTTTT
	Rev: AAACAAAAGCGCCGCCGCGAGCCTC

(Continued)

Primers	Sequence
CLN3 gRNA 3	**For:** CACCGGCGGCGCTTTTCGGATTCCG
	Rev: AAACCGGAATCCGAAAAGCGCCGC
CLN3 gRNA 4	**For:** CACCGGGACCTGAACTTGATGCGAT
	Rev: AAACATCGCATCAAGTTCAGGTCCC
Pen2 shRNA S2	**For:** CACCAGGCATAAATGATTATTAACGAATTAATAATCATTTATGCCT
	Rev: AAAAAGGCATAAATGATTATTAATTCGTTAATAATCATTTATGCCT
Pen2 shRNA S4	**For:** CACCAAATGATTATTAATATTTACGAATAAATATTAATAATCATTT
	Rev: AAAAAAATGATTATTAATATTTATTCGTAAATATTAATAATCATTT
Pen2 shRNA B1	**For:** CACCGGTTTGCTTTCCTGCCTTTCGAAAAAGGCAGGAAAGCAAACC
	Rev: AAAAGGTTTGCTTTCCTGCCTTTTTCGAAAGGCAGGAAAGCAAACC
hPen2 psi	**For:** GAACTCGAGATGAACCTGGAGCGAGTGTC
	Rev: GTCGCGGCCGCTCAGGGGGTGCCCAGGAGTATG

3.5.2 Sequencing primers

For: Forward, Rev: Reverse

Primers	Sequence
T7 promoter	**For:** TAATACGACTCACTATAGGG
BGH	**Rev:** TAGAAGGCACAGTCGAGG
L21	**For:** GGGGAAAGAATAGTAGACATAATAGCA
	Rev: CCACATAGCGTAAAAGGAGCA

3.6 Antibodies and Antibiotics

3.6.1 Primary antibodies

Antibodies	Company	Dilution
Chicken anti-GFP	Abcam, ab13970	1:10,000
Mouse anti-HA	Covance, MMS-101R	1:1000
Mouse anti β-actin	Sigma, A5441	1:100,000
Rabbit anti-dsRed	Clontech, 632496	1:500, 1:1000
Rabbit anti-LC3II	Novus, NB100-2220	1:1000
Rabbit anti-pS6	Cell signaling/NEB, 4858	1:2000

3.6.2 Secondary antibodies

Antibodies	Company	Dilution
Goat anti-chicken 633	Invitrogen, A21103	1:250
Goat anti-mouse 633	Thermo-scientific, 35513	1:250
Goat anti-rabbit 633	Thermo-scientific, 35563	1:250
Goat anti-chicken 555	Invitrogen, A21437	1:500
Goat anti-mouse 555	Invitrogen, A21422	1:500
Goat anti-rabbit 555	Invitrogen, A21428	1:500
Goat anti-chicken 488	Invitrogen, A11039	1:500
Goat anti-mouse 488	Invitrogen, A-11001	1:500
Goat anti-rabbit 488	Invitrogen, A11008	1:500
Rabbit anti-chicken HRP	Promega, G1351	1:10,000
Horse anti-mouse HRP	Vector laboratories, PI-2000	1:10,000
Goat anti-rabbit HRP	Vector laboratories, PI-1000	1:10,000

3.6.3 Antibiotics

Antibiotics	Company	Final concentration
Kanamycin	Applichem, A1493.0005	50µg/ml
Ampicillin	Applichem, A0839.0010	100µg/ml

3.7 Instruments

UV- transilluminator	BioRad
NanoDrop 2000 spectrophotometer	Peqlab
Ultrospec 2100 pro UV/visible spectrophotometer	Amersham Biosciences
Victor^3 light luminescence counter	PerkinElmer
Agarose-gelectrophoreses chamber PerfectBlue	PaqLab
ImageQuant LAS4000mini chemiluninescence detector	GE Healthcare
T-Professional Trio Thermocycler for PCR	Biometra
UV-gel-documentationsystemfor DNA-gels	BioRad

3.8 Microscopes

Confocal laser scanning microscope	Fluoview1000, Olympus
TCS SP5 confocal laser scanning microscope	Leica microsystems
TCS SP8 confocal laser scanning microscope	Leica microsystems
Apo fluorescence microscope	Zeiss Axio Imager Epifluorescence microscope

3.9 Software

DNASTAR Lasergene 9 Core Suite

SerialCloner 2.6.1

ImageJ/Fiji

Multi Gauge V3.2

Microsoft Office

4 Methods

4.1 Molecular biology

4.1.1 DNA preparation

For DNA-preparation on a small scale, the overnight culture of a picked colony from an LB-agar-plate in 4 ml of LB medium with an appropriate antibiotic was pelleted for 5 minutes at 4,500 rpm in a tabletop centrifuge. The pellet was resuspended in 200 µl of STET lysis buffer + Lysozyme (50 mg/ml) and shake for 2 minutes. After boiling the mixture for 2 minutes at 95°C and cooling on ice for 5 minutes a centrifugation step of 10 minutes at 13,000 rpm followed. The mucous pellet was removed, 10µl CTAB was added and centrifuged for 10 minutes at 13,000 rpm. The pellet was resuspended in 300µl NaCl (1-2M) after shaking for 5 minutes, 750µl absolute ethanol was added and spin at 13,000 rpm for 10 minutes. The pellet was washed with 500µl of 70 % ethanol and dried. The DNA was dissolved in 20 to 40 µl of distilled water. The preparations of larger scales of DNA were conducted with the nucleobondxtra midi kit (Machery-Nagel) and performed according to the manufacturer's protocol.

4.1.2 Extraction and purification of genomic DNA

Genomic DNA of HeLa cells was extracted and purified by using the genomic DNA mini kit (Invitrogen) and performed according to the manufacturer's recommended protocol. Briefly, HeLa cells were grown to $4x10^5$ per well in a 6 well plate in DMEM + 10%FCS + 1%PS medium. When cells were 80% confluent, the growth medium was removed, cells were harvested by trypsinization, resuspended in 200 µl PBS and 20µl Proteinase K was added. After addition of 20 µl RNase A, cells were mixed well by brief vortexing. This was followed by incubation at room temperature for 2 minutes. Then 200 µl PureLink Genomic Lysis/Binding Buffer was added, mixed well by vortexing to obtain a homogenous solution and incubated at 55°C for 10 minutes to promote protein digestion. 200 µl 100% ethanol was added to the lysate, mixed well by vortexing to yield a homogenous solution. Immediately after this step, the genomic DNA was purified.

The purification procedure is designed for purifying genomic DNA. Ethanol was added to the lysate (~640 µl) prepared with PureLink Genomic Lysis/Binding Buffer and poured on a spin column. This was centrifuged at 10,000 × g for 1 minute at room temperature. The collection tube was discarded and the spin column was placed into a clean pureLink collection tube. 500 µl Wash Buffer 1 was added to the column, centrifuged at 10,000 × g for 1 minute at room temperature, the collection tube discarded and the spin column was placed into a clean PureLink collection tube. 500 µl Wash Buffer 2 was added to the column, centrifuged at maximum speed for 3 minutes at room temperature, the collection tube was discarded, the spin column placed in a sterile 1.5-ml microcentrifuge tube, 100 µl of PureLink genomic elution buffer was added to the column, incubated at room temperature for 1 minute and the column centrifuged at maximum speed for 1 minute at room temperature. To recover more DNA, a second elution step was performed using the same elution buffer volume as for the first elution. The column was centrifuged at maximum speed for 1.5 minutes at room temperature and the purified genomic DNA collected.

4.1.3 DNA Extraction from single cell colony

HeLa cells from a well with a single colony were collected by trypsinization and split into two parts, one for future culturing and one for analysis. For analysis, cells were centrifuged at 1800xg for 2 min at 4°C. The supernatant was discarded and cells washed with PBS. The pellet was resuspended in Ohrlochpuffer + Proteinase K (50µl OLP + 6µl Proteinase K (10mg/µl). The volume of buffer was dependent on the cell pellet. Cells were incubated at 37°C for overnight with shaking. Cells were centrifuged at 4000xrpm for 1 min and the supernatant discarded. The pellet was dissolved in 100µl 1xTE buffer and incubated at 95°C for 15 minutes. The DNA was stored at 4°C.

4.1.4 RNA extraction by Phenol-Chloroform extraction with TRItidyG reagent

HeLa wild type, CLN3 and Pen2 knockout cells were seeded at $4x10^5$ per well on a 6 well plate in DMEM + 10% FCS + 1% PS medium and incubated overnight at 37°C. Before the RNA extraction 1ml Diethylpyrocarbonate (DEPC) was added to one liter millipore water and autoclaved. Cells were placed on ice and washed two times with ice-cold DEPC treated water. Per dish 1ml TRItidyG reagent (Thermo Fisher Scientific) was added and cells were

harvested using a cell scraper. The lysate was transferred into a 2ml reaction tube and incubated at room temperature for 10 minutes. For each milliliter of TRItidyG reagent, 200µl Chloroform was added. Reaction tubes were vigorously shaken for 15 seconds and then incubated at RT for another 10 minutes. Subsequent centrifugation for 15 minutes at 12000xg and 4°C resulted in three phases. The upper aqueous RNA containing phase was transferred into a new 1.5ml cup and 1Vol. isopropanol was added. After incubation at room temperature for 15 minutes, centrifugation step was repeated. The pellet was washed in 1ml 70% ethanol in DEPC-water and centrifuged again for 10 minutes at 4°C and 7500xg. The washing procedure was repeated with 1ml 100% ethanol. The pellet was then dried at 55°C and resolved in 50µl DEPC treated water at 55°C for 10 minutes before storage at -80°C.

4.1.5 Amplification of DNA fragments by polymerase chain reaction (PCR)

Amplification of DNA fragments was needed for the creation and alteration of expression constructs or other plasmids. For polymerase chain reactions (PCR) the following PCR reaction master mixtures were prepared (Table 2-5).

Table 2: DreamTaq PCR reaction master mixture.

Components	Volume/concentration
Template DNA	0.1-1µg
DreamTaq buffer, 10x	5µl
Forward primer, 10pmol/µl	1µl
Reverse primer, 10pmol/µl	1µl
dNTPs, 10mM	1µl
DreamTaq enzyme, 5U/µl	0.5µl
Distilled H_2O	Up to 50µl

Table 3: Pwo PCR reaction master mixture.

Components	Volume/concentration
Template DNA	0.1-1µg
Pwo master mixture	25 µl
Forward primer, 10pmol/µl	1µl
Reverse primer, 10pmol/µl	1µl
Distilled H_2O	Up to 50µl

Table 4: Pwo PCR reaction master mixture with and without Dimethyl sulfoxide (DMSO).

Genomic DNA without DMSO		**Genomic DNA with DMSO**	
Components	**Volume**	**Components**	**Volume**
Template genomic DNA	1 µl	Template genomic DNA	1 µl
Pwo master mix, 2x	25 µl	Pwo master mix, 2x	25 µl
Forward primer, 10pmol/µl	1 µl	Forward primer, 10pmol/µl	1 µl
Reverse primer, 10pmol/µl	1 µl	Reverse primer, 10pmol/µl	1 µl
Distilled H_2O	22 µl	DMSO, 5%	2.5 µl
		Distilled H_2O	19.5 µl
Total volume	50 µl	Total volume	50 µl
Genomic DNA (1/10) without DMSO		**Genomic DNA (1/10) with DMSO**	
Components	**Volume**	**Components**	**Volume**
Template genomic DNA (1/10)	1 µl	Template genomic DNA (1/10)	1 µl
Pwo master mix, 2x	25 µl	Pwo master mix, 2x	25 µl
Forward primer, 10pmol/µl	1 µl	Forward primer, 10pmol/µl	1 µl
Reverse primer, 10pmol/µl	1 µl	Reverse primer, 10pmol/µl	1 µl
Distilled H_2O	22 µl	DMSO, 5%	2.5 µl
		Distilled H_2O	19.5 µl
Total volume	50 µl	Total volume	50 µl

Table 5: Reverse transcription PCR reaction master mixture.

Transcriptor High Fidelity cDNA Synthesis Kit		**Superscript™ II RT kit**	
RT PCR Mixture	**Volume/Concentration/Incubation**	**cDNA synthesis mix**	**Volume**
Template RNA	6µg	1st standard buffer, 5x	4µl
Oligo dT Primer, 10µM	1µl	Dithiothreitol (DTT), 0.1M	2µl
dNTPs, 10mM	1µl	RNase OUT	1µl
Distilled H_2O	Up to 12µl	Superscript II	1µl
Incubate at 65°C	5 minutes		
Put on ice	2 minutes		
cDNA synthesis mix	8µl		

The annealing temperature for primers was determined by using the online tool Oligo calc (http://biotools.nubic.northwestern.edu/OligoCalc.html) and the annealing temperature was set according to the length of primers.

The elongation time is depended on the length of the expected PCR product for instance; the amplification time for 1kb of DNA fragment is roughly 45 seconds. Elongation times were set according to the length of the expected PCR product and usually, 30 reaction cycles were performed (Table 6).

Table 6: Protocol for amplification of PCR fragment.

Step	Time	Temperature	Number of cycles
Initial denaturation	120 sec	95°C	1
Denaturation	15 sec	95°C	30
Primer annealing	30 sec	Dependent on primers	
Elongation	30-250 sec	72°C	
Terminal elongation	420 sec	72°C	1
Resting temperature	---	4°C	∞

4.1.6 Gateway Cloning

Expression constructs for recombinant protein expression in mammalian cells were mostly generated by the Gateway system (Life Technologies). In the first cloning step, the sequence of interest was amplified with the addition of a Kozak consensus sequence (CACC) at the 5' end of the sequence. The PCR product was cloned into a pENTR/D-TOPO vector (ThermoFisher) according to the manufacturer's protocol. After 5-20 minutes of incubation 1.5µl of the reaction were transformed into Top10 E.coli bacteria. Correct integration of the sequence of interest into the pENTR/D-TOPO vector was assessed by antibiotic selection conditions for bacteria, restriction digestion of the purified plasmids and sequencing. pENTR/D-TOPO constructs can be sub-cloned into various destination vector (pDEST) with the Gateway LR clonase-II enzyme mix (Life Technologies) by DNA recombination. The pENTR/D-TOPO construct was combined with the desired pDEST vector in a recombination reaction which was set up according to the manufacturer's protocol. After an incubation time of 1 hour, 1.5µl of the reaction was transformed into Top10 E.coli bacteria. Correct recombination was assessed by the same method as for the TOPO cloning reaction.

4.1.7 Cloning of an expression vector encoding CLN3 with mutated lysosomal targeting motifs

In order to create mutations in CLN3 lysosomal targeting motifs, DreamTaq PCR reaction mixture was prepared (Table 2). For the first PCR, pDEST-LENTI-CMV-EGFP-RFA_hCLN3 was used as a template and PCR was performed by using the $E^{242}EE>AAA$, $L^{253}I>AA$, $M^{409}>A$ and $G^{419}>A$ primers which substitute the target nucleotide and change the amino acid.

For the second PCR, DreamTaq PCR reaction master mixture was prepared (Table 2) and the first PCR product was used as a template. PCR was performed by using the E^{242}EE>AAA forward and L^{253}I>AA reverse primers to combine the E^{242}EE>AAA with L^{253}I>AA mutant fragment. M^{409}>A forward and G^{419}>A reverse primers were used to combine the M^{409}>A with G^{419}>A mutant fragment.

The intermediate pcDNA3.1(+)-Zeocin vector was used to clone mutant fragments after the second PCR. The combined CLN3 E^{242}EE>AAA with L^{253}I>AA and M^{409}>A with G^{419}>A mutant fragment was cloned into the pcDNA3.1(+)-Zeocin vector by using NheI + KpnI and KpnI + BamHI restriction sites respectively. The cloned fragments were analyzed on an agarose gel and vectors sequenced by using the T7 promoter forward and BGH reverse primer to confirm mutations.

4.1.8 Cloning of shRNAs

To knockdown the human Pen2 mRNA three different shRNAs (shRNA S2, S4 and B1) were designed by using the online tools i-Score Designer (https://www.med.nagoyau.ac.jp/neurogenetics/i_Score/i_score.html) and Biosettia (http://biosettia.com/support/shrna-designer/).

The single-stranded oligos (Eurofins genomics) were resuspended in water to a concentration of 200 µM. The top and bottom strand oligos were annealed at 95C° for 4 minutes by using the following master mixture (Table 7).

Table 7: Master mixture for annealing the top and bottom single-stranded shRNAs oligos.

Components	Volume
shRNA top strand, 200 µM	5 µl
shRNA bottom strand, 200 µM	5 µl
Oligo annealing buffer, 10X	2 µl
Water	8 µl
Final volume	20 µl

The annealed oligos were cloned into the BLOCK-iT™ U6 entry vector (Life Technologies) according to the manufacturer's protocol. To analyze the shRNAs knockdown efficiency, human Pen2 was amplified in a DreamTaq PCR reaction master mixture (Table 2) by using the hPen2 psi primers and cloned into the psiCHECK™ vector (Promega).

4.1.9 Cloning of guide RNAs (gRNAs)

The guide RNAs (gRNAs) for Pen2 (gRNAs 1-4) and for CLN3 (gRNAs 1-4) were designed by using the online tools of the Feng Zhang lab (http://crispr.mit.edu/), GenScript (http://www.genscript.com/gRNA-database.html) and DNA20 (https://www.atum.bio/eCommerce/cas9/input).

The single-stranded (ss) oligos (Sigma) were resuspended in water to a concentration of 100 µM. For Phosphorylation and annealing, the top and bottom strand oligos the following master mixture was prepared (Table 8).

Table 8: Master mixture for annealing top and bottom single-stranded gRNAs oligos.

Components	Volume
sgRNA top, 100 µM	1 µl
sgRNA bottom, 100 µM	1 µl
T4 ligation buffer, 10X	1 µl
T4 Polynucleotide kinase (PNK)	1 µl
ddH2O	6 µl
Final volume	10 µl

The phosphorylation and annealing reaction condition were 1 cycle 37°C for 30 min, 1 cycle 95°C for 5 min, 70 cycle 95°C (delta T (C) = -1) for 12 sec and 25°C for 5 min. The phosphorylated gRNA oligos were diluted to 1:200 ratio in ddH_2O.

To clone the annealed oligos into the pX330 vector which was a gift from Feng Zhang (Addgene plasmid # 42230) the following reaction mixture was prepared (Table 9).

Table 9: Master mixture for cloning of gRNAs into pX330 vector.

Components	Volume
pX330 vector, 100ng	1 µl
Diluted oligo duplex	2 µl
Tango buffer, 10X	1 µl
Dithiothreitol, DTT, 10mM	1 µl
Adenosine-5`-triphosphate (ATP), 10mM	1 µl
Fast digest *Bbs*I	1 µl
T4 Ligase	0.5 µl
ddH2O	11.5 µl
Final volume	20 µl

The annealing conditions were 6 cycles 37°C for 5 min and 21°C for 5 min.

To digest any residual linearized DNA, the ligation reaction was treated with Exonuclease. For the reaction, each ligation reaction 11µl, 10x ExoIII buffer 1.5µl, 10mM ATP 1.5µl and 1µl fast digest ExoIII (Exonuclease) were mixed in a reaction tube and incubated at 37°C for 30 min and at 70°C for 30 min.

4.1.10 Restriction digestion

For cloning purposes and for the inspection of cloned plasmids digestions with restriction endonucleases were executed. Either conventional restriction endonucleases (Fermentas or New England Biolabs) were used for digestion from 1 hour to overnight or fast digest enzymes (Fermentas) were used for a digestion in 10 minutes. Restriction reactions were performed according to the product manual. To prevent re-ligation of plasmids with compatible overhangs the digested DNA was incubated with 1 unit Fast AP thermosensitive alkaline phosphatase (Fermentas) for the removal of 5'-phosphate groups. The digested DNA was separated on an agarose gel.

4.1.11 Ligation of DNA fragments

1 unit of T4-DNA ligase (Fermentas) was used to ligate 50ng of vector-DNA and suitable insert-DNA in a molar ratio of 5:1 or 10:1 to the vector. The reaction was set up according to the manufacturer's protocol and incubated for 60 minutes at room temperature or overnight at 4°C. The reaction was stopped by incubating at 65°C for 10 minutes.

4.1.12 Transformation

50µl Top 10 chemically competent Escherichia coli were thawed on ice and 5µl ligation reaction mixture was added and mixed by gentle tapping. Bacteria were incubated on ice for 15 min, transferred to 42°C for exactly 45 seconds and incubated on ice for 1-2 min. 250µl super optimal broth (SOC) medium was added and the suspension incubated on a horizontal shaker at 37°C for 1 hour. Transformed suspensions were plated onto LB agar plates with selection antibiotic and incubated at 37°C overnight.

4.1.13 Agarose gel electrophoresis

DNA fragments were separated on agarose-gels for the purpose of analysis and extraction of fragments of specific sizes. Agarose-gels were prepared with 0.5 - 2 % agarose (depending on the size of the relevant fragment) in TAE buffer. The agarose-TAE buffer mixture was heated and cooled at room temperature before pouring into the gel tracer. DNA was mixed with loading buffer and run on the gel. To assess the sizes of DNA fragments in the gel, GeneRuler 1kb plus DNA ladder (Thermo Fisher Scientific) was loaded in parallel to the DNA of interest. The gel was run at 10 V/cm. To stain the DNA, the gel was covered with TAE buffer + ethidium bromide (1:20,000) for 15-20 minutes at room temperature and documentation followed in the UV- transilluminator (BioRad).

4.1.14 Gel extraction and purification of PCR and cloning products

After restriction digestion and separation on an agarose gel, the relevant fragments were extracted from the agarose gel with the NucleoSpinR Gel and PCR Cleanup kit (Macherey-Nagel) according to the guidelines of the manufacturer. The kit was also used to purify DNA from PCR reactions.

4.1.15 DNA concentration assessment

The DNA concentration and purity of DNA preparations or of gel-extraction was determined with the NanoDrop 2000 spectrophotometer (Peqlab) by measurement of the optical density at 260nm.

4.1.16 DNA sequencing

Amplified DNA and plasmid DNA was analyzed by Sanger sequencing (Sanger *et al*. 1977). Sequencing was executed by the in-house service group Bioanalytics of PD Dr. Sabine Hoffmeister Ullerich. Sequence alignment and verification was performed with the help of the software package DNASTAR Lasergene 9 Core Suite.

4.2 Cell culture

4.2.1 Cultivation of secondary cell lines

Secondary cell lines (HeLa, COS-7, N2A and HEX 293) were maintained in 10cm plastic cell dishes (Cellstar®, Greiner Bio-one) at 37°C and 5% CO_2 with 95% humidity and split when 80% confluency was reached. Cells were washed 2x with sterile 1xPBS and detached by adding the 1ml trypsin solution (PAA) for 3 minutes at 37°C. The reaction was stopped by adding 10ml growth medium and cells were transferred to a 15ml falcon tube and centrifuged at 1200xg for 2 minutes. The pellet was resuspended in the desired volume of medium and if necessary cells were counted. Cells were cultured at a suitable density in 6 well, 24 well or 96 well plates (Greiner Bio-one).

For long-term storage the cell pellet was resuspended in freezing medium and frozen at -80°C for 24 hours before storage in liquid nitrogen.

4.2.2 Transfection of secondary cell lines

Secondary cell lines were transfected using Lipofectamine 2000 (Invitrogen) according to the manufacturer's protocol. For the transfection, Cells were incubated in OptiMEM without FCS medium which was exchanged for normal growth medium 4-6 hours after the transfection. N2A cells were kept in growth medium over the whole time of treatment. Stably transfected HeLa cells were generated under antibiotic selection conditions in DMEM + 10%FCS + 1%PS with zeocin (250µg/ml) medium.

4.2.3 Generation of stable transfected HeLa fluorescence tagged Pen2 cells

HeLa cells were seeded to $4x10^5$ per well in a 6 well plate in DMEM + 10%FCS + 1%PS medium and incubated overnight at 37°C. The following day HeLa cells were transfected with HA-tagged Pen2 and tdTomato-tagged Pen2 constructs which contain a zeocin resistance cassette. The transfection was performed with Lipofectamine 2000 (Invitrogen) reagent according to the manufacturer's protocol. After 48 hours of transfection, cells were trypsinized and diluted to 0.05cell/µl in the DMEM medium. Of these 2 cells/µl, 1 cell/µl and 0.5 cell/µl were cultured in a 96 well plate filled with DMEM + zeocin (250µg/ml) medium up to 200µl. Cells were incubated at 37°C for about 2 weeks or until single clones were grown sufficiently. HeLa cells from a well with a single colony were expended from 96 well plate to 6 well plate. To analyze the stable transfected fluorescence tag Pen2, the cells were seeded to $4x10^4$ per well in a 24 well plate on coverslips in the DMEM with zeocin medium and incubated overnight at 37°C. Next day, cells were fixed in 4% PFA and immunocytochemistry was performed. The fluorescence of specific tag was observed by fluorescence microscopy.

4.2.4 Immunocytochemistry

Cells were cultured at a suitable density in 6 well, 24 well or 96 well plates with coverslips. After transfection, cells were washed 2x with 1xPBS and fixed in 4% paraformaldehyde (PFA) under the hood for 15 minutes at room temperature. Cells were washed 2x with 1xPBS. To permeabilize membranes 0.5% saponin with 10% FCS was added to cells for 1-2 hours at room temperature or at 4°C overnight. The antibody labeling was performed on parafilm (Bemis) in a damp environment. The primary antibody was diluted in 0.5% saponin with 10% FCS and incubated for 1 hour at room temperature. Cells were washed three times with 0.5% saponin + 10% FCS, each washing step lasting for 5 minutes. The secondary antibody

was diluted in 0.5% saponin with 10% FCS and incubated for 1 hour at room temperature. Cells were washed three times with 0.5% saponin + 10% FCS, each washing step lasting for 5 minutes finally cells were washed with distilled water. Then coverslips were mounted with Immu-Mount (Thermo-scientific) containing 20% Prolong Gold anti fade with Dapi (Life Technologies) on a glass slide.

4.3 CLN3 and Pen2 knockout via CRISPR/Cas9 system

4.3.1 Verification and amplification of human CLN3 and Pen2 from genomic DNA

In order to verify human CLN3 and Pen2 sequence genomic DNA of HeLa cells was extracted and purified. The Pwo PCR reaction master mixture was prepared (Table 3). PCR was performed by using the CLN3 and Pen2 primers.

Different gRNAs were designed to knockout the CLN3 and Pen2, annealed and cloned into the pX330 vector a gift from Feng Zhang (Addgene plasmid # 42230). To test all gRNAs cloned into the pX330 vector, DreamTaq PCR reaction master mixture was prepared (Table 2). The respective colony was touched with a sterile tip and pipetted into the master mix. PCR was performed by using the U6 forward and each gRNA reverse primer.

To amplify the human CLN3 and Pen2 from HeLa genomic DNA, the Pwo PCR reaction master mixture with and without DMSO was prepared (Table 4). Pure genomic DNA and 1/10 diluted genomic DNA were added in both reaction mixtures. PCR was performed by using the HCLN3 EGxxFP and HPen2 EGxxFP primers. The amplified PCR fragments were cloned into the pCAG-EGxxFP vector, a gift from Masahito Ikawa (Addgene plasmid # 50716) and EGFP reconstitution test was performed to test the efficiency of gRNAs to knockout the gene.

4.3.2 EGFP reconstitution test

The assay is based on binding of gRNA to the target gene and Cas9 nuclease causes the double-stranded break. As a result, the split EGFP cassette is reconstituted via homologous recombination (HR) or single-strand annealing (SSA). The green fluorescence was observed under fluorescence microscope. To test the efficiency of gRNAs, human CLN3 and Pen2

genomic fragments corresponding to parts of the genes harboring the gRNA binding sites were cloned into the multiple cloning sites (MCS) of the pCAG-EGxxFP vector. NheI and EcoRI restriction sites were used for Pen2. BamHI and EcoRI restriction sites were used for CLN3. HeLa cells were cultured to $4x10^4$ cells per well in a 24 well plate on coverslips in DMEM + 10%FCS + 1%PS medium and incubated overnight at 37°C. Next day, cells were transfected according to the scheme shown in the table (Table 10-11).

Table 10: Transfection scheme of EGFP reconstitution test for Pen2.

Well #	**1**	**2**	**3**	**4**	**5**	**6**
Vector 1	pCAG_EGxxFP _pen2	pCAG_EGxxFP _pen2	pCAG_EGxxFP _pen2	pCAG_EGxxFP _pen2	pCAG_EGxxFP _pen2	pCAG_EGxxFP _pen2
Vector 2	pX330-Pen2 gRNA 1	pX330-Pen2 gRNA 2	pX330-Pen2 gRNA 3	pX330-Pen2 gRNA 4	pX330-empty vector	_____
Well #	**7**	**8**	**9**	**10**	**11**	**12**
Vector 1	pCAG_EGxxFP_ empty vector	pCAG_EGxxFP_ empty vector	pCAG_EGxxFP_ empty vector	pCAG_EGxxFP_ empty vector	pCAG_EGxxFP _empty vector	pCAG_EGxxFP _empty vector
Vector 2	pX330-Pen2 gRNA 1	pX330-Pen2 gRNA 2	pX330-Pen2 gRNA 3	pX330-Pen2 gRNA 4	pX330-empty plasmid	_____

Table 11: Transfection scheme of EGFP reconstitution test for CLN3.

Well #	**1**	**2**	**3**	**4**	**5**	**6**
Vector 1	pCAG_EGxxFP _CLN3	pCAG_EGxxFP _ CLN3	pCAG_EGxxFP _ CLN3	pCAG_EGxxFP _ CLN3	pCAG_EGxxFP _ CLN3	pCAG_EGxxFP _ CLN3
Vector 2	pX330-CLN3 gRNA 1	pX330- CLN3 gRNA 2	pX330-CLN3 gRNA 3	pX330-CLN3 gRNA 4	pX330-empty vector	_____
Well #	**7**	**8**	**9**	**10**	**11**	**12**
Vector 1	pCAG_EGxxFP_ empty vector	pCAG_EGxxFP_e mpty vector	pCAG_EGxxFP _empty vector	pCAG_EGxxFP _empty vector	pCAG_EGxxFP _empty vector	pCAG_EGxxFP _empty vector
Vector 2	pX330-CLN3 gRNA 1	pX330- CLN3 gRNA 2	pX330-CLN3 gRNA 3	pX330-CLN3 gRNA 4	pX330-empty plasmid	_____

4.3.3 Generation of human CLN3 and Pen2 knockout cells

HeLa cells were seeded to $6\text{-}8x10^4$ per well in a 24 well plates in DMEM + 10%FCS + 1%PS medium and incubated overnight at 37°C. 0.5µg each pX330_gRNA vector was added together with 1µg pcDNA3.1-zeocin (+) vector (Invitrogen) to 25µl OptiMEM (-FCS) medium in an eppendorf tube (mixture A). For each reaction, 2µl Lipofectamine 2000 was added to the 25µl OptiMEM medium in the eppendorf tube (mixture B). The mixture was incubated at room temperature for 5 minutes. The mixture A and B were combined and incubated at room temperature for 20 minutes. The DMEM + 10%FCS + 1%PS medium was removed from the cells. These were washed with PBS and subsequently 1ml OptiMEM (-FCS) medium was added to the cells. The transfection mix was added to HeLa cells and mixed well. Cells were

incubated at 37°C overnight. The following day, HeLa cells were trypsinized and reseeded into 6 well plate in the DMEM + 10%FCS + 1%PS with zeocin (250µg/ml) medium and incubated at 37°C for 5 days. Cells were trypsinized and diluted to 0.05 cell/µl in DMEM + 10%FCS + 1%PS medium. Of these 2 cells/well, 1 cell/well and 0.5 cell/well were cultured in a 96 well plates filled with the DMEM + 10%FCS + 1%PS medium up to 200µl. Cells were incubated at 37°C for about 2 weeks or until single clones were grown sufficiently.

HeLa cells from a well with a single colony were collected by trypsinization and split into two parts, one for future culturing and one for analysis. DNA extraction from cell colonies was performed. To confirm the CLN3 and Pen2 knockout from single cell clones, DreamTaq PCR reaction master mixture was prepared (Table 2). PCR was performed by using the Pen2 CRISPR and hCLN3 RT primers. The PCR product was analyzed on agarose gel and sequenced.

4.3.4 Verification of CLN3 and Pen2 knockout HeLa cells by reverse transcription

The other possible way to verify mutations in HeLa wild type, CLN3 and Pen2 knockout cells is reverse transcription. RNA was extracted by phenol-chloroform extraction with TRItidyG reagent. Reverse transcription PCR (RT-PCR) was performed to synthesize the cDNA from RNA of HeLa wild type, CLN3 and Pen2 knockout cells by using the transcriptor High Fidelity cDNA Synthesis (Roche) together with superscript^{TM} II RT (GIBCO BRL) kits. For RT-PCR, reverse transcriptase PCR reaction mixture was prepared (Table 5). The reverse transcription PCR reaction condition was 1 cycle at 50°C for 60 min, 1 cycle at 70°C for 45 min and 1 cycle at 4°C for 5 min.

After the reverse transcription PCR, to confirm mutations in a CLN3 and Pen2 knockout, DreamTaq PCR reaction master mixture was prepared (Table 2). cDNA of HeLa wild type, CLN3 and Pen2 knockout cells were used as a template. PCR was performed by using the hCLN3 RT and hPen2 RT primers. The PCR product was analyzed on agarose gel and sequenced.

4.4 Luciferase assay

A Luciferase assay was used for the assessment of the knockdown efficiency of shRNAs and for the γ-secretase activity assay. Luciferase assay for Dual-Glo® luciferase assay system (Promega) and Bright-Glo™ luciferase assay system (Promega) was conducted according to the guidelines of the manufacturer.

4.4.1 Test of shRNAs

The shRNAs were constructed with the BLOCK-iT™ U6 RNAi entry vector kit (Life Technologies) and tested with the Dual-Glo® luciferase assay system in combination with the psiCHECK™ vector system (Promega).

The knockdown capacity of the constructed shRNAs was compared to the specific knockdown of the Renilla luciferase with a Renilla specific shRNA (pSuperrenilla). As negative controls, the empty shRNA vector (pENTR-U6 vector) and a scrambled shRNA (pSuper TRONO) were used. The psiCHECK™ vector with human Pen2 and specific shRNAs were transfected into N2A cells with Lipofectamine 2000 (Invitrogen) according to the manufacturer's protocol. Each reaction mixture was tested in 4 replicates. Cells in the 8th row of the 96 well plate remained un-transfected for normalization (Table 12).

Table 12: Scheme of transfection to test the knockdown efficiency of shRNAs.

Line 1	Line 2	Line 3	Line 4	Line 5	Line 6	DNA µg/well
pSuperRenilla	pSuper TRONO	shRNA S2	shRNA B1	shRNA S4	pENTR-U6	0.15
psiCHECK2-hPen2	psiCHECK2-hPen2	psiCHECK2-hPen2	psiCHECK2-hPen2	psiCHECK2-hPen2	psiCHECK2-hPen2	0.15

The efficiency of the shRNAs was assessed with the Dual-Glo® luciferase assay system according to the manufacturer's protocol briefly, after removing the medium 25µl Bright-Glo™ luciferase substrate and 25µl OptiMEM were added to each of the 96 well plates. Plates were incubated with slight shaking at room temperature for 5 minutes. The liquid was transferred to a white measuring plate. The luminosity of firefly luciferase was measured with the Victor^3 light luminescence counter (PerkinElmer). After firefly luciferase measurement, Dual-Glo luciferase substrate and Dual-Glo stop substrate with 1:100 ratio

was added to each well of the 96 well plates. The luminosity of Renilla luciferase was measured with the Victor^3 light luminescence counter. The Renilla caused luminosity was normalized to the measured firefly activity for each well.

4.4.2 γ- secretase assay

As sensors for the γ-secretase activity, γ-secretase substrates were inserted into a vector by using a Gateway pDEST vector as a template. The insert consists of a nuclear localization sequence (NLS), a Gal-4 promoter binding domain and a VP16 transcriptional activation domain at the C-terminus which induce the transcription of a Gal-4 promoter driven reporter gene. Firefly luciferase was used as a reporter and activity was measured with the Bright-Glo™ reagent (Promega).

The developed constructs were transfected into HeLa wild type and Pen2 knockout cells with Lipofectamine 2000 (Invitrogen) reagent according to the manufacturer's protocol. As a transfection control GFP was co-transfected and in addition, the reporter plasmid bearing the Gal-4 promoter driven firefly luciferase gene was transfected. Each reaction mixture was tested in 7 replicates. Cells in the 8th row of the 96 well plate remained un-transfected for normalization (Table 13).

Table 13: Scheme of transfection to test the γ-secretase activity.

Line 1	Line 2	Line 3	Line 4	Line 5	DNA µg/well
NotchΔE	Notch-ICD	APP-FL	APP-ICD	CLN3	0.0125 to 0.1
GFP	GFP	GFP	GFP	GFP	0.1125
UAS	UAS	UAS	UAS	UAS	0.0125

The reporter gene expression was assessed with the Bright-Glo™ luciferase system. The Bright-Glo™ reagent and OptiMEM were warmed to room temperature. The GFP fluorescence was measured with the Victor^3 light luminescence counter (PerkinElmer). The media was removed from wells and 25µl fresh OptiMEM and 25µl Bright-Glo™ reagent were added to each well of the 96 well plates. After 5 minutes incubation with slight shaking, the liquid was transferred to a white measuring plate and the luminosity was measured with the Victor^3 light luminescence counter. The luminosity was normalized to the measured GFP intensity for each well.

4.5 Biochemistry

4.5.1 Lysosomal enzymatic activity measurement from cell lysates and medium

In order to measure the β-hexosaminidase A (β-Hex A) and Arylsulfatase A (ARSA) enzymatic activity from cell lysates and β-hexosaminidase A enzymatic activity from the cell medium, HeLa wild type, CLN3 and Pen2 knockout cells were seeded at $4x10^5$ per well on a 6 well plate in DMEM + 10%FCS + 1%PS medium and incubated overnight at 37°C. For one readout cell lines were cultured in 3 wells of a 6 well plate. For the measurement of β-hexosaminidase A and Arylsulfatase A activity, cell lysates were prepared by using a classical lysis buffer. BCA protein assay (Thermo Fisher Scientific) was performed according to manufacturer's protocol and measured the protein concentration at 550nm. From each well, 100µg protein was added in two eppendorf tubes and filled water up to 100µl. For the β-hexosaminidase A from each well 100µl cell medium was added in two eppendorf tubes. For control experiments, 100µl water was added in two eppendorf tubes for each cell line. To cell lysates and medium 100µl β-hexosaminidase A substrate was added. The incubation time for β-hexosaminidase A was 30 minutes at 37°C and for Arylsulfatase A was 24 hours at 37°C. The reaction was stopped by adding 800µl stop buffer. The β-hexosaminidase A enzymatic activity was measured by taking the absorbance by using a spectrophotometer (Amersham Biosciences) at 405nm and for Arylsulfatase A at 515nm.

4.5.2 Inhibition and induction of autophagy pathway

4.5.2.1 Inhibition of the autophagy pathway

In order to inhibit autophagy, HeLa wild type, CLN3 and Pen2 knockout cells were seeded at $4x10^5$ per well on a 6 well plate in DMEM + 10% FCS + 1% PS medium and incubated overnight at 37°C. The following day, cells were washed and treated with NH_4Cl (Sigma) (10mM/ml) alone and together with the protease inhibitors E-64d (Sigma) + Pepstatin A (Applichem) (each 10µg/ml) in DMEM medium without FCS for 6 hours. In parallel control experiments, cells were cultured in DMEM + 10%FCS + 1% PS medium without any inhibitor treatment.

4.5.2.2 Induction of the mTor-dependent and mTor-independent autophagy pathway

In order to induce mTor-dependent and mTor-independent autophagy, HeLa wild type, CLN3 and Pen2 knockout cells were cultured at $4x10^5$ per well on a 6 well plate in DMEM + 10% FCS + 1% PS medium and incubated overnight at 37°C. The following day, cells were washed 2x with 1xPBS. To induce the mTor-dependent autophagy cells were treated with Earle's Balanced Salt Solution (EBSS) medium (Life Technologies) alone and together with rapamycin (Selleckchem) (2µM/ml) and Torin1 (Selleckchem) (2µM/ml) for 8 hours at 37°C. To induce the mTor-independent autophagy cells were treated with trehalose (Sigma) (100mM/ml) in DMEM + FCS medium for 24 hours at 37°C. In parallel control experiments, cells were cultured in DMEM + 10%FCS + 1% PS medium without treatment.

4.5.3 Immunoblot

The separation of proteins according to molecular weight was conducted by sodium dodecyl sulfate-polyacrylamide gel electrophoresis (SDS-PAGE). Discontinuous 10 or 12 % SDS-gels were prepared with a polymerization time of 30 minutes for each separating and stacking gel. The separating gel part was overlaid with isopropanol after casting to create a clean edge. After polymerization, the isopropanol was discarded and the stacking gel was casted around a comb for the creation of pockets for the samples. The protein samples were loaded into the pockets of the stacking gel and the SDS-PAGE was run in running buffer at 80 V to allow focusing of the proteins above the separating gel. For the following separation in the separating gel 150 V was applied for about 1.5 hours. For molecular weight-comparison of the proteins page ruler pre-stained protein Ladder (Thermo Fisher Scientific) was used.
After the completed separation process on the SDS-PAGE, the proteins from the gel were transferred to a PVDF membrane (Immobilon-P TransferMembran, Millipore) by western blotting. Prior to setting up the western blot the PVDF membrane was activated for 15 seconds in methanol, washed with distilled water for 2 minutes and then equilibrated in precooled blotting buffer for 5 minutes. The composition of the transfer-system was fixed in a sandwich chamber and setup as follows:

1. 1 sponge
2. 2x Whatmann-3MM-paper
3. PVDF membrane
4. SDS-gel
5. 2x Whatmann-3MM -paper
6. 1 sponge

Proteins were transferred onto the PVDF membrane in blotting buffer by the application of electric current at a tension of 100 V for 1.5 hours at 4 °C or at 80 mA overnight. Subsequently, the PVDF-membrane with the transferred proteins was washed in water and treated with methanol for 10 seconds and dried for 15 minutes. Another reactivation with methanol for 5 seconds was followed by washing in water for 2 minutes. The membrane was incubated with ponceau red-solution for 15 minutes to visualize the transferred proteins. After 2 washing steps in PBS-Tween (1x PBS; 0.1 % Tween20) the membrane was incubated with 5 % skimmed milk powder in PBS-Tween to block unspecific binding of antibodies. If necessary, the membrane was dissected into different parts and incubated with the primary antibody in PBS-Tween for either 1 hour at RT or overnight at 4 °C under slight agitation. After 3 washing steps in PBS-Tween, the incubation with the horseradish peroxidase-coupled secondary antibody followed for 1 hour at RT. The membrane was washed 3 times in PBS-Tween and subsequently incubated with ECL-solution (SuperSignalWest Pico, Thermo-scientific) for 1 minute. The detection of the chemiluminescence signal was conducted with the LAS4000Mini system (GE Healthcare).

4.6 Statistics

For quantification and statistical analysis at least four times an experiment was performed. Quantification of immunoblots was done by using the Multi Gauge V3.2 and ImageJ/Fiji software. For autophagic flux analysis, numbers of puncta were counted manually and by using the ImageJ/Fiji software. Quantification of luciferase assay and lysosomal enzymatic activity was done by using the Microsoft Excel. For statistical analysis t-test was performed by using the Microsoft Excel. The results with p-value <0.05 are considered as a statistically significant. The p-value equal or >0.05 fail to reject the null hypothesis.

5 Results

5.1 Co-localization of CLN3 and Pen2

5.1.1 CLN3 and Pen2 co-localize in late endosomes/lysosomes

In order to analyze the co-localization of CLN3 with Pen2, HeLa and COS-7 cells were co-transfected with EGFP-tagged CLN3 and tdTomato-tagged constructs. The following day, cells were fixed with 4% paraformaldehyde (PFA) and analyzed by confocal microscopy. Both proteins co-localized on identical vesicular structures (Figures 10). This result verifies the previous finding by Sandra Oetjen, who showed that both proteins co-localize and are co-transported in late endosomes/lysosomes. In addition, in-situ hybridizations demonstrated that both proteins were expressed on the same tissue (Sandra Oetjen; Ph.D. Thesis).

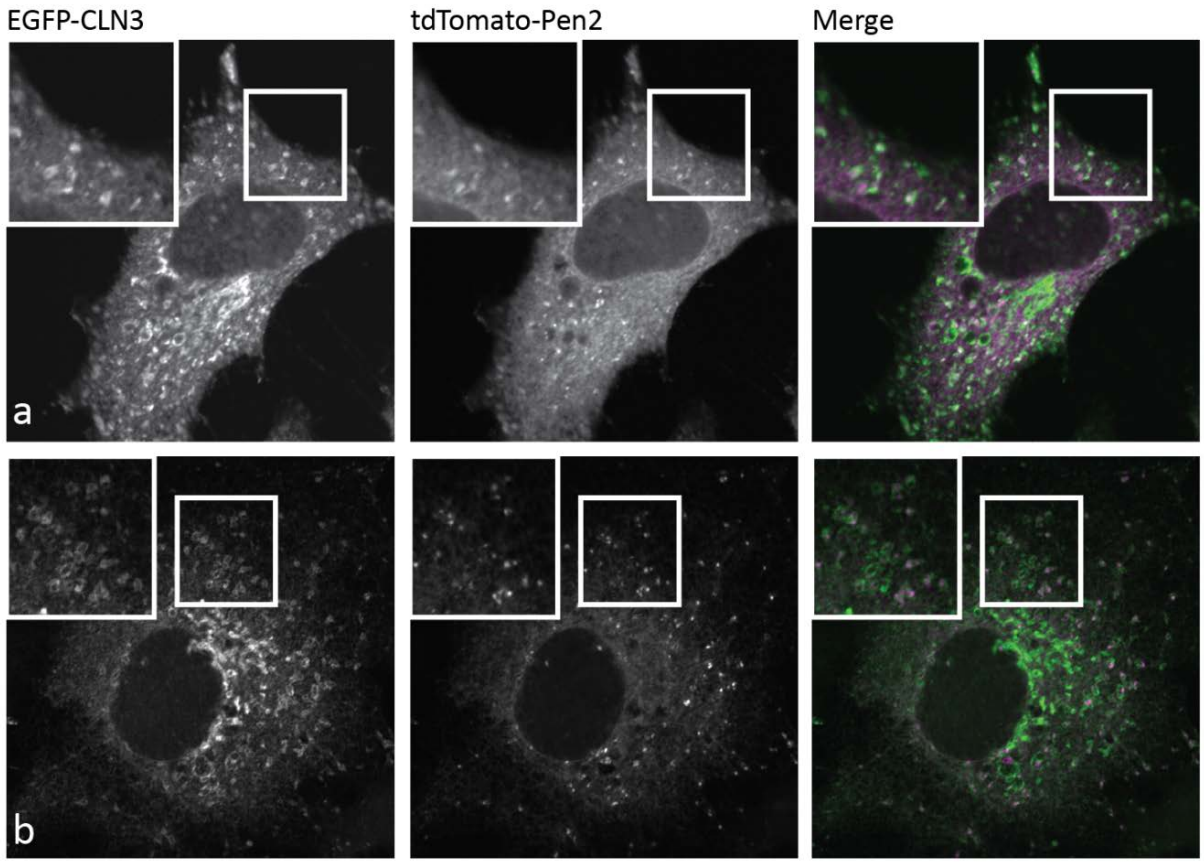

Figure 10: Co-localization of CLN3 with Pen2 to identical vesicular structures. (a) Co-localization of EGFP-tagged CLN3 and tdTomato-tagged Pen2 in HeLa cells. (b) Co-localization of EGFP-tagged CLN3 and tdTomato-tagged Pen2 in COS-7 cells.

5.1.2 Stable expression of Pen2

Stable transfected HeLa EGFP-CLN3 cells were already generated and available (Oetjen et al., 2016). In order to generate stable transfected HeLa cells expressing tagged Pen2, HeLa cells were transfected with constructs encoding HA-tagged Pen2 or tdTomato-tagged Pen2 respectively. For selection, the cells were cultured in 96 well plates with the presence of zeocin for about 2 weeks or until single clones were grown sufficiently. HeLa cells from a well with a single colony were cultured, fixed with 4% PFA and analyzed by immunocytochemistry. Two HeLa cell clones of stably expressing HA-tagged Pen2 and three clones of stably expressing tdTomato-tagged Pen2 were generated (Figure 11).

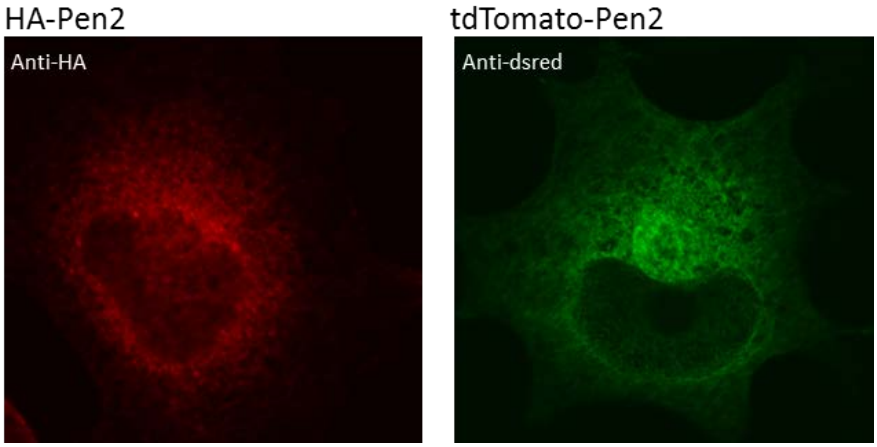

Figure 11: Stable transfected HeLa cells expressing tagged Pen2. Stable transfected HeLa cells expressing HA-tagged Pen2 (red) and stable transfected HeLa cells expressing tdTomato-tagged Pen2 (green) are shown.

5.1.3 Analysis of the CLN3 and Pen2 interaction using a FRET assay

Fluorescence resonance energy transfer (FRET) is a mechanism in which the donor protein (protein A tagged with GFP) is excited at a wavelength 488nm. The donor protein absorbs the light energy and transfers this to an acceptor protein (Protein B tagged with RFP) which emits fluorescence at a wavelength 630nm. The FRET technique can be used to analyze the close co-localization between two proteins. The FRET technique can be applied if the distance between two proteins is less than 10nm. Additionally, the N- or C-terminus of two analyzed transmembrane proteins should face either the cytosolic or luminal sides (Figure 12).

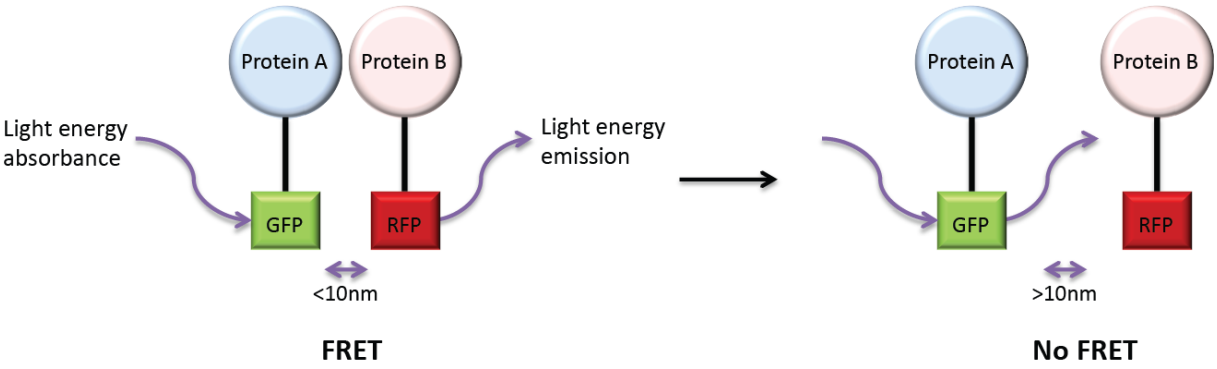

Figure 12: FRET mechanism. In FRET light energy is absorbed by the donor protein (protein A with GFP-tagged) and transferred to the acceptor protein (Protein B with RFP-tagged) which emits fluorescence at a specific wavelength. Acceptor protein losses fluorescence if the distance is more than 10nm between two proteins. Modified after (van der Ploeg et al., 2015).

Pen2 is a two transmembrane protein with the N- and C-terminus facing the lumen or extracellular space. CLN3 is six transmembrane protein with the N- and C-terminus facing the cytosol. Because of such a different topology of these two proteins, the FRET technique was regarded as not useful to analyze the interaction of these two proteins. However, an alternative structure of Pen2 was proposed in late 2015 (Zhang et al., 2015). The data suggest that the N-terminus is facing the cytosol and the C-terminus is facing the lumen or extracellular space. If this suggested topology would be the actual topology of Pen2 the FRET could be applied to analyze the interaction of CLN3 with Pen2.

Therefore HeLa cells were co-transfected with EGFP-tagged Pen2 and mCherry-tagged CLN3. For control experiments, cells were transfected only with EGFP or mCherry constructs and cells were excited by 488nm and 580nm respectively and emitted light was detected at 530nm and 630nm respectively. After transfection FRET analysis was performed by confocal laser scanning microscopy at a wavelength 488-630nm (Figure 13 a, b). For FRET analysis cells were co-transfected with EGFP-tagged Pen2 and mCherry-tagged CLN3 and excited at 488nm. Emitted light was detected only at 530nm and not at 630nm. (Figure 13 c, d). This indicates no close co-localization between CLN3 and Pen2 or that the alternative Pen2 topology suggested by Zhang et al., 2015 is not right.

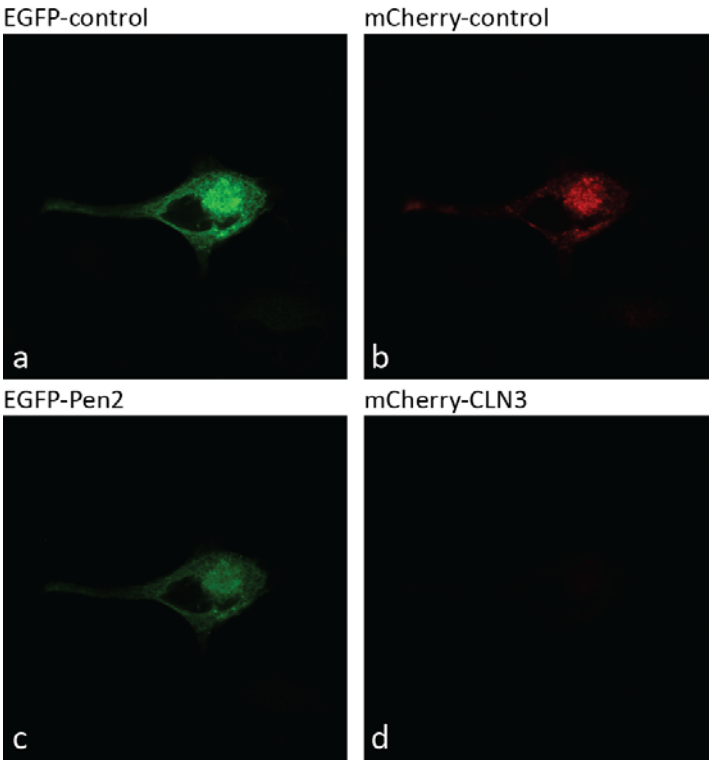

Figure 13: FRET analysis of CLN3 with Pen2 in HeLa cells. For control experiments, HeLa cells were transfected only with EGFP and mCherry constructs. The excitation at 488nm and 580nm emits light at 530nm (a) and 630nm (b) respectively. For FRET analysis Hela cells were co-transfected with EGFP-tagged Pen2 and mCherry-tagged CLN3 constructs. The excitation at 488nm emits light only at 530nm (c) but not at 630nm (d).

5.1.4 Deletion of the lysosomal targeting motifs of CLN3 hampers co-localization with Pen2

Specific primers were designed to mutate the lysosomal targeting motifs of CLN3 in expression constructs by site-directed mutagenesis. Because of the lack of suitable unique restriction sites in the pDEST-LENTI-CMV-EGFP-RFA_hCLN3 vector, pcDNA3.1(+)-Zeocin was used as an intermediate vector. The mutated CLN3 cDNA was finally cloned from the pcDNA3.1(+)-Zeocin into the pDEST-LENTI-CMV-EGFP-RFA_hCLN3 vector. The mutations of the CLN3 lysosomal targeting motifs were confirmed by DNA sequencing (Figure 14).

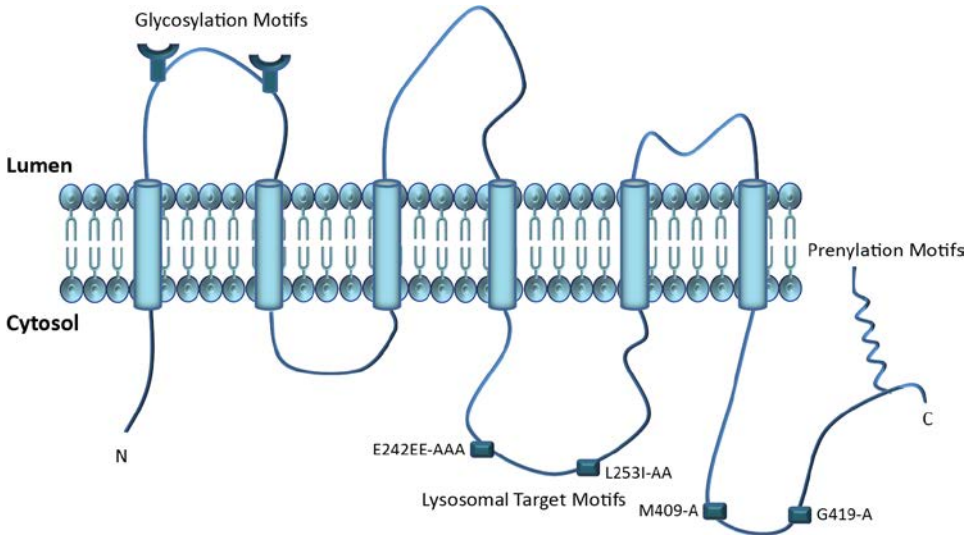

Figure 14: A CLN3 protein with its lysosomal targeting motifs mutations (LTM). The cartoon illustrates the mutation of specific amino acids in lysosomal targeting motifs of CLN3. Modified after (Cotman and Staropoli, 2012).

In order to analyze the localization of wild type CLN3 and CLN3 with its mutated lysosomal targeting motifs (CLN3-LTM) first, two different constructs encoding wild type CLN3 fused to two different protein-tags, HA and GFP were co-expressed in HeLa cells. Both constructs co-localized to identical vesicular structures (Figure 15a). Next, EGFP-tagged CLN3 mutated in its lysosomal targeting motifs (EGFP-CLN3-LTM), was co-expressed with HA-tagged wild type CLN3 in HeLa cells. The wild type CLN3 was localized to vesicles while CLN3-LTM was mainly targeted to the plasmamembrane (Figure 15b).

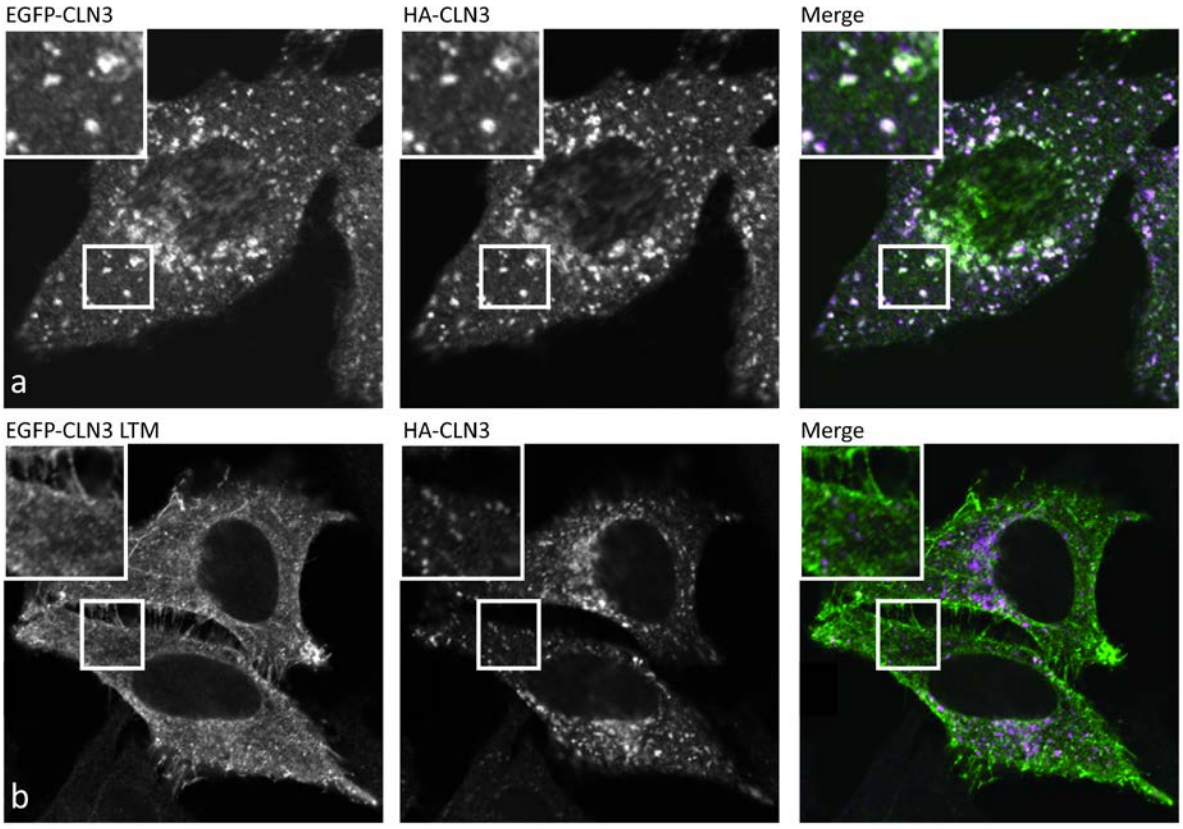

Figure 15: Localization of wild type CLN3 and CLN3 with mutated lysosomal targeting motifs (CLN3-LTM). (a) Localization of wild type CLN3, EGFP-tagged (green) and HA-tagged CLN3 (Magenta) in HeLa cells. (b) Altered localization of CLN3 with mutations in its lysosomal targeting motifs. EGFP-tagged CLN3-LTM was co-expressed with HA-tagged wild type CLN3 in HeLa cells. Whereas wild type CLN3 still localized to vesicular structures, CLN3-LTM was targeted mainly to the plasmamembrane.

To assess co-localization of CLN3 with Pen2, HeLa and COS-7 cells were co-transfected with EGFP-tagged CLN3 and tdTomato-tagged Pen2. Both proteins co-localized on identical vesicular structures (Figures 16a, c). To examine if a change in the subcellular localization of CLN3 would recruit Pen2 to the same subcellular compartment EGFP-tagged CLN3-LTM and tdTomato-tagged Pen2 were co-expressed in HeLa and COS-7 cells. Co-localization of both proteins was not observed anymore. In HeLa cells, CLN3-LTM localized to the plasmamembrane while Pen2 mostly localized to endoplasmic reticulum-like structures and only partially to vesicles (Figure 16b). In COS-7 cells, CLN3-LTM localized to the plasmamembrane while Pen2 was present in vesicular structures (Figure 16d).

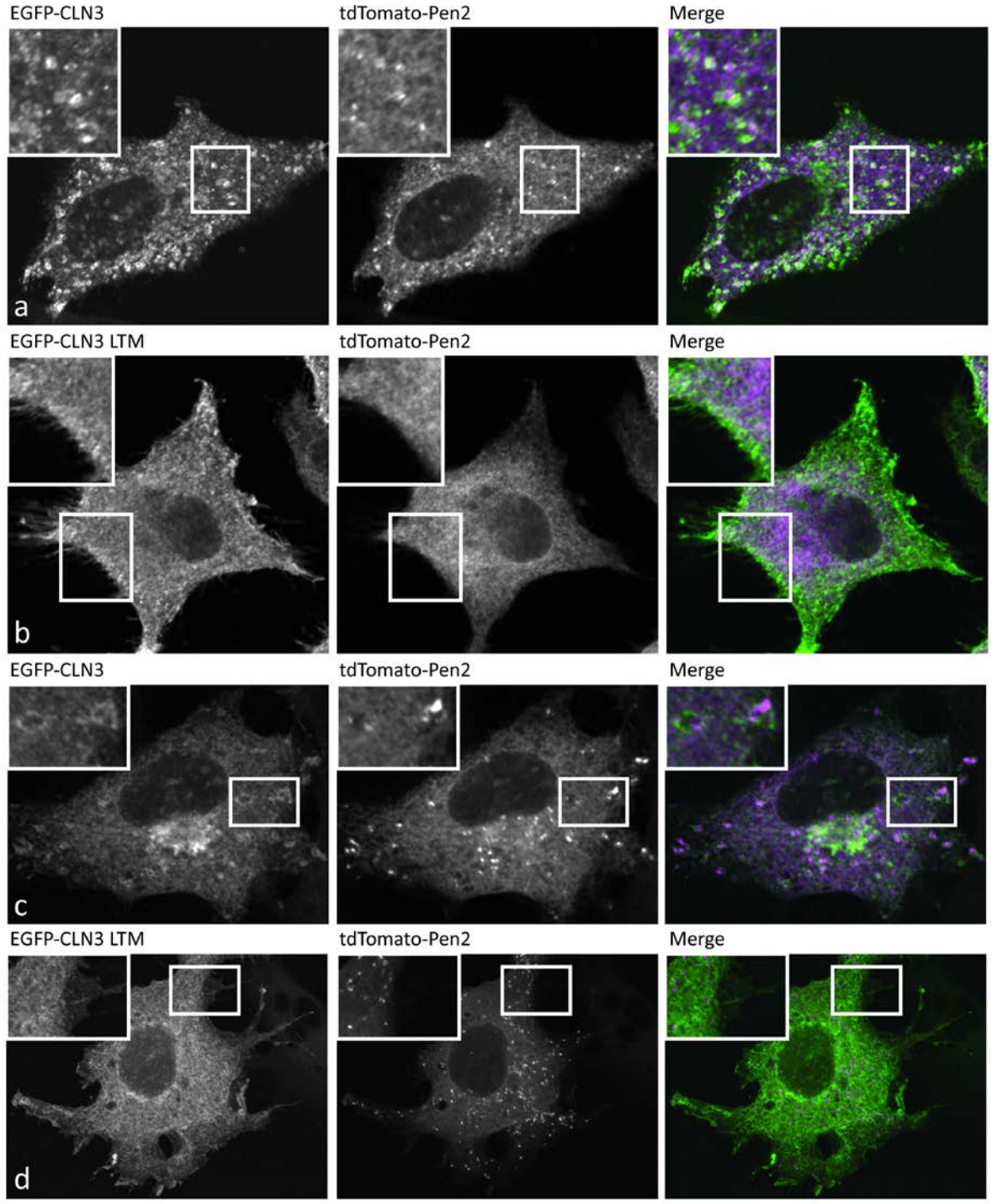

Figure 16: Altered co-localization of wild type CLN3 and CLN3 with mutations in its lysosomal targeting motifs (CLN3-LTM) with Pen2. (a) Co-localization of EGFP-tagged CLN3 and tdTomato-tagged Pen2 in HeLa cells. (b) Altered co-localization of EGFP-tagged CLN3-LTM and tdTomato-tagged Pen2 in HeLa cells. (c) Co-localization of EGFP-tagged CLN3 and tdTomato-tagged Pen2 in COS-7 cells. (d) Altered co-localization of EGFP-tagged CLN3-LTM and tdTomato-tagged Pen2 in COS-7 cells.

5.2 Pen2 knockdown in N2A cells

5.2.1 Pen2 knockdown by shRNAs

To knockdown murine CLN3 and Pen2 different shRNAs were tested before. In order to knockdown the human Pen2, three different shRNAs were designed by using online tools. The single-stranded oligos were annealed and cloned into the pENTR-U6 vector by using specific restriction sites.

To estimate the efficiencies of the three different shRNAs N2A cells were cultured and co-transfected with the vectors psiCHECK2-hPen2 and pENTR-U6 shRNA (1-3). As a negative control, the empty pENTR-U6 vector and scrambled shRNA (pSuper TRONO) were used. To knockdown the Renilla mRNA, Renilla shRNA (pSuperRenilla) was used, which served as a positive control. The psiCHECK2 vector contains two different luciferase genes, Renilla and Firefly luciferase. The human Pen2 gene was cloned in the frame with Renilla luciferase to generate psiCHECK-hPen2. Because Pen2 and Renilla luciferase are transcribed to a fused mRNA the shRNA knockdown of human Pen2 reduces the luciferase activity of Renilla. The Renilla luciferase activity was normalized with Firefly luciferase activity which is transcribed independently. Transfection with one shRNA (shRNA-B1) resulted in reduced luciferase activity as compared to shRNA-S2 and shRNA-S4 after 24 hours of transfection (Figure 17).

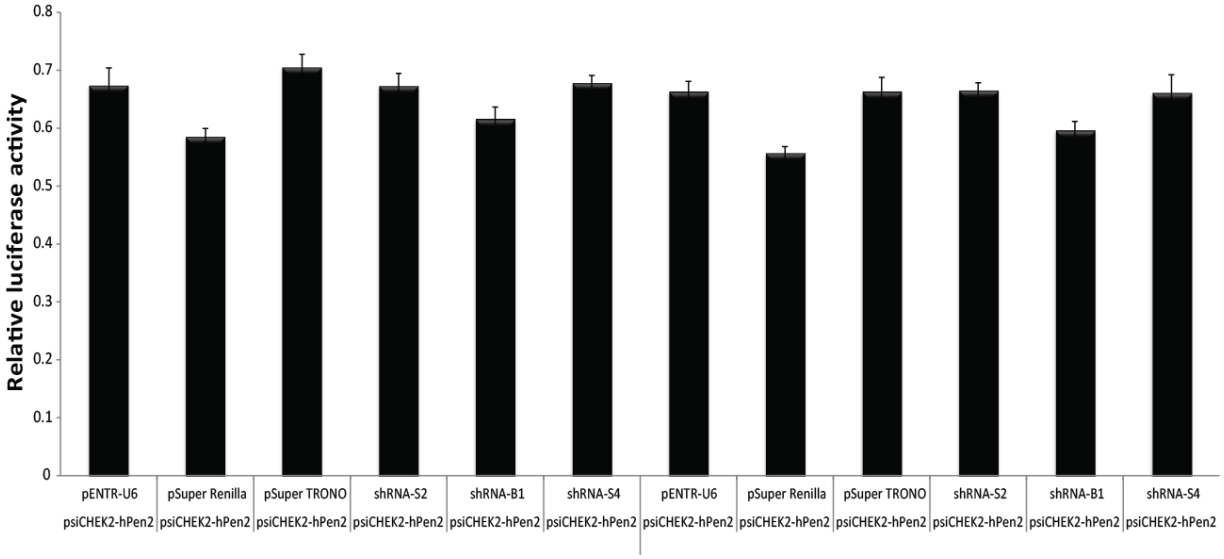

Figure 17: Knockdown effect of shRNAs on human Pen2. One out of three shRNA (shRNA-B1) reduced luciferase activity to a comparable level as the positive control (pSuperRenilla). The negative controls empty U6 vector and scrambled shRNA against Renilla mRNA showed no knockdown effect. The mean value is presented with a standard deviation of 4 independent experiments.

5.3 Generation of CLN3 and Pen2 Knockout HeLa cell lines

5.3.1 The CRISPR/Cas9 system was applied to knockout the CLN3 and Pen2 gene respectively

Knockdown of RNA is one possibility to hamper gene expression. Another possible way is to knockout the genes of interest, here CLN3 and Pen2, e.g through the CRISPR/Cas9 system. On protein level, the amino acid sequence of Pen2 is 96% and of CLN3 is 93.38% identical, while on DNA level, the nucleotide sequence of Pen2 is 91.18% and of CLN3 is 82.76% identical between mouse and human. Moreover, minor differences in the genomic sequences of individuals of one species exist. For specific CRISPR/Cas9 mediated knockout of genes efficient binding of guide RNAs (gRNAs) to the target sequence is required to enable the Cas9 endonuclease to cause a single/double-strand breaks. Therefore, the precise design of gRNAs requires the exact knowledge of genomic CLN3 and Pen2 sequences in the target organism or cells, here HeLa cells. To this end genomic DNA was extracted from HeLa cells, CLN3 and Pen2 genomic sequence were amplified by PCR using specific primers and sequence from genomic HeLa cell DNA were determined by DNA sequencing.

To knockout the Pen2 and the CLN3 gene respectively in HeLa cells four different gRNAs for Pen2 and four different gRNAs for CLN3 were designed by using bioinformatics tools. Corresponding single-stranded oligos were annealed and cloned into the pX330 vector (Cong et al., 2013) by utilizing the unique BbsI site (Figure 18a). A fragment corresponding to the genomic Pen2 and the genomic CLN3 sequence was cloned from HeLa cells and transferred into the pCAG-EGxxFP vector (Mashiko et al., 2013) to check the efficiency of the different gRNAs (Figure 18b). The resulting pCAG-EG-Pen2-FP and pCAG-EG-CLN3-FP plasmid were co-transfected with the pX330 vector which expressed one of the four different gRNAs for Pen2 and one of four different gRNAs for CLN3 into HeLa cells to assess the efficiency of the different gRNAs. The Cas9 endonuclease forms a complex with hybrids of gRNAs specifically bound to DNA and causes double standard breaks. A CLN3 and Pen2 specific gRNA mediates cleavage of the CLN3 and Pen2 gene respectively which is then followed by homologous recombination (HR) or single-strand annealing (SSA). This would reconstitute the EGFP expression cassette of pCAG-EG-Pen2-FP and pCAG-EG-CLN3-FP. The efficiency of gRNAs was analyzed by observing green fluorescence caused by the reconstitution of the split EGFP (Figure 18c).

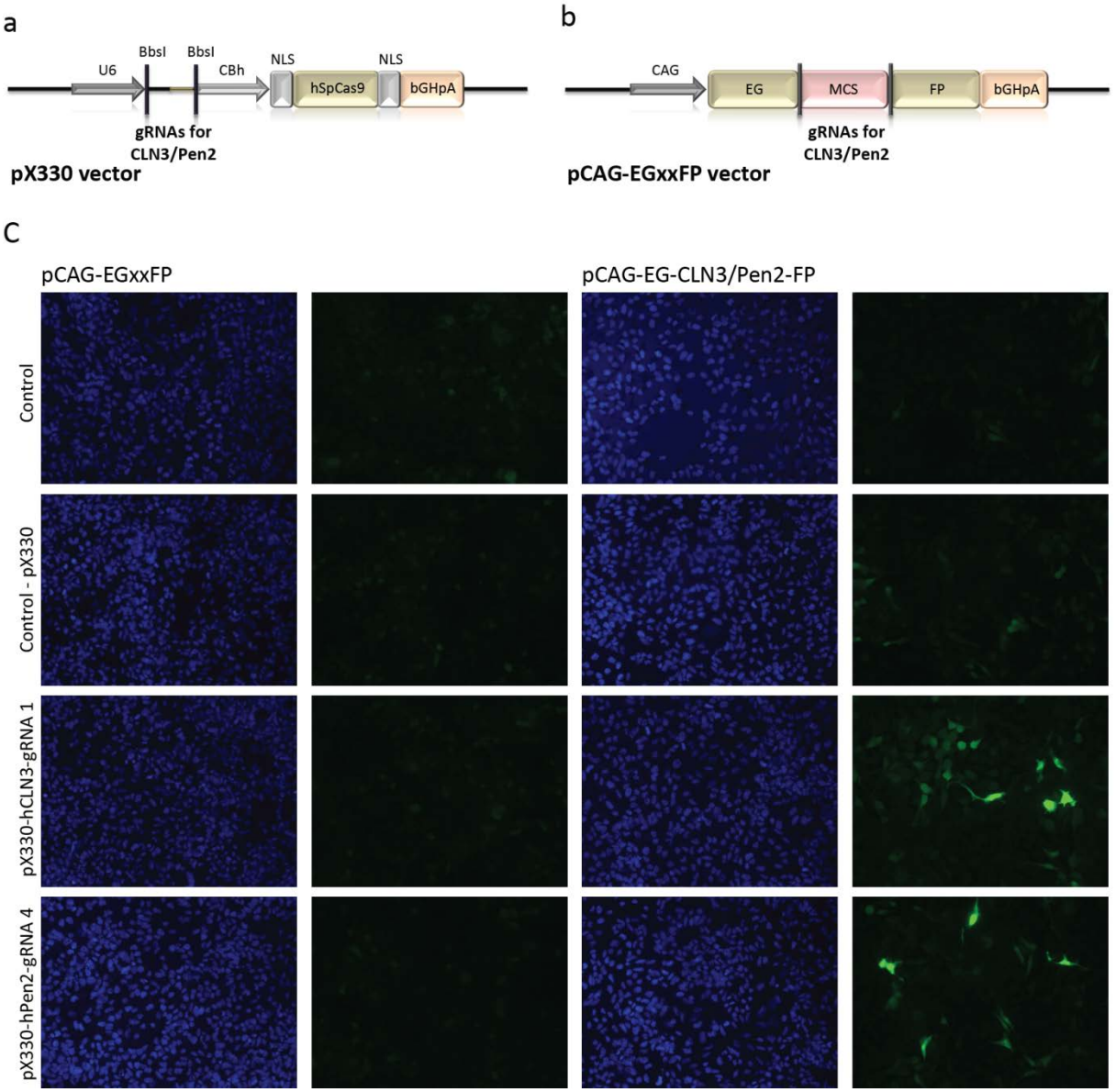

Figure 18: Efficiency test of gRNAs. (a) Four different gRNAs for Pen2 and four different gRNAs for CLN3 were designed and cloned into the pX330 vector. (b) The human CLN3 and Pen2 gene were cloned into the pCAG-EGxxFP vector between the N- and C- terminal part of EGFP by using specific restriction sites. (c) In order to test the efficiency of the different gRNAs, each gRNA cloned into pX330 was co-transfected with pCAG-EG-xx-FP and pCAG-EG-Pen2/CLN3-FP into HeLa cells. In parallel control experiments, HeLa cells were transfected with pCAG-EGxxFP and pCAG-EG-CLN3/Pen2-FP vectors alone and together with the empty pX330 vector. The performed assay is based on the assumption that specific gRNA target the sequence of CLN3 and Pen2, the Cas9 endonuclease forms a complex with hybrids of gRNA specifically bound to DNA, the targeted DNA is cleaved by a Cas9 endonuclease and this causes a double-strand break. Homologous recombination or single-strand annealing reconstitutes the split EGFP and results in green fluorescence as exemplified for Pen2 gRNA4 and CLN3 gRNA 1 (right panel). Blue fluorescence represents the DAPI staining (left panel). CAG, CAG promotor; cBh, cBh promotor; gRNA, guide RNA; MCS, multiple cloning sites; NLS, nuclear localization signal; U6, U6 promoter.

In order to knockout CLN3 and Pen2, HeLa cells were cultured and co-transfected with pX330-CLN3 gRNA (1-4) and pX330-Pen2 gRNA (1-4) respectively together with pcDNA3.1-zeocin(+) plasmids. For selection, cells were trypsinized 24 hours after transfection and cultured in medium supplemented with zeocin for 5 days. The cells were split and cultured in normal medium in 96 well plates for two weeks or until single colonies appeared. These were analyzed by PCR of genomic DNA and subsequent sequencing of products. The sequencing result showed that one out of four gRNAs for Pen2 (Pen2 gRNA 4) and one out of four gRNAs for CLN3 (CLN3 gRNA 1) were most efficient. In the case of Pen2, an insertion of one adenosine 22 base pairs after the start codon was found in three clones (Figure 19a). In the case of CLN3, three mutant clones were found. In one clone a deletion of 7 base pairs from position 35 to 41 and in two clones an identical deletion of 1 base pair at position 41 after the start codon was found (Figure 19b). In these clones, the mutation appeared homozygous because only one trace was present in the sequencing result. In other clones, an additional trace was present after the mutation indicating that the cells were heterozygous or mutated and mixed with wild type cells.

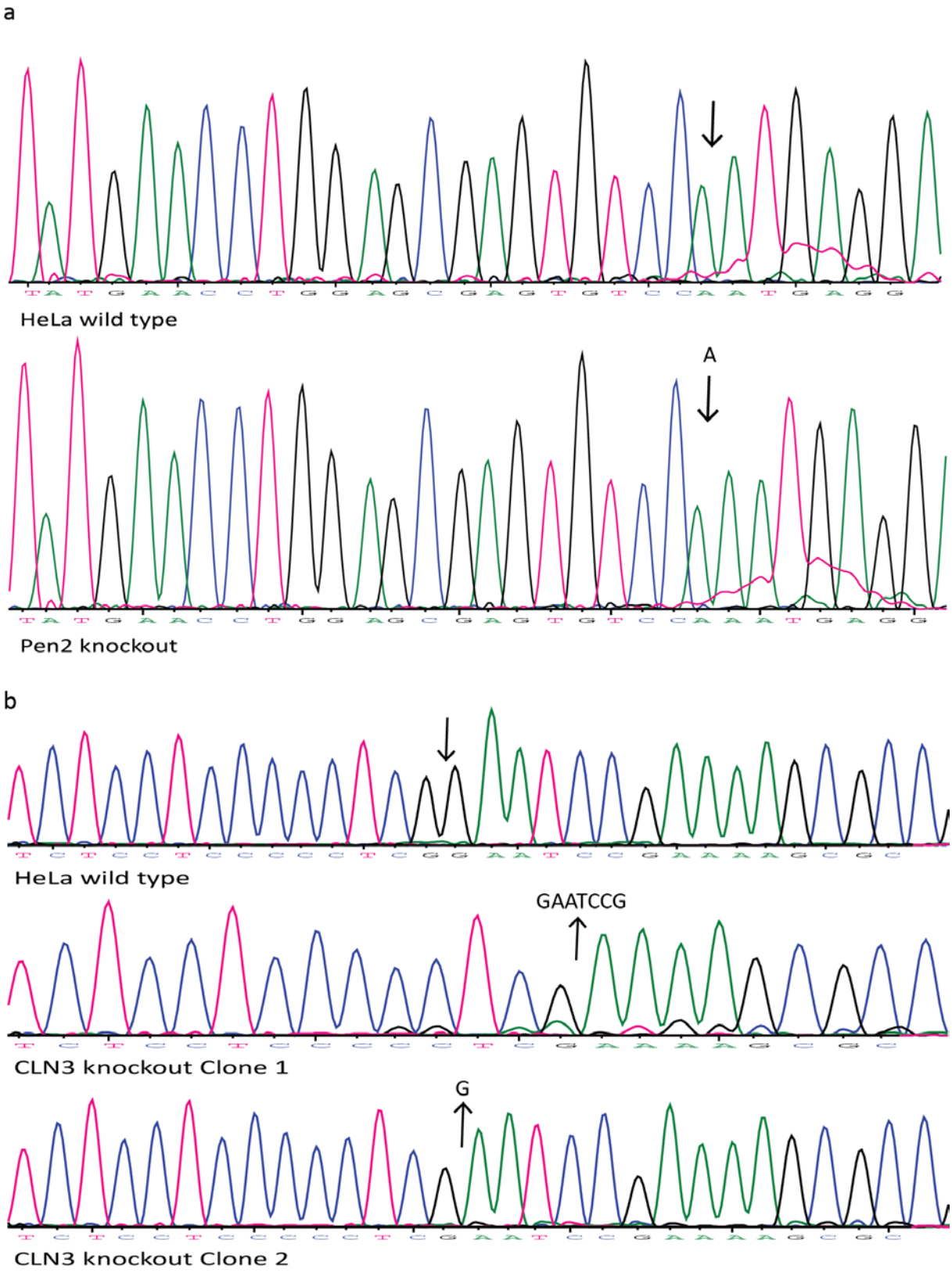

Figure 19: Sequencing results of HeLa wild type, CLN3 and Pen2 knockout cell lines. Genomic DNA of cells was amplified by PCR and sequenced. (a) Sequencing shows an adenosine insertion in the Pen2 gene. (b) Sequencing shows two different deletion events in the CLN3 gene observed in two different cell clones. Arrows indicate an Indel mutation.

To verify mutations in CLN3 and Pen2 knockout HeLa cell clones, reverse transcriptase (RT) PCR was performed after single cell clones have been expanded. Wild type HeLa, three independent CLN3 and Pen2 knockout cell clones were analyzed. Total RNA was extracted and RT PCR using CLN3 and Pen2 specific primers was performed. The sequencing results validated the insertion mutation in Pen2 and deletion mutations in CLN3 knockout cell clones (Figure 19). In one CLN3 knockout cell clone deletion of 7 base pairs from position 35 to 41 after the start codon changed the amino acid at position 13 from Aspartic acid to Arginine ($D^{13}R$) which leads to a premature stop codon at position 52. In two CLN3 knockout cell clones, similar deletion of 1 base pair at position 41 after start codon changed the amino acid at position 15 from Glutamic acid to Arginine ($E^{15}R$) which leads to a premature stop codon at position 54 (Figure 20a). In three Pen2 knockout cell clones, the insertion of an Adenine at 22 base pairs after the start codon changed the amino acid at position 8 from Asparagine to Lysine ($N^{8}K$) and leads to a premature stop codon at position 9 (Figure 20b). In conclusion, these mutations result in the expression of truncated proteins which are likely to be unstable and to lack of function.

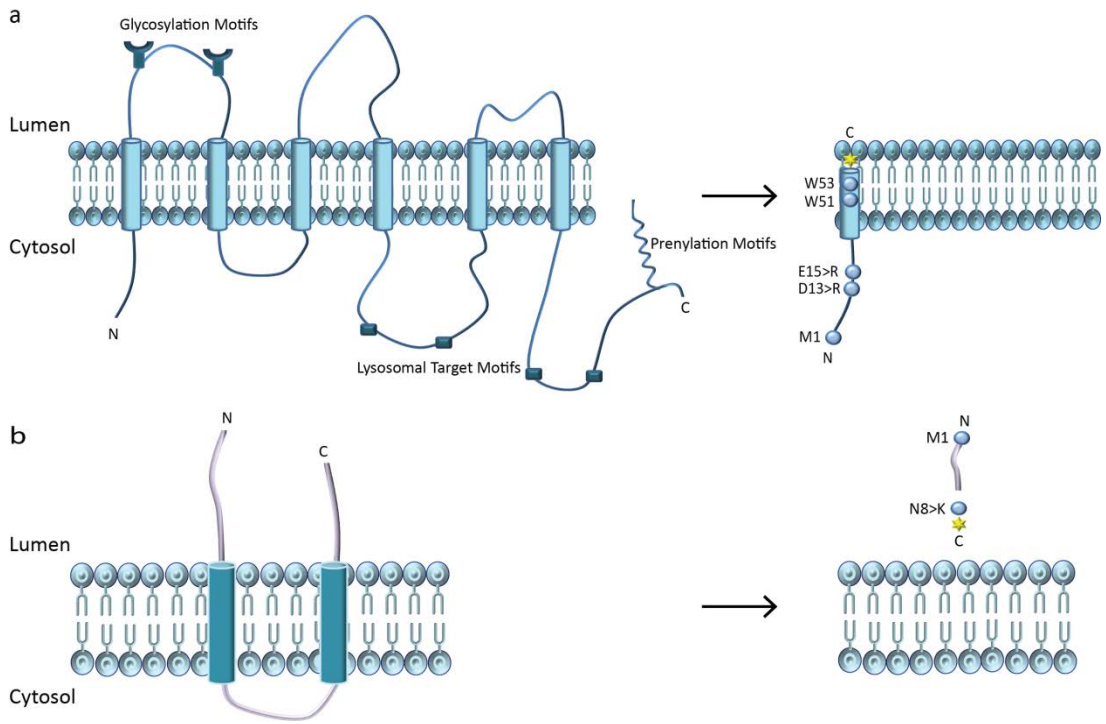

Figure 20: Mutations in CLN3 and Pen2 lead to premature stop codons. (a) The CLN3 protein consists of 6 transmembrane domains in which N- and C-terminal ends are facing the cytosolic site. Mutations in CLN3 cause a premature stop codon after 51 in one clone and 53 amino acid in two clones respectively as a result, a truncated protein is formed. (b) The Pen2 protein consists of 2 transmembrane domains in which N- and C-terminal ends are facing the luminal site. The mutation in Pen2 causes a premature stop codon after 8 amino acids as a result, a truncated protein is formed.

5.4 Interaction of CLN3 with the γ-secretase complex

5.4.1 Assessing γ-secretase activity through luciferase assay

Pen2 has been identified as an interaction partner of CLN3. Pen2 is an integral part of γ-secretase complex and plays a vital role in γ-secretase complex stability and export from the endoplasmic reticulum. Many type-1 transmembrane proteins such as amyloid precursor protein (APP) and Notch are cleaved by two proteases α- or β-secretase and subsequently by γ-secretase (Pajak et al., 2016; Steiner and Haass, 2000). APP and Notch are first cleaved by α- or β-secretase in their extracellular moiety and the remaining transmembrane stub is processed by the γ-secretase (Figure 8 and 9).

In order to address the question if CLN3 is involved in the γ-secretase complex activity and to validate the Pen2 knockout, a γ-secretase activity luciferase assay was performed. For this assay, APP full length (APP-FL) and modified NotchΔE constructs were used. The APP-FL is first cleaved by α- or β-secretase and subsequently by γ-secretase. The modified NotchΔE is directly cleaved by the γ-secretase and this cleavage is independent of a preceding α- or β-secretase processing. As a positive control, the APP intracellular domain (APP-ICD) and the Notch intracellular domain (Notch-ICD) were used, which are expressed in the cytosol. Because the lack of cleavage site for secretase, CLN3 was used as a negative control. All these constructs contained a nuclear localization sequence (NLS), a Gal-4 promoter binding domain and VP16 transactivation domain (TAD) at the C-terminus (Figure 21). GFP was used as a transfection control. After γ-secretase cleavage, the C-terminus of APP or Notch is released into the cytoplasm and the NLS directs the fragment into the nucleus. Gal-4 together with VP16 drives the transcription of the luciferase gene which is used as a reporter.

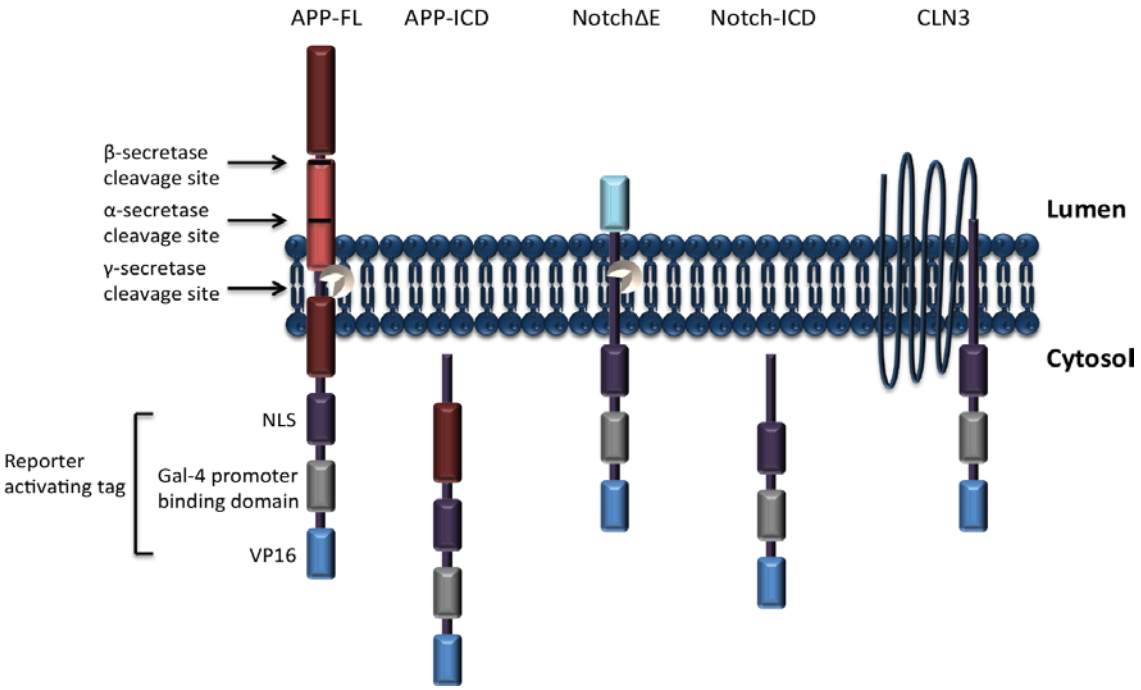

Figure 21: Constructs used for the γ-secretase luciferase assay. All constructs for γ-secretase luciferase assay contain nuclear localization sequence (NLS), a Gal-4 promoter binding domain and VP16 transcriptional activation domain at the C-terminus. After γ-secretase cleavage, APP-FL and NotchΔE release their C-termini into the cytosol. APP-ICD and Notch-ICD were used as positive controls which are expressed in the cytosol. CLN3 was used as a negative control because of the lack of a γ-secretase cleavage site.

HeLa wild type and Pen2 knockout cells were cultured in a 96 well plate and transfected with the constructs presented in figure 21 together with a reporter construct in which the upstream activator sequence (UAS) of Gal-4 drives luciferase expression and with GFP for normalization. After 24 hours of transfection, the luciferase activity was measured and normalized to GFP. In the CLN3 negative control lower luciferase activity was detected, while in APP-ICD and Notch-ICD positive controls highest luciferase activity was observed in HeLa and Pen2 knockout cells. In cleavable NotchΔE transfected cells, the luciferase activity was slightly increased while in cleavable APP-FL the luciferase activity was almost similar to negative control in both cell lines (Figure 22).

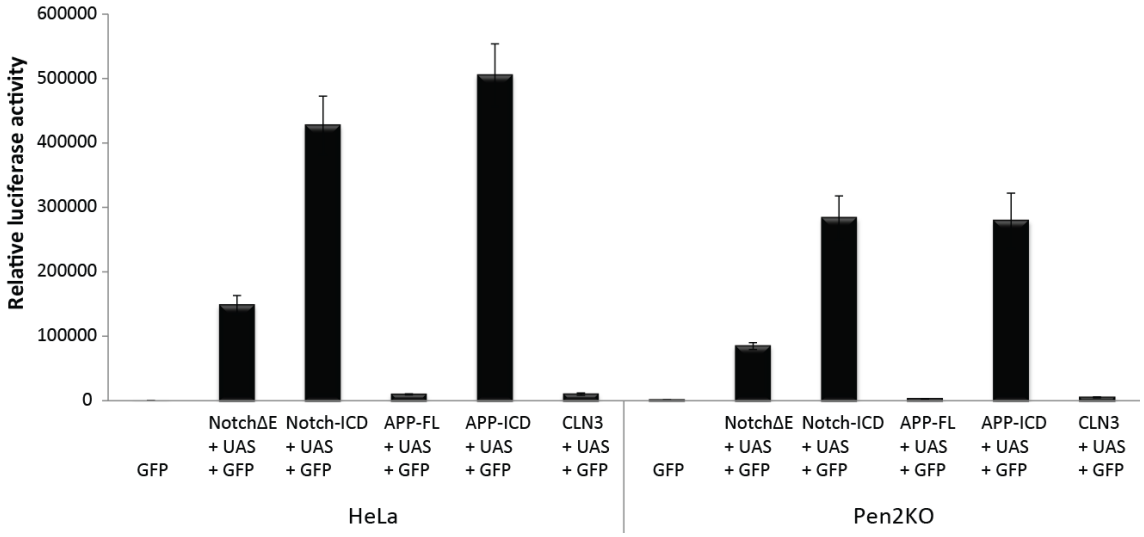

Figure 22: γ-secretase processing measured by luciferase activity. In order to measure the γ-secretase activity in the luciferase assay, HeLa wild type and Pen2 knockout cells were transfected with developed constructs together with reporter UAS and GFP. The luciferase activity was measured after 24 hours of transfection and normalized with GFP. The luciferase activity was higher in positive control and lower in negative control in both cell lines. In cleavable NotchΔE transfected cells, the luciferase activity was induced while in cleavable APP-FL the luciferase activity was almost similar to negative control in HeLa wild type and Pen2 knockout cells. The mean value is presented with a standard deviation of 3 independent experiments.

The results of the luciferase activity assay were not conclusive. Surprisingly, the γ-secretase activity was not altered in a Pen2 knockout as compared to HeLa wild type cells. In both cell lines, no significant difference of γ-secretase activity was observed. This suggests that the Pen2 knockout cells still express Pen2, which is regarded as indispensable for γ-secretase activity or that the assay is not suitable due to a strong background luciferase activity.

5.4.2 Assessing γ-secretase activity through immunoblotting

An alternative assay to analyze the γ-secretase activity is detecting cleavage products of a substrate in immunoblots. The β- and γ-secretase cleave substrates at different sites and this results in fragments of different size. These can be detected in immunoblots. To address the question if CLN3 is involved in a γ-secretase complex activity and to validate the Pen2 knockout cells, NotchΔE and amyloid precursor protein (APP) constructs were used to transfect the cells. The C-terminal EGFP-tagged full-length APP is a type-I transmembrane protein which is first cleaved by α- or β-secretase. Subsequently, γ-secretase cleavage releases the C-terminal APP-ICD into the cytosol. The modified C-terminally HA-tagged NotchΔE serves as a substrate which is directly cleaved by the γ-secretase and this cleavage is independent of initial α- or β-secretase processing. After cleavage of NotchΔE by γ-secretase, the C-terminal Notch-ICD is released into the cytosol. For control experiments, the

C-terminal HA-tagged Notch intracellular domain (Notch-ICD) and the C-terminal EGFP-tagged APP intracellular domain (APP-ICD) were used (Figure 23).

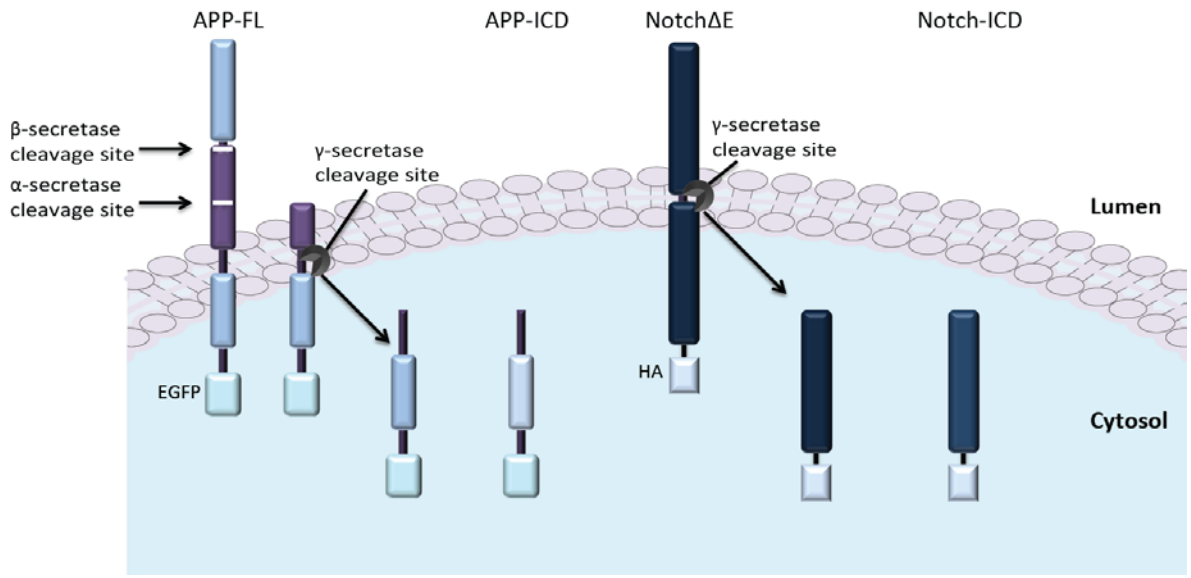

Figure 23: APP and Notch constructs generated for analysis of γ-secretase activity through immunoblotting. Full-length amyloid precursor protein (APP) with a C-terminal EGFP-tag is first cleaved by the α- or β-secretase and subsequently processed by γ-secretase. This leads to the release of the APP intracellular domain (APP-ICD) into the cytosol. NotchΔE with a C- terminal HA-tag serves directly as a substrate for γ-secretase. After cleavage, Notch intracellular domain (Notch-ICD) is released into the cytosol. APP-ICD and Notch-ICD were used as controls to estimate sizes of proteins.

HeLa wild type, CLN3 and Pen2 knockout cells were cultured and transfected with the generated constructs. The cell lysates were analyzed by immunoblotting. In cell lysates of cells transfected with NotchΔE, the upper band represents the full-length protein while the lower band represents the cleaved NotchΔE-ICD which is equal to the size of the control construct Notch-ICD. NotchΔE cleavage was observed in HeLa wild type and in CLN3 knockout cells, but not in Pen2 knockout cells (Figure 24). This strongly suggests γ-secretase inactivity in Pen2 knockout cells. In cell lysates of cells transfected with APP the upper band corresponds to the full-length protein; the middle band corresponds to APP cleaved by α- or β-secretase and lower band represents APP subsequently cleaved by γ-secretase which is equal to the size of APP-ICD. Again γ-secretase cleavage was observed in HeLa wild type and in CLN3 knockout cells, but, the lower band was absent in Pen2 knockout cells (Figure 24). These results strongly suggest hampered γ-secretase activity in Pen2 knockout cells whereas, γ-secretase activity was observed in HeLa wild type and CLN3 knockout cells.

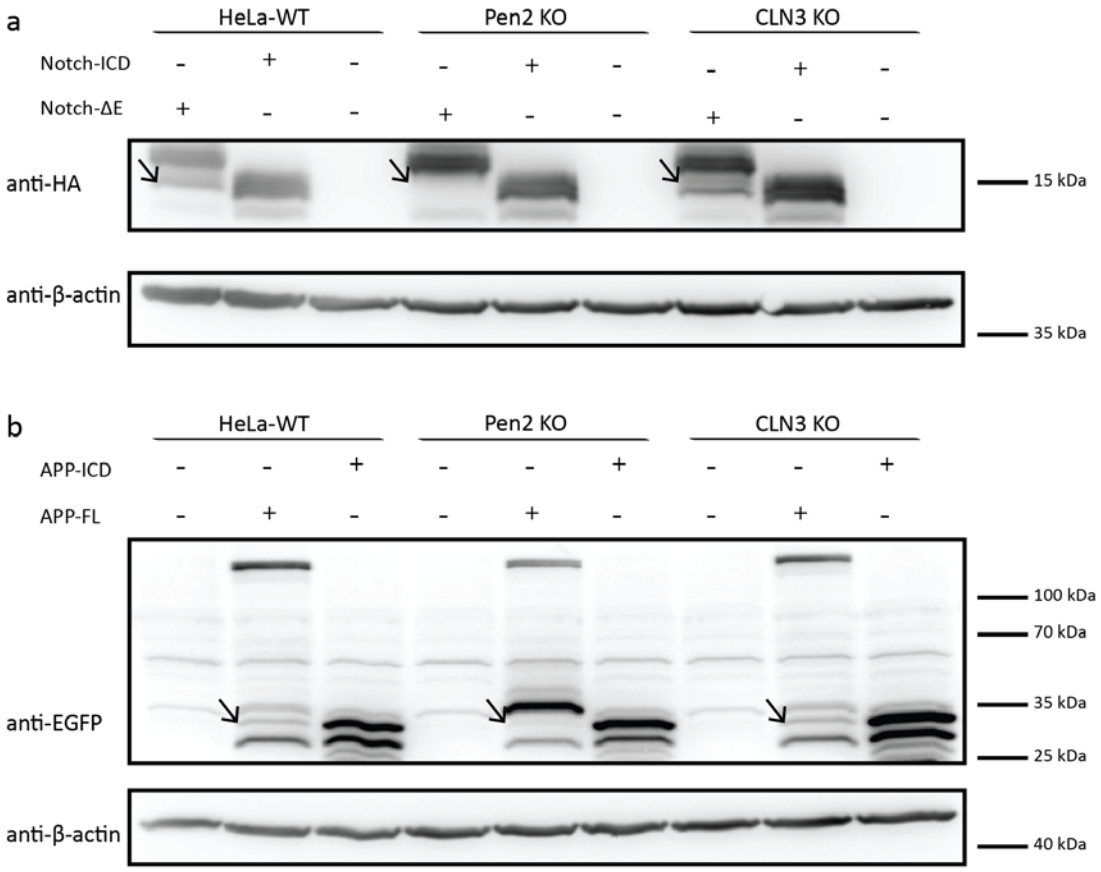

Figure 24: γ-secretase is hampered in Pen2 knockout cells and unchanged in the CLN3 knockout cells. HeLa wild type, CLN3 and Pen2 knockout cells were transfected with C-terminally HA-tagged full-length NotchΔE and Notch-ICD constructs (a) or with C-terminally EGFP-tagged full-length APP and APP-ICD (b). Cell lysates were analyzed by immunoblotting using anti HA (a) and anti EGFP (b) antibodies. Arrows indicate the Notch-ICD band of cleaved NotchΔE (a) and the APP-ICD band of the cleaved APP by γ-secretase (b) in HeLa wild type and CLN3 knockout cells and its absence in Pen2 knockout cells. This indicates the hampered γ-secretase activity in Pen2 knockout cells as compared to HeLa wild type and CLN3 knockout cells. As controls untransfected cells and to compare the fragment size, APP-ICD and Notch-ICD were used. β-actin was used as a loading control.

In order to rescue the γ-secretase activity in Pen2 knockout cells, HeLa wild type and Pen2 knockout cells were transfected with NotchΔE-HA and APP-FL-EGFP constructs. As a control Notch-ICD and APP-ICD were used. Pen2 knockout cells were co-transfected with NotchΔE-HA and EGFP-Pen2 to analyze the NotchΔE cleavage. To analyze the APP cleavage Pen2 knockout cells were co-transfected with APP-FL-EGFP and HA-Pen2. Cell lysates were prepared and analyzed by immunoblotting. The Notch-ICD and APP-ICD band of cleaved NotchΔE and APP by γ-secretase was observed in HeLa wild type while the lower band was absent in Pen2 knockout cells. The co-expression of EGFP-Pen2 or HA-Pen2 in Pen2 knockout cells promoted the appearance of the lower band. In cells transfected with APP-FL-EGFP co-transfection of HA-Pen2 caused a disappearance of a 35 kDa band presumably corresponding to the fragment generated by α- or β-secretase cleavage (Figure 25).

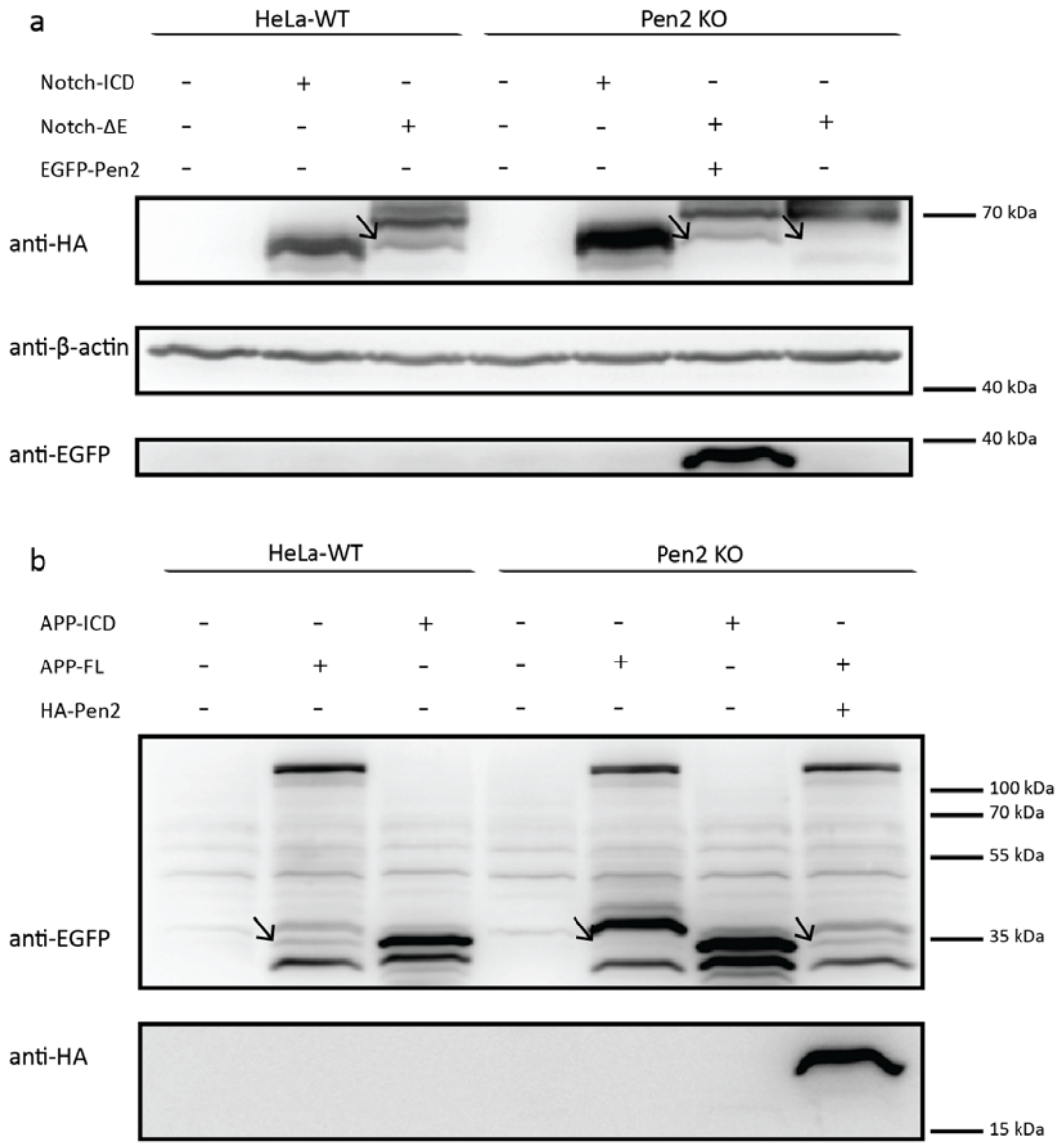

Figure 25: Rescue of γ-secretase activity in Pen2 knockout cells. To rescue the γ-secretase activity, HeLa wild type and Pen2 knockout cells were either mock transfected, transfected with NotchΔE-HA or with Notch-ICD or with co-transfected with NotchΔE-HA and EGFP-Pen2 (a). Alternatively, the cells were mock transfected, transfected with APP-FL-EGFP or with APP-ICD-EGFP or with co-transfected with APP-FL-EGFP and HA-Pen2 (b). Cell lysates were analyzed by immunoblotting using anti HA and anti EGFP antibodies. (a) Arrows indicate the Notch-ICD band of cleaved NotchΔE and (b) APP-ICD band of the cleaved APP by γ-secretase which was observed in HeLa wild type and in rescued Pen2 knockout cells. The lower band was absent in Pen2 knockout cells. β-actin was used as a loading control.

These results indicate that Pen2 is indispensable for γ-secretase activity and CLN3 is not involved in the γ-secretase activity additionally, the specificity of the Pen2 knockout was verified by these experiments.

5.5 Analysis of lysosomal enzymatic activity in CLN3 and Pen2 knockout cells

5.5.1 β-hexosaminidase A (β-Hex A) enzymatic activity

CLN3 and Pen2 co-localize in the late endosomal/lysosomal compartments. To test the hypothesis if both proteins are involved in the normal functioning of the late endosomes/lysosomes, different lysosomal enzymatic activities were measured. First β-hexosaminidase A (β-Hex A) enzymatic activity was measured. HEXA and HEXB genes are involved in the synthesis of alpha and beta subunit of β-hexosaminidase A. These two subunits join together and make a functional enzyme. GM2 activator protein (GM2A) acts as a co-factor to stabilize the enzyme (Mahuran, 1999). In lysosomes β-hexosaminidase A hydrolyses the fatty substance GM2 ganglioside by targeting the N-acetyl group. In humans, a deficiency of β-hexosaminidase A causes the accumulation of GM2 ganglioside which leads to lysosomal storage diseases such as Tay-Sachs disease. HeLa wild type, CLN3 and Pen2 knockout cells were cultured and cell lysates were prepared. β-hexosaminidase A substrate was added to cell lysates for 30 minutes at 37°C. Stop buffer was added to terminate the reaction and enzymatic activity was measured by spectrophotometry at 405nm. Quantification of the results indicated that β-hexosaminidase A enzymatic activity was significantly reduced in CLN3 and Pen2 knockout cells as compared to HeLa wild type (Figure 26a).

The reduction of β-hexosaminidase A enzymatic activity in lysosomes leads to the question if the knockout of CLN3 and Pen2 proteins could cause mislocalization of β-hexosaminidase A enzyme to the cell surface and its release into the medium. To test this hypothesis HeLa wild type, CLN3 and Pen2 knockout cells were cultured. β-hexosaminidase A substrate was added to the medium for 90 minutes at 37°C. Stop buffer was added to terminate the reaction and enzymatic activity was measured by spectrophotometry at 405nm. Quantification of the results indicated that β-hexosaminidase A enzymatic activity was slightly increased in the medium of CLN3 and Pen2 knockout cells as compared to HeLa wild type (Figure 26b).

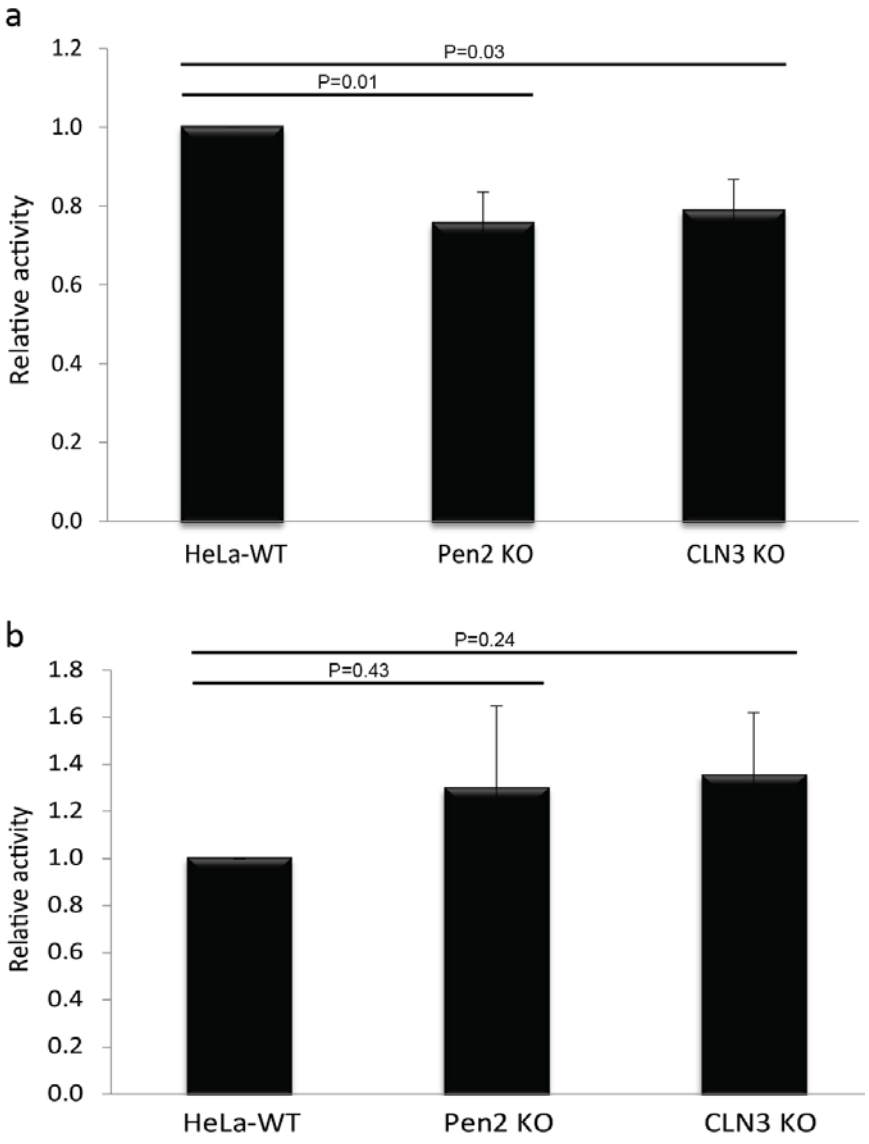

Figure 26: β-hexosaminidase A (β-Hex A) enzymatic activity. In order to measure the β-hexosaminidase A enzymatic activity HeLa wild type, CLN3 and Pen2 knockout cells were cultured. (a) β-hexosaminidase A substrate was added to the cell lysates and (b) to the cell medium. The enzymatic activity was measured by spectrophotometry at 405nm. The enzymatic activity was significantly reduced in cell lysates and slightly increased in cell medium of a CLN3 and Pen2 knockout as compared to HeLa wild type. Quantification of the relative activity of the enzyme is represented as the mean ± SEM of 9 and 7 independent experiments respectively.

5.5.2 Arylsulfatase A (ARSA) enzymatic activity

Next arylsulfatase A (ARSA) enzymatic activity was measured which is another lysosomal enzyme. The ARSA gene is responsible for the synthesis of arylsulfatase A which breaks down the sulfatides (glycolipid which comprises a sulfate group) in lysosomes. Deficiency of this enzyme leads to lysosomal storage diseases such as metachromatic leukodystrophy.

HeLa wild type, CLN3 and Pen2 knockout cells were cultured and cell lysates were prepared. Arylsulfatase A substrate was added to cell lysates for 24 hours at 37°C. Stop buffer was added to terminate the reaction and enzymatic activity was measured by spectrophotometry 515nm. Quantification of the results indicated that Arylsulfatase A enzymatic activity was slightly increased in CLN3 and Pen2 knockout cells as compared to HeLa wild type (Figure 27).

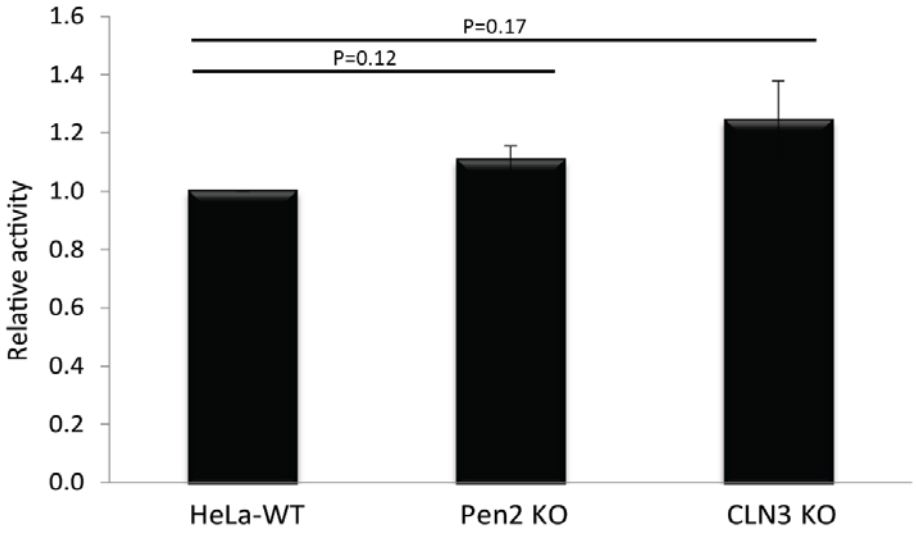

Figure 27: Arylsulfatase A (ARSA) enzymatic activity. In order to measure the Arylsulfatase A (ARSA) enzymatic activity HeLa wild type, CLN3 and Pen2 knockout cells were cultured. Arylsulfatase A substrate was added to cell lysates. The enzymatic activity was measured by spectrophotometry at 515nm. The enzymatic activity was slightly increased in CLN3 and Pen2 knockout as compared to HeLa wild type. Quantification of the relative activity of the enzyme is represented as the mean ± SEM of 4 independent experiments.

These results indicate that knockout of CLN3 and Pen2 proteins cause misbalance in lysosomes which, altered lysosomal enzymatic activities.

5.6 Analysis of the autophagy pathway in CLN3 and Pen2 knockout cells

5.6.1 Induction and inhibition of the autophagy pathway

One important lysosomal function is in the autophagy pathway. In this pathway, autolysosomes are formed by the fusion of autophagosomes with lysosomes which, are involved in degradation of cytoplasmic materials like old mitochondria. Autophagy inducers and inhibitors treatment interrupt the autophagy pathway at different points. Inducers such as starvation medium, torin1 and rapamycin treatment induce the mTOR-dependent

autophagy. Disaccharide sugars such as trehalose and sucrose treatment induce the mTOR-independent autophagy. Protease inhibitors such as NH_4Cl, E-64d and pepstatin A treatment inhibit the fusion of autophagosomes with lysosomes. Different autophagy markers such as Atg proteins, LC3-II and lysosomal proteins can be used to monitor the autophagy pathway (Figure 28).

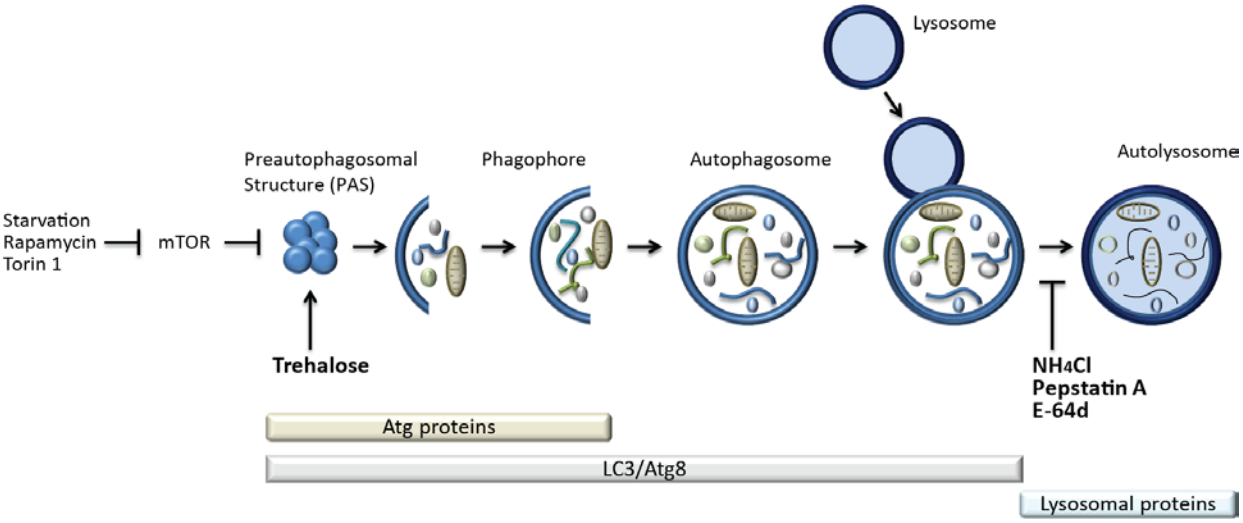

Figure 28: Induction and inhibition of the autophagy pathway. The inducers and inhibitors treatment disrupts the autophagy pathway at different points and monitor by using the different autophagy markers. Modified after (Melendez and Levine, 2009).

5.6.2 Induction of autophagy in CLN3 and Pen2 knockout cells

CLN3 and Pen2 co-localize in the late endosomal/lysosomal compartments. The interaction of both proteins could be involved in normal functioning of lysosomes and knockout of these proteins may have some effect on lysosomes or lysosomal related pathways like autophagy. To assess the effect of CLN3 and Pen2 knockout on autophagy, HeLa wild type, CLN3 and Pen2 knockout cells were cultured in DMEM + 10%FCS + 1%PS medium. The following day, cell lysates were prepared and analyzed by immunoblotting. LC3-II was used as a marker to monitor autophagy. Quantification of immunoblot results indicated that under steady state condition the LC3-II levels were increased in CLN3 and Pen2 knockout cells as compared to HeLa wild type while the LC3-II levels were higher in CLN3 as compared to Pen2 knockout cells (Figure 29). This result shows that the autophagy pathway is changed in CLN3 and Pen2 knockout cells.

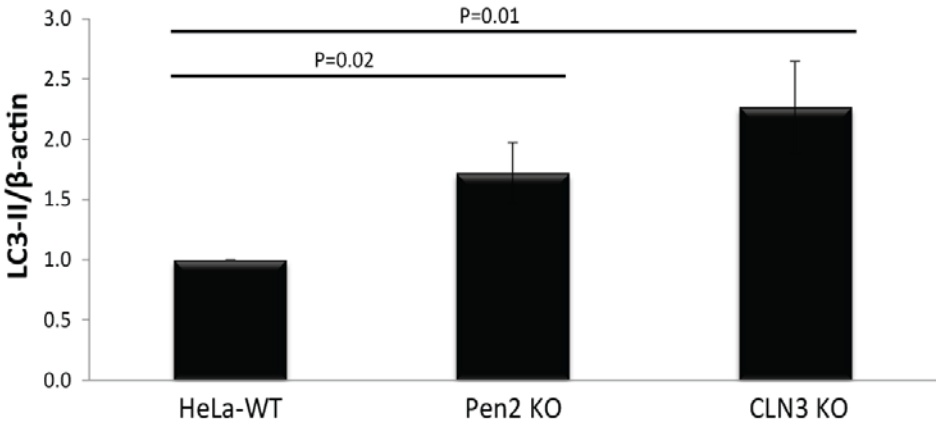

Figure 29: Endogenous LC3-II levels in HeLa wild type, CLN3 and Pen2 knockout cells. In order to analyze the effect of CLN3 and Pen2 knockout on autophagy HeLa wild type, CLN3 and Pen2 knockout cells were cultured. Cell lysates were analyzed by immunoblotting using an LC3 antibody. β-actin was used as a loading control and for normalization of the LC3-II levels. Quantification of immunoblot results showed that under steady-state conditions the LC3-II levels were increased in CLN3 and Pen2 knockout cells as compared to HeLa wild type cells. Quantification of endogenous LC3-II/β-actin levels is represented as the mean ± SEM of 10 independent experiments.

5.6.3 Analysis of autophagy with inhibitors treatment

In order to analyze alterations in autophagy HeLa wild type, CLN3 and Pen2 knockout cells were cultured. The following day, cells were treated with NH_4Cl alone and together with the protease inhibitors pepstatin A and E-64d in DMEM medium without FCS for 6 hours. For control experiments, cells were cultured in DMEM + 10%FCS + 1%PS medium without any inhibitor treatment. The fusion of autophagosomes with lysosomes is hampered by the inhibitors. As a result, autophagosomes accumulate. LC3-II and P62 were used as markers to monitor altered autophagy. Analysis of cell lysates by immune blotting revealed induced LC3-II levels in wild type cells after NH_4Cl treatment alone and in combination with the protease inhibitors pepstatin A + E-64d treatment. Both treatments strongly induced LC3-II levels in CLN3 and Pen2 knockouts as compared to HeLa wild type cells (Figure 30a). P62 levels appeared unchanged in HeLa wild type, CLN3 and Pen2 knockout cells (Figure 31). Quantification of immunoblot results demonstrated that the LC3-II levels were significantly increased by more than factor 2 in CLN3 and Pen2 knockout cells as compared to HeLa wild type cells after NH_4Cl treatment (Figure 30b). NH_4Cl treatment combined with Pepstatin A + E-64d protease inhibitors treatment significantly increased LC3-II levels in CLN3 and Pen2 knockout cells as compared to wild type cells. The combined inhibitor effect was somewhat increased in Pen2 knockout cells while no additional effect of combined treatment was observed in CLN3 knockout cells (Figure 30c).

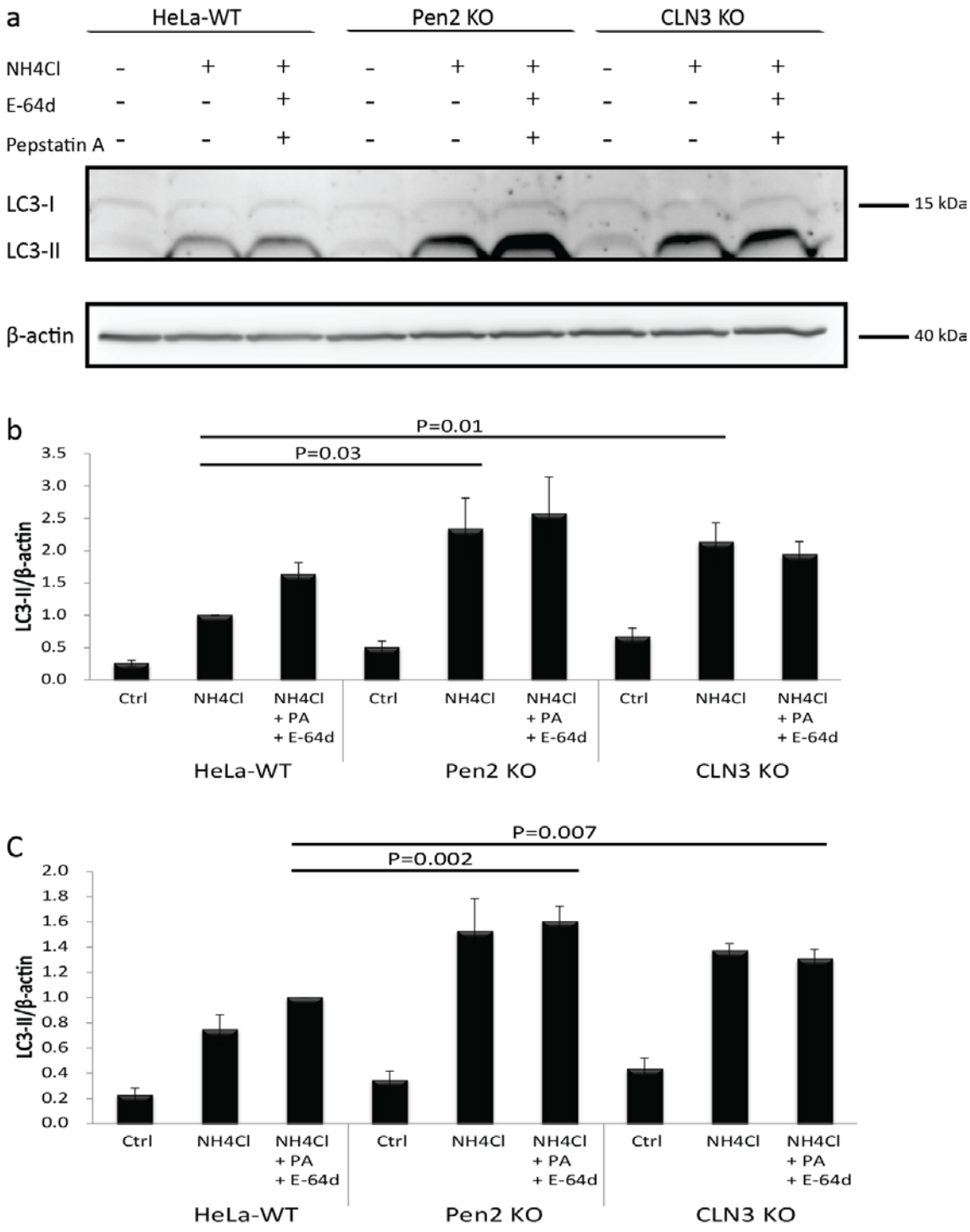

Figure 30: Autophagy inhibitor treatment induced LC3-II levels in HeLa wild type, CLN3 and Pen2 knockout cells. (a) To inhibit the autophagy pathway HeLa wild type, CLN3 and Pen2 knockout cells were cultured and treated with NH_4Cl alone and together with Pepstatin A + E-64d inhibitors for 6 hours. Cell lysates were analyzed by immunoblotting using an LC3 antibody. β-actin was used as a loading control and for normalization of the LC3-II levels. (b) Quantification of immunoblot results showed the increased LC3-II levels in CLN3 and Pen2 knockout cells as compared to HeLa wild type after NH_4Cl treatment. (c) Quantification of the western blot results indicated that NH_4Cl combined with protease inhibitors pepstatin A + E-64d treatment strongly induced the LC3-II levels in Pen2 knockout cells as compared to CLN3 knockout cells. The LC3-II levels were significantly increased in a CLN3 and Pen2 knockout as compared to HeLa wild type. Quantification of LC3-II/β-actin levels is represented as the mean ± SEM of 7 independent experiments.

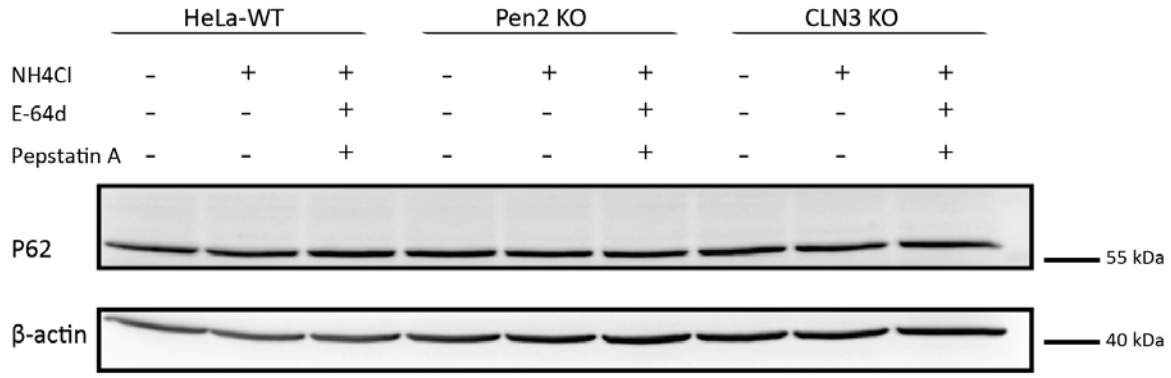

Figure 31: P62 levels are unchanged in HeLa wild type, CLN3 and Pen2 knockout cells. In order to analyze the altered autophagy by using a P62 as a marker, HeLa wild type, CLN3 and Pen2 knockout cells were cultured and treated with NH_4Cl alone and combined with protease inhibitors Pepstatin A + E-64d for 6 hours. Cell lysates were analyzed by immunoblotting using a P62 antibody. Immunoblot results showed no change of p62 levels in HeLa wild type, CLN3 and Pen2 knockout cells. β-actin was used as a loading control.

5.6.4 Induction of mTOR-dependent autophagy

In order to induce mTOR-dependent autophagy, HeLa wild type, CLN3 and Pen2 knockout cells were cultured and treated with Torin1 and rapamycin in Earle's Balanced Salt Solution (EBSS) as a starvation medium for 8 hours. For control experiments, cells were cultured in DMEM + 10%FCS medium without treatment. LC3-II was used as a marker to monitor the altered autophagy and phosphorylated S6 (pS6) was used as a marker to observe the mTOR activity. Immunoblot results showed induced LC3-II levels in HeLa wild type cells after EBSS alone and together with torin1 and rapamycin treatment as compared to untreated HeLa wild type cells. The LC3-II levels were increased in CLN3 and Pen2 knockout cells as compared to wild type cells. This is in agreement with the previous experiments. However, LC3-II levels were not further increased in CLN3 and Pen2 knockout cells with and without inducer treatment. The lack of S6 phosphorylation indicated that EBSS alone and together with torin1 and rapamycin treatment blocked mTOR activity in all cell types. Hyperphosphorylation of S6 was observed in untreated CLN3 and Pen2 knockout cells as compared to HeLa wild type. In CLN3 knockout cells, the pS6 signal was more increased as compared to Pen2 knockout cells (Figure 32).

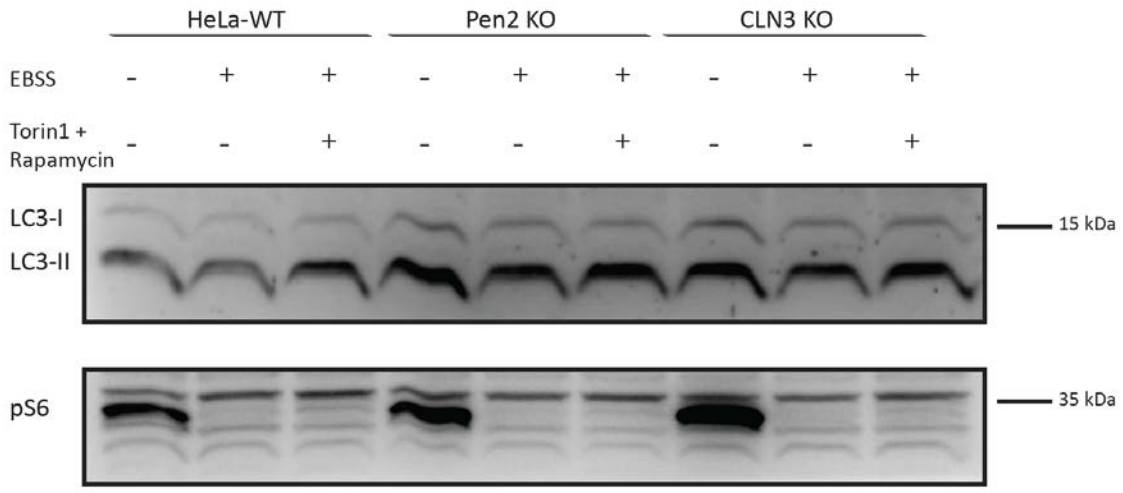

Figure 32: mTOR-dependent autophagy was observed in HeLa wild type and compared to CLN3 and Pen2 knockout cells. To induce the mTOR-dependent autophagy HeLa wild type, CLN3 and Pen2 knockout cells were treated with EBSS alone and together with torin1 and rapamycin for 8 hours. Cell lysates were analyzed by immunoblotting using LC3 and pS6 antibodies. The LC3-II levels were induced in HeLa wild type cells after EBSS alone and together with torin1 and rapamycin treatment as compared to CLN3 and Pen2 knockout cells. The untreated CLN3 and Pen2 knockout cells showed hyperphosphorylation of s6 as compared to HeLa wild type.

5.6.5 Induction of mTOR-independent autophagy

Autophagy can be induced either by a mTOR-dependent or mTOR-independent pathway. In order to induce the mTOR-independent autophagy pathway, HeLa wild type, CLN3 and Pen2 knockout cells were cultured and treated with trehalose for 24 hours. For control experiments, cells were cultured in DMEM + FCS medium without treatment. LC3-II was used as a marker to monitor the altered autophagy. The LC3-II levels were induced in HeLa wild type, CLN3 and Pen2 knockout cells after trehalose treatment (Figure 33a). Quantification of immunoblot results indicated the significantly increased LC3-II levels in CLN3 and Pen2 knockout cells as compared to HeLa wild type. In Pen2 knockout the LC3-II levels were strongly induced after trehalose treatment as compared to CLN3 knockout cells (Figure 33b).

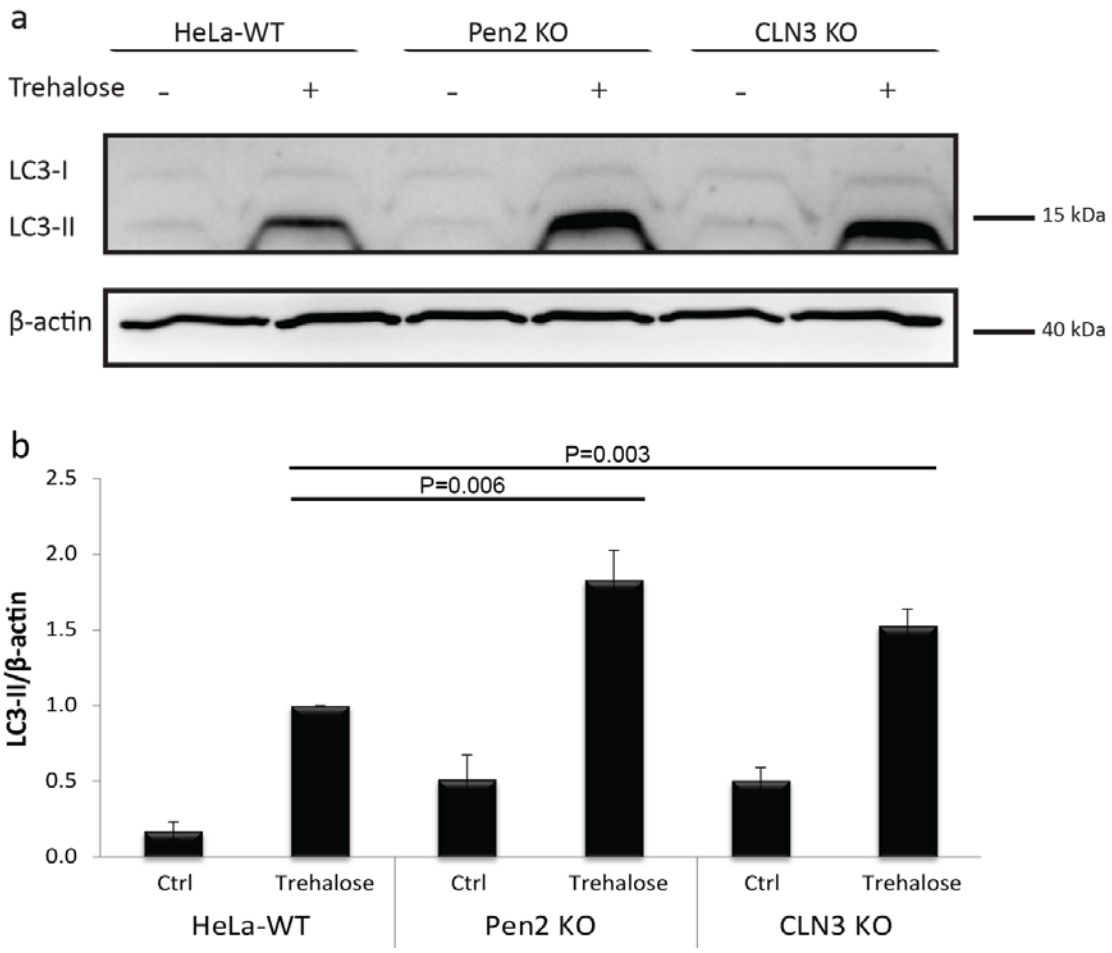

Figure 33: Trehalose treatment induces the mTOR-independent autophagy pathway in HeLa wild type, CLN3 and Pen2 knockout cells. (a) To induce the mTOR-independent autophagy pathway HeLa wild type, CLN3 and Pen2 knockout cells were cultured and treated with trehalose for 24 hours. Cell lysates were analyzed by immunoblotting using an LC3-II antibody. β-actin was used as a loading control and for normalization of the LC3-II levels. (b) Quantification of immunoblot results showed the significantly increased LC3-II levels in CLN3 and Pen2 knockout cells as compared to HeLa wild type after trehalose treatment. Quantification of LC3-II/β-actin levels is represented as the mean ± SEM of 7 independent experiments.

5.6.6 Autophagic flux analysis in CLN3 and Pen2 knockout cells

Autophagic flux was analyzed in HeLa wild type, CLN3 and Pen2 knockout cells by using the two tags mCherry and EGFP fused to LC3-II. The fluorophore EGFP is acid sensitive while mCherry is acid insensitive. In autophagosomes excitation of EGFP and mCherry tags with specific wavelengths results in the emission of green and red fluorescence, this occurs as yellow. The fusion of autophagosomes with lysosomes results in autolysosomes which are more acidic than autophagosomes. In acidic conditions, the green fluorescence is lost and only the mCherry emits red fluorescence. The two tagged proteins are degraded in autolysosomes which causes the loss of mCherry fluorescence as well and no fluorescence is observed (Figure 34).

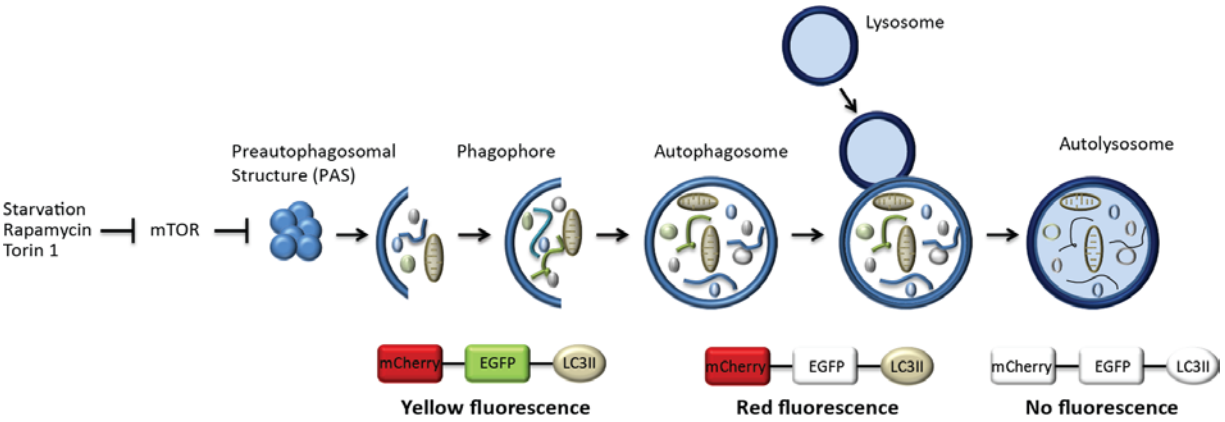

Figure 34: Autophagic flux constructs. The mCherry-EGFP-LC3-II construct was used to analyze the autophagic flux which emits green and red fluorescence in autophagosomes, red fluorescence after the fusion of autophagosomes with lysosomes and no fluorescence when the two tags fused to the protein are degraded in autolysosomes. Modified after (Hansen and Johansen, 2011).

HeLa wild type, CLN3 and Pen2 knockout cells were transfected with the mCherry-EGFP-LC3-II construct. After 48 hours of transfection, images were taken from live cells by confocal microscopy. Under steady state conditions HeLa wild type, CLN3 and Pen2 knockout cells showed no difference in yellow and red puncta (Figure 35a). For quantification, numbers of yellow and red puncta were counted manually and through Fiji software by applying identical maxima conditions to all images. Quantification of the puncta demonstrated a reduced number of red puncta in CLN3 and Pen2 knockout cells as compared to HeLa wild type. The number of yellow puncta was almost equal in HeLa wild type, CLN3 and Pen2 knockout cells (Figure 35b). The results indicate that the autophagic flux is reduced in CLN3 and Pen2 knockout cells as compared to HeLa wild type.

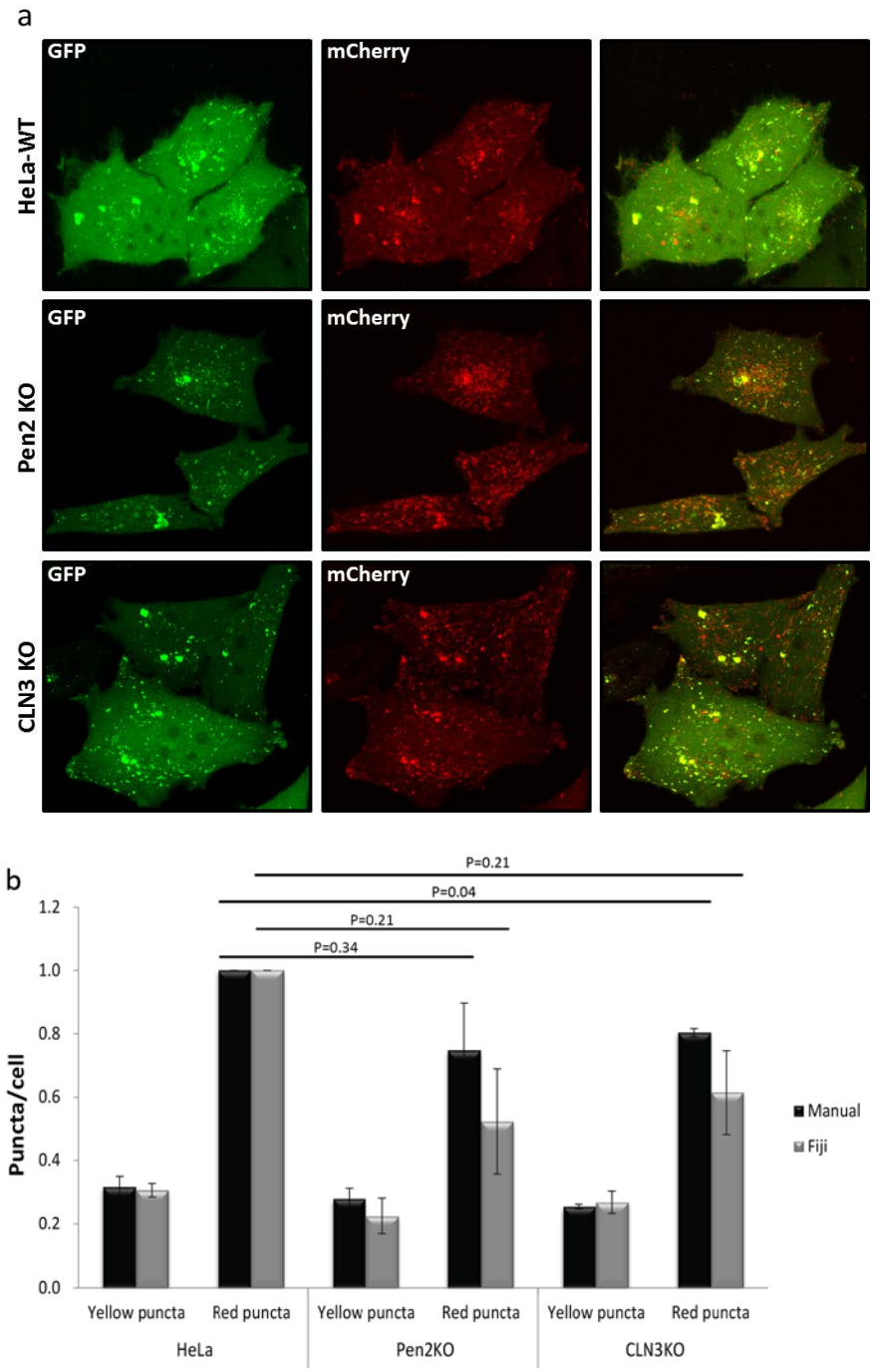

Figure 35: Autophagic flux analysis in HeLa wild type, CLN3 and Pen2 knockout cells. (a) HeLa wild type, CLN3 and Pen2 knockout cells were transfected with the mCherry-EGFP-LC3-II. Images were taken after 48 hours of transfection. Under steady state conditions cells showed no difference in yellow and red puncta. (b) Numbers of puncta were counted manually (black bars) and by Fiji software (gray bars). Quantification of the puncta results showed a reduced number of red puncta in CLN3 and Pen2 knockout cells as compared to HeLa wild type while the number of yellow puncta was almost equal in all cells. Quantification puncta per cell are represented as the mean ± SEM of 2 independent experiments.

These results indicate that the autophagy pathway is altered in CLN3 and Pen2 knockout cells and autophagosomal accumulation is higher in a CLN3 and Pen2 knockout as compared to HeLa wild type cells.

6 Discussion

Mutations in the CLN3 gene are the main cause of Juvenile Neuronal Ceroid Lipofuscinosis (JNCL). In this disease many organs are affected, particularly the brain. JNCL patients show accumulation of autofluorescent material “mitochondrial ATP subunit C” in lysosomes. To date the function of the CLN3 protein is unclear. Several interaction partners have been identified for CLN3. These interactions suggested possible roles of this protein but the cellular mechanisms it is involved in are still not conclusive. CLN3 is localized to late endosomal/lysosomal compartments. Pen2 has been found as a new interaction partner for CLN3. In this project, the functional characterization of this interaction was analyzed. This could be helpful to understand the role of CLN3 in JNCL pathology, to rule out common mechanisms in JNCL and Alzheimer’s disease, and to add novel information to the cellular role of Pen2.

6.1 CLN3 and Pen2 co-localize in late endosomes/lysosomes

Juvenile Neuronal Ceroid Lipofuscinosis (JNCL) is one form of Neuronal Ceroid Lipofuscinosis (NCL) which is an autosomal recessive neurodegenerative disease mainly affecting children. Mutations in the CLN3 gene are responsible for JNCL. Around 15% of JNCL patients carry different missense, nonsense and Indel mutations while 85% contain a 1kb deletion of exon 7/8 ($CLN3^{\Delta ex7/8}$) which leads to a truncation of the CLN3 protein (Cotman and Staropoli, 2012). The primary function of CLN3 is still unknown. One possible way to unravel its function is identifying interaction partners of CLN3 which could have a dynamic role in protein stability and function. Some studies have presented the interaction of CLN3 with other NCL associated genes such as CLN5 (Lyly et al., 2009) and with microtubule binding protein Hook1 (Luiro et al., 2004). These findings highlighted the possible role of these interactions in CLN3 intracellular trafficking but did not unravel CLN3 functions.

In a TAP-tag screening, Pen2 has been identified as an interaction partner of CLN3. Pen2 is an important subunit of the γ-secretase complex. Biochemical studies have shown that the Pen2 subunit is the final component added to the γ-secretase complex whereupon the presenilin holoprotein undergoes autoproteolysis (Takasugi et al., 2003). The suggested function of Pen2 is allowing full assembly, stabilizing the complex and proper trafficking of the γ-secretase complex (Holmes et al., 2014). The CLN3 protein is localized to late

endosomal/lysosomal compartments (Haskell et al., 1999; Oetjen et al., 2016; Phillips et al., 2005). In this thesis, co-localization of CLN3 with Pen2 was examined in HeLa and COS-7 cells. Tagged versions of CLN3 and Pen2 were generated due to lack of specific antibodies for both proteins. In order to achieve long-term expression of a CLN3 and Pen2 genes, stable HeLa cell lines were generated. Stable transfected EGFP-tagged CLN3 HeLa cells were already available in the lab. For Pen2, HeLa cells were transfected with HA and fluorophore protein tags. The single stably transfected cell clones of HeLa cells were picked and immunocytochemistry was performed on fixed cells. Both proteins co-localized on identical vesicular structures. The result verifies previous findings by Sandra Oetjen, who showed that both proteins co-localize and are co-transported in late endosomes/lysosomes in undifferentiated cells and primary cultured neurons. In addition, in-situ hybridizations demonstrated that both proteins are expressed in the same tissue and co-immunoprecipitations validated the interaction of both proteins (Sandra Oetjen; Ph.D. Thesis). Fluorescence resonance energy transfer (FRET) technique was applied as a second approach to analyze the close localization of CLN3 and Pen2. Many factors take into account for this technique but important aspects are the distance between two proteins is less than 10nm (Lalonde et al., 2008) furthermore the N- or C-terminus of both proteins facing either cytosolic or luminal sides allowing fluorophore tagging in identical cellular compartments (Ratajczak et al., 2014). This technique was applied on the basis of a newly suggested Pen2 structure which proposed that the N-terminus is facing the cytosolic side and the C-terminus is facing the luminal side (Zhang et al., 2015). CLN3 is a six transmembrane protein with the N- and C-terminus facing the cytosolic side (Ratajczak et al., 2014). Therefore, the newly suggested structure of Pen2 would enable FRET analysis. HeLa cells were co-transfected with EGFP-tagged Pen2 and mCherry-tagged CLN3 constructs. FRET analysis was performed by confocal laser scanning microscope at a wavelength of 488-630nm. The result showed no close co-localization between CLN3 and Pen2 proteins. One reason might be the distance between two proteins is more than 10nm. A possible underlying mechanism could be that another protein interferes between CLN3 and Pen2 and both proteins have indirect interaction (Lalonde et al., 2008). Another reason might be that the newly suggested Pen2 topology is wrong.

The CLN3 protein contains lysosomal targeting motifs (LTM) in its long C-terminal cytosolic tail. It is thought that adaptor proteins bind CLN3-LTM and mediate trafficking to late endosomes/lysosomes. It has been shown that mutations in CLN3-LTM mistarget the CLN3 protein to the plasmamembrane (Kyttala et al., 2004; Storch et al., 2004). To examine if CLN3 with its lysosomal targeting motifs mutated would recruit Pen2 to the plasmamembrane, HeLa and COS-7 cells were transiently co-transfected with EGFP-tagged CLN3-LTM and tdTomato-tagged Pen2. The result shows full-length CLN3 protein carrying LTM mutation is localized to the plasmamembrane whereas, Pen2 remains in endoplasmic reticulum-like structures or partially localizes to vesicular structures. One reason for Pen2 not following CLN3 translocation might be that the mutated cytosolic domain of CLN3 is important for interaction with Pen2 and mutation in CLN3-LTM may interrupt this interaction. Partial localization of Pen2 to vesicular structures gives another reason that it might be CLN3 with its lysosomal targeting motifs mutation still interacts with Pen2 and traffic to the Golgi but expressed in different cell organelle. Another reason could be due to its overexpression Pen2 is partially localized to vesicular structures. More experiments need to be done and further, the localization of both proteins should be analyzed in knockout cells. In CLN3 and Pen2 knockout HeLa cells a tag knock-in via the CRISPR/Cas9 system would be a valuable method to analyze the location of both proteins. In addition, expression of CLN3 with four core components of γ-secretase in a 1:1:1:1 stoichiometry would be worthwhile to prove interaction and localization of CLN3 with γ-secretase complex (Meckler and Checler, 2016).

These results indicate that CLN3 and Pen2 are co-localized to late endosomal/lysosomal compartments and interaction of both proteins might have a functional role in the lysosomes.

6.2 Generation of CLN3 and Pen2 knockout HeLa cell lines

If both proteins interact it is likely that they function in a common cellular pathway. Thus, deletion of each protein alone is probably leading to identical phenotypes. To study gene function and physiological phenotype on a cellular level, CLN3 and Pen2 genes were inactivated. A first approach was to knockdown by shRNA. This technique has been widely used to silence target genes by inactivation of its mRNA (Moore et al., 2010). Previously, mouse CLN3 was knocked down by shRNAs (Sandra Oetjen; Ph.D. Thesis). In this thesis, the

knockdown effect of shRNAs on human Pen2 was assessed in N2A cells by using a luciferase activity based test. The result showed highest luciferase activity in negative controls. Among others, shRNA-B1 displayed reduced luciferase activity to a comparable level as the positive control. Specific shRNA has shown the reduced activity but competency to knockdown the Pen2 was not efficient. One reason might be insufficient shaking after adding luciferase substrate to cells. Another reason might be firefly luciferase didn't quench properly as a result, Renilla luciferase activity was not expressively reduced.

Another method to inactivate genes is knockout via the CRISPR/Cas9 system. This method has been widely used for genome editing in a variety of species and cell types (Hsu et al., 2014). In this thesis, the knockout effect of different gRNAs on human CLN3 and Pen2 genes was evaluated in HeLa cells. Using split-EGFP reconstitution as an efficiency test of gRNAs green fluorescence was observed in HeLa cells treated with all gRNAs. However, signal intensity was strong in the tests for gRNA-1 for CLN3 and gRNA-4 for Pen2. The result indicates the good binding efficiency of guide RNAs (gRNAs) to the respective target sequence and causes a single/double-strand break by the Cas9 endonuclease.

In a comparison of efficiency tests, the knockout effect of gRNAs was more pronounced as compared to the knockdown effect of shRNAs. For this reason, the knockout approach was adopted to inactivate CLN3 and Pen2 genes. The proved specific gRNAs were used to mutate CLN3 and Pen2 genes from HeLa cells. Mutations in both cell lines were examined through DNA sequencing. A technique to verify the knockout of the encoded protein is immunoblotting but due to lack of suitable antibodies for both proteins, this approach was not feasible. However, DNA sequencing after reverse transcriptase (RT) PCR verified mutations in both genes. The result demonstrated that CRISPR/Cas9 system worked and through this method CLN3 and Pen2 knockout HeLa cell lines were generated.

6.3 CLN3 does not modulate processing by γ-secretase

The γ-secretase complex consists of four subunits Presenilin (PS), anterior pharynx defective 1 (APH-1), nicastrin and Presenilin enhancer 2 (Pen2) (De Strooper, 2003). Pen2 mutations alter γ-secretase complex formation, PS endoproteolysis and trafficking from the endoplasmic reticulum to Golgi (Dries and Yu, 2008; Holmes et al., 2014). Some studies have highlighted that Pen2 mutations do not only lead to a familial Alzheimer's disease (Andreoli

et al., 2011; Sala Frigerio et al., 2005; Tanzi, 2012) but also is embryonic lethal due to defect in Notch signaling (Francis et al., 2002). On the other hand, some findings have suggested altered amyloid precursor protein (APP) processing in the brain of NCL patients (Wisniewski et al., 1990a; Wisniewski et al., 1990b). Interaction of CLN3 with Pen2 leads to the hypothesis that CLN3 could be involved in a γ-secretase activity. CLN3 deficiency might be altering APP and Notch processing due to a defect in γ-secretase activity. To test this hypothesis a γ-secretase activity assay was performed by using the APP and modified Notch, NotchΔE, well-known substrates for γ-secretase. The APP is first cleaved by α- or β-secretase and then within the transmembrane domain through γ-secretase. Modified NotchΔE is independent of α-secretase and directly cleaved by γ-secretase. First, γ-secretase processing was measured by a luciferase assay. To establish this method HeLa wild type and Pen2 knockout cells were used. In Pen2 knockout cells, altered APP and NotchΔE processing were expected when compared to wild type cells. Therefore, these cells were used to optimize experimental conditions which would be useful to critically analyze γ-secretase activity in CLN3 knockout cells. Luciferase assay demonstrated highest and lowest luciferase activity in positive and negative controls respectively. Luciferase activity in cleavable NotchΔE was induced whereas, in the cleavable APP was almost similar to negative control between both cell lines. No expected difference between an APP and NotchΔE processing by γ-secretase among HeLa wild type and Pen2 knockout cells was detected. The results of the luciferase assay were unexpected and not conclusive. Therefore, immunoblotting was used as an alternative methodology to investigate γ-secretase activity in HeLa wild type, CLN3 and Pen2 knockout cells. This method was based on analyzing fragments of different size produced by α- , β- and γ-secretase cleavage. The immunoblot results indicate that γ-secretase activity is hampered in Pen2 knockout cells and unchanged in CLN3 knockout cells as compared to wild type. In Pen2 knockout cells, γ-secretase activity is restored by overexpression of Pen2. It has been revealed before that Pen2 mutation altered APP and Notch processing (De Strooper et al., 1999; De Strooper et al., 1998) by troubling γ-secretase activity, stability and PS1 endoproteolysis(Francis et al., 2002; Luo et al., 2003; Steiner et al., 2002). Indirect effects of the CLN3 knockout cannot be excluded. Thus it has been shown that overexpression of mutated CLN3p in human embryonal kidney cells increases lysosomal pH. The misbalance in pH could be a reason for alterations in APP processing (Golabek et al., 2000) in addition, it is suggested that ubiquitously overexpression of CLN3 in Drosophila might be affecting Notch

processing (Tuxworth et al., 2009). However, the here presented results lead to the conclusion that Pen2 is crucial for γ-secretase activity and strongly suggest that CLN3 is not involved in the γ-secretase activity. Therefore, it is tempting to speculate that the interaction of CLN3 with Pen2 plays a role in γ-secretase independent processes in the late endosomal/lysosomal system. Pen2 knockout cells are also validated in the assessment of γ-secretase activity through immunoblot assay.

6.4 Altered lysosomal enzymatic activity in CLN3 and Pen2 knockout cells

Lysosomal transmembrane proteins have a crucial role in many cellular events such as lysosomal acidification, transport of metabolites and membrane fusion. Defects in these proteins can lead to an imbalance in the lysosomal pH. As a result, many enzymatic activities are disturbed which could lead to lysosomal storage diseases (Ruivo et al., 2009; Schwake et al., 2013). CLN3 and Pen2 are transmembrane proteins, co-localizing in the late endosomal/lysosomal compartments. Deletion or mutation of each of the proteins could have identical consequences on lysosomes such as imbalance in lysosomal pH which could change enzymatic activities. To test this hypothesis β-hexosaminidase A (β-Hex A) and Arylsulfatase A (ARSA) enzymatic activities were measured in CLN3 and Pen2 knockout HeLa cell lines. Cell lysates of both knockout cells showed significantly reduced β-hexosaminidase A and slightly increased Arylsulfatase A enzymatic activities as compared to HeLa wild type. Cell culture medium of both knockout cells displayed slightly increased in β-hexosaminidase A activity as compared to HeLa wild type. Other studies have presented that CLN3 is important for lysosomal pH regulation and cathepsin D activity. CLN3 mutation raises lysosomal pH as a result cathepsin D activity is altered (Carcel-Trullols et al., 2017; Holopainen et al., 2001; Vidal-Donet et al., 2013). In Alzheimer's disease dysregulation of lysosomal pH and calcium have been reported due to mutations in presenilin 1 (PS1) (Coffey et al., 2014; Lee et al., 2015; McBrayer and Nixon, 2013). The current observation suggests that deletion of CLN3 and Pen2 alters lysosomal enzymatic activities. This effect could be due to changes in lysosomal pH. To further validate the current results more experiments need to be done such as measuring cathepsin B and D enzymatic activity and assessing lysosomal pH in both knockout cells.

6.5 Autophagy is altered in CLN3 and Pen2 knockout cells

Lysosomes play a central role in the autophagy pathway. Alteration in lysosomes such as changes in pH affects the autophagy pathway (Raben et al., 2009). Deletion of CLN3 and Pen2 altered enzymatic activities. This could be due to an imbalance in the lysosomal pH. The interaction of both proteins and their effect on lysosomes led to the hypothesis that their deletion could have identical physiological consequences on the autophagy pathway. To test this hypothesis the autophagy pathway was examined in different ways. To observe changes in this pathway autophagy markers LC3-II and p62 were used (Mizushima et al., 2010).

To assess the effect of CLN3 and Pen2 knockout on the autophagy, cell lysates were analyzed by immunoblotting. Under steady state conditions increased LC3-II levels in the knockout cells provided the first indication of shared changes in the autophagy. LC3-II/LC3-I levels determine the autophagosome contents. In certain cell lines such as HeLa cells, the visibility of LC3-I is reduced as compared to LC3-II whereas LC3-I is highly visible in other cells or in brain tissue. To quantify immunoblots by LC3-II/β-actin levels is a reliable method to determine the change in autophagosome contents (Chu et al., 2009; Klionsky et al., 2016).

Alterations in the autophagy were analyzed after inhibitor treatment. HeLa wild type, CLN3 and Pen2 knockout cells were treated with NH_4Cl alone and together with Pepstatin A + E-64d inhibitors in DMEM medium without FCS. Inhibitors effect on HeLa cells were analyzed at different time points. Finally, the treatment time was set to 6 hours. The NH_4Cl treatment increases lysosomal pH which inhibits the fusion of autophagosomes with lysosomes (Yu et al., 2013). Pepstatin A and E-64d inhibit aspartic and cysteine proteases respectively. These proteases are active at acidic pH in lysosomes (Klionsky et al., 2016). The NH_4Cl alone and together with Pepstatin A + E-64d inhibitors treatment induced LC3-II levels in CLN3 and Pen2 knockout cells as compared to HeLa wild type. Comparison between two treatments demonstrated that combined inhibitors treatment effect is not significantly higher than NH_4Cl alone treatment in both knockout cells. The reason might be that in CLN3 and Pen2 knockout cells the lysosomal pH is already increased. This is further boosted by the NH_4Cl treatment. The increased pH may affect aspartic and cysteine proteases activity. Due to this reason Pepstatin A and E-64d inhibitor treatment might not have an additional effect in both knockout cells. Some studies have presented increased LC3-II levels in JNCL patients

fibroblasts after bafilomycin A_1 or $CINH_4$ plus leupeptin inhibitors treatment (Vidal-Donet et al., 2013) and thapsigargin treated human iPSC-derived neuronal progenitor cells from JNCL affected patients (Chandrachud et al., 2015). Similar effects were observed in Alzheimer's disease due to mutations in presenilin which is the main cause of autophagy impairment in this disease (Neely et al., 2011; Orr and Oddo, 2013). In the presented study, p62 levels appeared unchanged with and without inhibitor treatment in all cells. One reason might be that upon prolonged starvation p62 expression is restored. Another reason might be that amino acids starvation or selective inhibitors treatment is not sufficient to induce p62 level in HeLa cells (Sahani et al., 2014). Both amino acids starvation and serum starvation or using alternative inhibitors of the autophagic pathway such as bafilomycin and leupeptin could be useful to induce p62 levels in HeLa cells. However, the altered LC3-II levels strongly suggest that the autophagy is altered in CLN3 and Pen2 knockout cells.

Autophagy induced through the mTOR-dependent pathway was analyzed in HeLa wild type, CLN3 and Pen2 knockout cells. Active mTOR phosphorylates ribosomal protein S6 kinase and other substrates which regulate protein synthesis (Magnuson et al., 2012). Inactivating mTOR inhibits translation and induces autophagy by dephosphorylation of ULK1 (Shang et al., 2011). It has been shown that mTOR is not completely inhibited by rapamycin. Combination of rapamycin with torin1 has the potential to completely block the mTOR complex (Thoreen et al., 2009). Effect of mTOR inhibitors alone and in combination on HeLa cells was determined with different concentration and at different time points. Finally, cells were treated with both mTOR inhibitors for 8 hours in starvation medium. The LC3-II levels were increased in CLN3 and Pen2 knockout cells as compared to wild type cells. However, LC3-II levels were not further increased in both knockout cells with and without mTOR inhibitors treatment. The yeast CLN3 disease model exhibits a defect in TORC pathway (Bond et al., 2015) also, JNCL patients fibroblasts show more phosphorylation of the mTOR complex (Vidal-Donet et al., 2013). On the other hand, high levels of the phospho-mTOR complex have been reported in human Alzheimer's disease brain (Oddo, 2012). The mTOR inhibitors treatment might not be effective due to a defect in the mTOR complex. For this reason, LC3-II is not further increased in both knockout cells. Lack of S6 phosphorylation indicated that mTOR activity is completely blocked in all mTOR inhibitors treated cells. Whereas, untreated CLN3 and Pen2 knockout cells showed hyperphosphorylation of S6 as compared to wild type cells. Some finding suggests that due to a high level of mTOR

phosphorylation the downstream target of mTOR, ribosomal protein S6 (pS6) is hyperphosphorylated in JNCL patient fibroblasts (Vidal-Donet et al., 2013) and human Alzheimer's disease brain (Oddo, 2012). However, results presented in this thesis demonstrate that the autophagy through the mTOR-dependent pathway is affected in CLN3 and Pen2 knockout cells. The reason might be due to an increase in the mTOR phosphorylation downstream substrate of mTOR ribosomal protein S6 is hyperphosphorylated in both knockout cells which could be one of the reasons for JNCL progression.

Next, Autophagy induced through the mTOR-independent pathway was analyzed in HeLa wild type, CLN3 and Pen2 knockout cells. Trehalose is a natural disaccharide that is found in plants and many organisms excluding mammals. Trehalose induces autophagy by direct activation of ULK1 through phosphorylation. It has been shown that prolonged trehalose incubation time induces autophagy in HeLa cells (Chen et al., 2016; Kim et al., 2011). Accordingly, cells were treated with trehalose for 24 hours. Trehalose treatment induced autophagy in all cells. LC3-II levels were significantly higher in both knockout cells as compared to wild type. Some studies highlighted mTOR-independent autophagy induction by trehalose which increases the LC3-II levels. It has been shown that trehalose administration in JNCL mice could be a therapeutic approach to improve disease pathology (Palmieri et al., 2017). In human neuroblastoma H4 cells trehalose treatment inhibits lysosomal degradation of APP and decreases Aβ secretion without affecting the γ-secretase (Tien et al., 2016). The result clearly demonstrates that trehalose treatment induces autophagy through the mTOR-independent pathway in CLN3 and Pen2 knockout cells. Treatment of these cells with another disaccharide (sucrose) or trisaccharide (raffinose) could further validate the current result.

Autophagic flux was analyzed in HeLa wild type, CLN3 and Pen2 knockout cells by using two tags mCherry and EGFP fused to LC3-II. Images were taken from live cells after 48 hours of transfection. The result was interpreted on the basis of yellow and red fluorescence (Hansen and Johansen, 2011). Under steady state condition cells revealed no difference in yellow and red puncta. For quantification two different ways were adopted to count yellow and red puncta. Manual counting and counting by using the Fiji software was performed by applying identical maxima conditions to all images. Quantification results of both counting methods

showed unchanged numbers of yellow puncta in all cells. The numbers of red puncta were reduced in CLN3 and Pen2 knockout cells as compared to wild type. Some finding by others demonstrated altered autophagic flux in Alzheimer's disease (Orr and Oddo, 2013) and iPSC-derived neuronal progenitor cells from JNCL affected patients (Chandrachud et al., 2015). The data presented here illustrate that autophagic flux is decreased in CLN3 and Pen2 knockout cells. More experiments need to be performed to obtain statistically significant results. In addition, analysis of autophagic flux in both knockout cells after autophagy inhibitors (NH_4Cl) and inducers (trehalose, rapamycin and torin1) could further validate the current result.

Collectively, these results demonstrate that CLN3 and Pen2 knockout affect the autophagy pathway. The mTOR-independent autophagy pathway and autophagic flux are changed in CLN3 and Pen2 knockout cells. Autophagy induction through the mTOR-independent pathway could be a potential therapeutic approach to treat the JNCL.

7 Conclusions

Results of this project lead to the conclusion that CLN3 and Pen2 proteins are co-localized to late endosomal/lysosomal compartments. The γ-secretase activity is hampered in Pen2 knockout cells and unchanged in CLN3 knockout cells as compared to HeLa wild type. CLN3 and Pen2 interaction could have a physiological role to maintain different cell functions. Deletion of these proteins has highly similar consequences on lysosomes and the autophagy pathway. CLN3 deletion altered lysosomal enzymatic activities and the autophagy pathway. Similar effects were reported in the Alzheimer's disease mainly due to mutations in the presenilin (PS), a functionally important subunit of the γ-secretase complex. In this thesis, it has been reported for the first time that Pen2 deletion causes also changes lysosomal enzymatic activities and the autophagy pathway. Pen2 deletion may have an indirect effect, for instance by interrupting PS endoproteolysis activity in the endoplasmic reticulum. Due to this alteration in PS the v-ATPase pump and TRPML1 ion channel are unable to maintain the lysosomal pH and calcium homeostasis. The suggested function of Pen2 is allowing full assembly, stabilizing the complex and proper trafficking of the γ-secretase complex. It could also be possible that CLN3 interaction with Pen2 makes a γ-secretase independent functional unit. Pen2 could be involved in trafficking of CLN3 from the endoplasmic reticulum. The interaction of both proteins may have a direct role in maintaining lysosomal functions and the autophagy pathway.

8 References

Aberg, L.E., Backman, M., Kirveskari, E., and Santavuori, P. (2000). Epilepsy and antiepileptic drug therapy in juvenile neuronal ceroid lipofuscinosis.pdf.

Andreoli, V., Trecroci, F., La Russa, A., Cittadella, R., Liguori, M., Spadafora, P., Caracciolo, M., Di Palma, G., Colica, C., Gambardella, A.*, et al.* (2011). Presenilin enhancer-2 gene: identification of a novel promoter mutation in a patient with early-onset familial Alzheimer's disease. Alzheimers Dement *7*, 574-578.

Appelqvist, H., Nilsson, C., Garner, B., Brown, A.J., Kagedal, K., and Ollinger, K. (2011). Attenuation of the lysosomal death pathway by lysosomal cholesterol accumulation. Am J Pathol *178*, 629-639.

Augustine, E.F., Adams, H.R., Beck, C.A., Vierhile, A., Kwon, J., Rothberg, P.G., Marshall, F., Block, R., Dolan, J., Mink, J.W.*, et al.* (2015). Standardized assessment of seizures in patients with juvenile neuronal ceroid lipofuscinosis. Dev Med Child Neurol *57*, 366-371.

Autti, T., Hamalainen, J., Aberg, L., Lauronen, L., Tyynela, J., and Van Leemput, K. (2007). Thalami and corona radiata in juvenile NCL (CLN3) a voxel-based morphometric study.pdf.

Ballabio, A., and Gieselmann, V. (2009). Lysosomal disorders: from storage to cellular damage. Biochim Biophys Acta *1793*, 684-696.

Bandyopadhyay, D., Cyphersmith, A., Zapata, J.A., Kim, Y.J., and Payne, C.K. (2014). Lysosome transport as a function of lysosome diameter. PLoS One *9*, e86847.

Belzile, J.P., Sabalza, M., Craig, M., Clark, E., Morello, C.S., and Spector, D.H. (2015). Trehalose, an mTOR-Independent Inducer of Autophagy, Inhibits Human Cytomegalovirus Infection in Multiple Cell Types. J Virol *90*, 1259-1277.

Bond, M.E., Brown, R., Rallis, C., Bahler, J., and Mole, S.E. (2015). A central role for TOR signalling in a yeast model for juvenile CLN3 disease. Microb Cell *2*, 466-480.

Boulton, M.E., Cai, J., and Grant, M.B. (2008). gamma-Secretase: a multifaceted regulator of angiogenesis. J Cell Mol Med *12*, 781-795.

Boya, P., Reggiori, F., and Codogno, P. (2013). Emerging regulation and functions of autophagy.pdf. Nat Cell Biol.

Braakman, I., and Hebert, D.N. (2013). Protein folding in the endoplasmic reticulum. Cold Spring Harb Perspect Biol *5*, a013201.

Braulke, T., and Bonifacino, J.S. (2009). Sorting of lysosomal proteins. Biochim Biophys Acta *1793*, 605-614.

Bray, S.J. (2016). Notch signalling in context. Nat Rev Mol Cell Biol *17*, 722-735.

Breitling, J., and Aebi, M. (2013). N-linked protein glycosylation in the endoplasmic reticulum. Cold Spring Harb Perspect Biol *5*, a013359.

Bulleid, N.J. (2012). Disulfide bond formation in the mammalian endoplasmic reticulum. Cold Spring Harb Perspect Biol *4*.

Burkovetskaya, M., Karpuk, N., and Kielian, T. (2017). Age-dependent alterations in neuronal activity in the hippocampus and visual cortex in a mouse model of Juvenile Neuronal Ceroid Lipofuscinosis (CLN3). Neurobiol Dis *100*, 19-29.

Cai, D., Leem, J.Y., Greenfield, J.P., Wang, P., Kim, B.S., Wang, R., Lopes, K.O., Kim, S.H., Zheng, H., Greengard, P.*, et al.* (2003). Presenilin-1 regulates intracellular trafficking and cell surface delivery of beta-amyloid precursor protein. J Biol Chem *278*, 3446-3454.

Callen, D.F., Baker, E., Lane, S., Nancarrow, J., Thompson, A., Whitmore, S.A., MacLennan, D.H., Berger, R., Cherif, D., Jarvela, I.*, et al.* (1991). Regional mapping of the Batten disease locus (CLN3) to human chromosome 16p12.pdf.

Carcel-Trullols, J., Kovacs, A.D., and Pearce, D.A. (2015). Cell biology of the NCL proteins: What they do and don't do. Biochim Biophys Acta *1852*, 2242-2255.

Carcel-Trullols, J., Kovacs, A.D., and Pearce, D.A. (2017). Role of the Lysosomal Membrane Protein, CLN3, in the Regulation of Cathepsin D Activity. J Cell Biochem *118*, 3883-3890.

Chami, L., and Checler, F. (2012). BACE1 is at the crossroad of a toxic vicious cycle involving cellular stress and β-amyloid production in Alzheimer's disease..pdf. Molecular Neurodegeneration.

Chan, C.H., Mitchison, H.M., and Pearce, D.A. (2008). Transcript and in silico analysis of CLN3 in juvenile neuronal ceroid lipofuscinosis and associated mouse models. Hum Mol Genet *17*, 3332-3339.

Chan, C.H., Ramirez-Montealegre, D., and Pearce, D.A. (2009). Altered arginine metabolism in the central nervous system (CNS) of the Cln3-/- mouse model of juvenile Batten disease. Neuropathol Appl Neurobiol *35*, 189-207.

Chandrachud, U., Walker, M.W., Simas, A.M., Heetveld, S., Petcherski, A., Klein, M., Oh, H., Wolf, P., Zhao, W.N., Norton, S.*, et al.* (2015). Unbiased Cell-based Screening in a Neuronal Cell Model of Batten Disease Highlights an Interaction between Ca2+ Homeostasis, Autophagy, and CLN3 Protein Function. J Biol Chem *290*, 14361-14380.

Chattopadhyay, S., and Pearce, D.A. (2000). Neural and extraneural expression of the neuronal ceroid lipofuscinoses genes CLN1, CLN2, and CLN3: functional implications for CLN3. Mol Genet Metab *71*, 207-211.

Chen, X., Li, M., Li, L., Xu, S., Huang, D., Ju, M., Huang, J., Chen, K., and Gu, H. (2016). Trehalose, sucrose and raffinose are novel activators of autophagy in human keratinocytes through an mTOR-independent pathway. Sci Rep *6*, 28423.

Chu, C.T., Plowey, E.D., Dagda, R.K., Hickey, R.W., Cherra, S.J., and Clark, R.S.B. (2009). Chapter 11 Autophagy in Neurite Injury and Neurodegeneration. *453*, 217-249.

Cialone, J., Adams, H., Augustine, E.F., Marshall, F.J., Kwon, J.M., Newhouse, N., Vierhile, A., Levy, E., Dure, L.S., Rose, K.R.*, et al.* (2012). Females experience a more severe disease course in Batten disease. J Inherit Metab Dis *35*, 549-555.

Coffey, E.E., Beckel, J.M., Laties, A.M., and Mitchell, C.H. (2014). Lysosomal alkalization and dysfunction in human fibroblasts with the Alzheimer's disease-linked presenilin 1 A246E mutation can be reversed with cAMP. Neuroscience *263*, 111-124.

Colacurcio, D.J., and Nixon, R.A. (2016). Disorders of lysosomal acidification-The emerging role of v-ATPase in aging and neurodegenerative disease. Ageing Res Rev *32*, 75-88.

Cong, L., Ran, F.A., Cox, D., Lin, S., Barretto, R., Habib, N., Hsu, P.D., Wu, X., Jiang, W., Marraffini, L.A.*, et al.* (2013). Multiplex genome engineering using CRISPR/Cas systems. Science *339*, 819-823.

Cooper, J.D. (2008). Moving towards therapies for juvenile Batten disease? Exp Neurol *211*, 329-331.

Cotman, S.L., and Staropoli, J.F. (2012). The juvenile Batten disease protein, CLN3, and its role in regulating anterograde and retrograde post-Golgi trafficking. Clin Lipidol *7*, 79-91.

Coutinho, M.F., Prata, M.J., and Alves, S. (2012). Mannose-6-phosphate pathway: a review on its role in lysosomal function and dysfunction. Mol Genet Metab *105*, 542-550.

Crystal, A.S., Morais, V.A., Pierson, T.C., Pijak, D.S., Carlin, D., Lee, V.M., and Doms, R.W. (2003). Membrane topology of gamma-secretase component PEN-2. J Biol Chem *278*, 20117-20123.

De Strooper, B. (2003). Aph-1, Pen-2, and Nicastrin with Presenilin generate an active gamma-Secretase complex..pdf. Neuron.

De Strooper, B., Annaert, W., Cupers, P., Saftig, P., Craessaerts, K., Mumm, J.S., Schroeter, E.H., Schrijvers, V., Wolfe, M.S., Ray, W.J.*, et al.* (1999). A presenilin-1-dependent gamma-secretase-like protease mediates release of Notch intracellular domain..pdf. Nature.

De Strooper, B., Saftig, P., Craessaerts, K., Vanderstichele, H., Guhde, G., Annaert, W., Von Figura, K., and Van Leuven, F. (1998). Deficiency of presenilin-1 inhibits the normal cleavage of amyloid precursor protein..pdf. Nature.

Ding, S.L., Tecedor, L., Stein, C.S., and Davidson, B.L. (2011). A knock-in reporter mouse model for Batten disease reveals predominant expression of Cln3 in visual, limbic and subcortical motor structures. Neurobiol Dis *41*, 237-248.

Donoviel, D.B., Hadjantonakis, A.K., Ikeda, M., Zheng, H., Hyslop, P.S., and Bernstein, A. (1999). Mice lacking both presenilin genes exhibitearlyembryonic patterningdefects.pdf. Genes Dev.

Dries, D.R., and Yu, G. (2008). ASSEMBLY MATURATION AND TRAFFICKING OF THE γ SECRETASE COMPLEX IN ALZHEIMER'S DISEASE.pdf. Curr Alzheimer Res.

Duve, C. (1975). Exploring cells with a centrifuge.pdf. Science.

Elrick, M.J., and Lieberman, A.P. (2013). Autophagic dysfunction in a lysosomal storage disorder due to impaired proteolysis. Autophagy *9*, 234-235.

Finn, R., Kovacs, A.D., and Pearce, D.A. (2011). Altered sensitivity of cerebellar granule cells to glutamate receptor overactivation in the Cln3(Deltaex7/8)-knock-in mouse model of juvenile neuronal ceroid lipofuscinosis. Neurochem Int *58*, 648-655.

Francis, R., McGrath, G., Zhang, J., Ruddy, D.A., Sym, M., Apfeld, J., Nicoll, M., Maxwell, M., Hai, B., Ellis, M.C.*, et al.* (2002). aph-1 and pen-2 are required for Notch pathway signaling, gamma-secretase cleavage of betaAPP, and presenilin protein accumulation..pdf. Dev Cell.

Fukumori, A., Fluhrer, R., Steiner, H., and Haass, C. (2010). Three-amino acid spacing of presenilin endoproteolysis suggests a general stepwise cleavage of gamma-secretase-mediated intramembrane proteolysis. J Neurosci *30*, 7853-7862.

Futerman, A.H., and van Meer, G. (2004). The cell biology of lysosomal storage disorders. Nat Rev Mol Cell Biol *5*, 554-565.

Gaut, J.R., and Hendershot, L.M. (1993). The modification and assembly of proteins in the ER.pdf. Curr Opin Cell Biol.

Glick, D., Barth, S., and Macleod, K.F. (2010). Autophagy: cellular and molecular mechanisms. J Pathol *221*, 3-12.

Goate, A., Chartier-Harlin, M.C., Mullan, M., Brown, J., Crawford, F., Fidani, L., Giuffra, L., Haynes, A., Irving, N., James, L.*, et al.* (1991). Segregation of a missense mutation in the amyloid precursor protein gene with familial Alzheimer's disease..pdf. Nature.

Golabek, A.A., Kida, E., Walus, M., Kaczmarski, W., Michalewski, M., and Wisniewski, K.E. (2000). CLN3 protein regulates lysosomal pH and alters intracellular processing of Alzheimer's amyloid-beta protein precursor and cathepsin D in human cells. Mol Genet Metab *70*, 203-213.

Gotzl, J.K., Mori, K., Damme, M., Fellerer, K., Tahirovic, S., Kleinberger, G., Janssens, J., van der Zee, J., Lang, C.M., Kremmer, E.*, et al.* (2014). Common pathobiochemical hallmarks of progranulin associated frontotemporal lobar degeneration and neuronal ceroid lipofuscinosis.pdf. Acta Neuropathol.

Greene, N.D., Bernard, D.L., Taschner, P.E., Lake, B.D., de Vos, N., Breuning, M.H., Gardiner, R.M., Mole, S.E., Nussbaum, R.L., and Mitchison, H.M. (1999). A murine model for juvenile NCL gene targeting of mouse Cln3.pdf.

Greenfield, J.P., Gross, R.S., Gouras, G.K., and Xu, H. (2000). Cellular and molecular basis of beta-amyloid precursor protein metabolism..pdf. Front Biosci.

Groh, J., Berve, K., and Martini, R. (2017). Fingolimod and Teriflunomide Attenuate Neurodegeneration in Mouse Models of Neuronal Ceroid Lipofuscinosis. Mol Ther *25*, 1889-1899.

Guruharsha, K.G., Kankel, M.W., and Artavanis-Tsakonas, S. (2012). The Notch signalling system: recent insights into the complexity of a conserved pathway. Nat Rev Genet *13*, 654-666.

Haass, C., and De Strooper, B. (1999). The presenilins in Alzheimer's disease--proteolysis holds the key.pdf. Science.

Hafler, B.P., Klein, Z.A., Jimmy Zhou, Z., and Strittmatter, S.M. (2014). Progressive retinal degeneration and accumulation of autofluorescent lipopigments in Progranulin deficient mice. Brain Res *1588*, 168-174.

Haltia, M. (2003). The neuronal ceroid-lipofuscinoses. J Neuropathol Exp Neurol *62*, 1-13.

Hansen, T.E., and Johansen, T. (2011). Following autophagy step by step.pdf. BMC Biol.

Haskell, R.E., Derksen, T.A., and Davidson, B.L. (1999). Intracellular trafficking of the JNCL protein CLN3.pdf.

Hayashi-Nishino, M., Fujita, N., Noda, T., Yamaguchi, A., Yoshimori, T., and Yamamoto, A. (2009). A subdomain of the endoplasmic reticulum forms a cradle for autophagosome formation. Nat Cell Biol *11*, 1433-1437.

Hebert, S.S., Serneels, L., Dejaegere, T., Horre, K., Dabrowski, M., Baert, V., Annaert, W., Hartmann, D., and De Strooper, B. (2004). Coordinated and widespread expression of gamma-secretase in vivo: evidence for size and molecular heterogeneity. Neurobiol Dis *17*, 260-272.

Hersrud, S.L., Kovacs, A.D., and Pearce, D.A. (2016). Antigen presenting cell abnormalities in the Cln3(-/-) mouse model of juvenile neuronal ceroid lipofuscinosis. Biochim Biophys Acta *1862*, 1324-1336.

Holler, C.J., Taylor, G., Deng, Q., and Kukar, T. (2017). Intracellular Proteolysis of Progranulin Generates Stable, Lysosomal Granulins that Are Haploinsufficient in Patients with Frontotemporal Dementia Caused by GRN Mutations. eNeuro *4*.

Holmes, O., Paturi, S., Selkoe, D.J., and Wolfe, M.S. (2014). Pen-2 is essential for gamma-secretase complex stability and trafficking but partially dispensable for endoproteolysis. Biochemistry *53*, 4393-4406.

Holopainen, J.M., Saarikoski, J., Kinnunen, P.K., and Jarvela, I. (2001). Elevated lysosomal pH in neuronal ceroid lipofuscinoses (NCLs).pdf. Eur J Biochem.

Hsu, P.D., Lander, E.S., and Zhang, F. (2014). Development and applications of CRISPR-Cas9 for genome engineering. Cell *157*, 1262-1278.

https://www.fda.gov/NewsEvents/Newsroom/PressAnnouncements/ucm555613.htm?ftag=MSF095

1a18%7Caccessdate=30

Ishida, Y., Nayak, S., Mindell, J.A., and Grabe, M. (2013). A model of lysosomal pH regulation. J Gen Physiol *141*, 705-720.

J. O. Rinne , H. M. Ruottinen, K. Någren, L. E. Åberg, and Santavuori, P. (2002). Positron emission tomography shows reduced striatal dopamine D1 but not D2 receptors in juvenile neuronal ceroid lipofuscinosis.pdf.

Jalanko, A., and Braulke, T. (2009). Neuronal ceroid lipofuscinoses. Biochim Biophys Acta *1793*, 697-709.

Johnson, N., Powis, K., and High, S. (2013). Post-translational translocation into the endoplasmic reticulum. Biochim Biophys Acta *1833*, 2403-2409.

Jung, C.H., Jun, C.B., Ro, S.H., Kim, Y.M., Otto, N.M., Cao, J., Kundu, M., and Kim, D.H. (2009). ULK-Atg13-FIP200 Complexes Mediate mTOR Signaling to the Autophagy Machinery.pdf. Mol Biol Cell.

Kaether, C., Capell, A., Edbauer, D., Winkler, E., Novak, B., Steiner, H., and Haass, C. (2004). The presenilin C-terminus is required for ER-retention, nicastrin-binding and gamma-secretase activity..pdf. EMBO J.

Kaether, C., Scheuermann, J., Fassler, M., Zilow, S., Shirotani, K., Valkova, C., Novak, B., Kacmar, S., Steiner, H., and Haass, C. (2007). Endoplasmic reticulum retention of the gamma-secretase complex component Pen2 by Rer1. EMBO Rep *8*, 743-748.

Kang, R., Zeh, H.J., Lotze, M.T., and Tang, D. (2011). The Beclin 1 network regulates autophagy and apoptosis. Cell Death Differ *18*, 571-580.

Kim, J., Kundu, M., Viollet, B., and Guan, K.L. (2011). AMPK and mTOR regulate autophagy through direct phosphorylation of Ulk1. Nat Cell Biol *13*, 132-141.

Kirveskari, E., Partinen, M., Salmi, T., Sainio, K., Telakivi, T., Hamalainen, M., Larsen, A., and Santavuori, P. (2000). Sleep alterations in juvenile neuronal ceroid lipofuscinosis.pdf.

Klionsky, D.J., Abdelmohsen, K., Abe, A., Abedin, M.J., Abeliovich, H., Acevedo Arozena, A., Adachi, H., Adams, C.M., Adams, P.D., Adeli, K.*, et al.* (2016). Guidelines for the use and interpretation of assays for monitoring autophagy (3rd edition). Autophagy *12*, 1-222.

Kohan, R., Cismondi, I.A., Oller-Ramirez, A.M., Guelbert, N., Anzolini, T.V., Alonso, G., Mole, S.E., de Kremer, D.R., and de Halac, N.I. (2011). Therapeutic approaches to the challenge of neuronal ceroid lipofuscinoses.pdf. Curr Pharm Biotechnol.

Kollmann, K., Uusi-Rauva, K., Scifo, E., Tyynela, J., Jalanko, A., and Braulke, T. (2013). Cell biology and function of neuronal ceroid lipofuscinosis-related proteins. Biochim Biophys Acta *1832*, 1866-1881.

Kopan, R., and Ilagan, M.X. (2009). The canonical Notch signaling pathway: unfolding the activation mechanism. Cell *137*, 216-233.

Kopan, R., Schroeter, E.H., Weintraub, H., and Nye, J.S. (1996). Signal transduction by activated mNotch importance of proteolytic processing and its regulation by the extracellular domain..pdf. Proc Natl Acad Sci U S A.

Kovacs, A.D., Hof, C., and Pearce, D.A. (2015). Abnormally increased surface expression of AMPA receptors in the cerebellum, cortex and striatum of Cln3(-/-) mice. Neurosci Lett *607*, 29-34.

Kovacs, A.D., Saje, A., Wong, A., Ramji, S., Cooper, J.D., and Pearce, D.A. (2012). Age-dependent therapeutic effect of memantine in a mouse model of juvenile Batten disease. Neuropharmacology *63*, 769-775.

Kovacs, A.D., Saje, A., Wong, A., Szenasi, G., Kiricsi, P., Szabo, E., Cooper, J.D., and Pearce, D.A. (2011). Temporary inhibition of AMPA receptors induces a prolonged improvement of motor performance in a mouse model of juvenile Batten disease. Neuropharmacology *60*, 405-409.

Kovacs, A.D., Weimer, J.M., and Pearce, D.A. (2006). Selectively increased sensitivity of cerebellar granule cells to AMPA receptor-mediated excitotoxicity in a mouse model of Batten disease. Neurobiol Dis *22*, 575-585.

Kudchodkar, S.B., Yu, Y., Maguire, T.G., and Alwine, J.C. (2004). Human cytomegalovirus infection induces rapamycin-insensitive phosphorylation of downstream effectors of mTOR kinase. J Virol *78*, 11030-11039.

Kyttala, A., Ihrke, G., Vesa, J., Schell, M.J., and Luzio, J.P. (2004). Two motifs target Batten disease protein CLN3 to lysosomes in transfected nonneuronal and neuronal cells. Mol Biol Cell *15*, 1313-1323.

Kyttala, A., Yliannala, K., Schu, P., Jalanko, A., and Luzio, J.P. (2005). AP-1 and AP-3 facilitate lysosomal targeting of Batten disease protein CLN3 via its dileucine motif. J Biol Chem *280*, 10277-10283.

Lalonde, S., Ehrhardt, D.W., Loque, D., Chen, J., Rhee, S.Y., and Frommer, W.B. (2008). Molecular and cellular approaches for the detection of protein-protein interactions: latest techniques and current limitations. Plant J *53*, 610-635.

Larsen, E.P., and Ostergaard, J.R. (2014). Valproate-induced hyperammonemia in juvenile ceroid lipofuscinosis (Batten disease). Seizure *23*, 429-434.

LaVoie, M.J., Fraering, P.C., Ostaszewski, B.L., Ye, W., Kimberly, W.T., Wolfe, M.S., and Selkoe, D.J. (2003). Assembly of the gamma-secretase complex involves early formation of an intermediate subcomplex of Aph-1 and nicastrin. J Biol Chem *278*, 37213-37222.

Lee, J.H., McBrayer, M.K., Wolfe, D.M., Haslett, L.J., Kumar, A., Sato, Y., Lie, P.P., Mohan, P., Coffey, E.E., Kompella, U.*, et al.* (2015). Presenilin 1 Maintains Lysosomal Ca(2+) Homeostasis via TRPML1 by Regulating vATPase-Mediated Lysosome Acidification. Cell Rep *12*, 1430-1444.

Leem, J.Y., Vijayan, S., Han, P., Cai, D., Machura, M., Lopes, K.O., Veselits, M.L., Xu, H., and Thinakaran, G. (2002). Presenilin 1 is required for maturation and cell surface accumulation of nicastrin. J Biol Chem *277*, 19236-19240.

Levine, B., and Kroemer, G. (2008). Autophagy in the pathogenesis of disease. Cell *132*, 27-42.

Levy, J.M.M., Towers, C.G., and Thorburn, A. (2017). Targeting autophagy in cancer. Nat Rev Cancer *17*, 528-542.

Li, J., Fici, G.J., Mao, C.A., Myers, R.L., Shuang, R., Donoho, G.P., Pauley, A.M., Himes, C.S., Qin, W., Kola, I.*, et al.* (2003). Positive and negative regulation of the gamma-secretase activity by nicastrin in a murine model. J Biol Chem *278*, 33445-33449.

Lieberman, A.P., Puertollano, R., Raben, N., Slaugenhaupt, S., Walkley, S.U., and Ballabio, A. (2012). Autophagy in lysosomal storage disorders. Autophagy *8*, 719-730.

Lim, M.J., Alexander, N., Benedict, J.W., Chattopadhyay, S., Shemilt, S.J., Guerin, C.J., Cooper, J.D., and Pearce, D.A. (2007). IgG entry and deposition are components of the neuroimmune response in Batten disease. Neurobiol Dis *25*, 239-251.

Lippincott-Schwartz, J., Roberts, T.H., and Hirschberg, K. (2000). Secretory Protein Trafficking and Organelle Dynamics in Living Cells.pdf. Annu Rev Cell Dev Biol.

Luiro, K., Yliannala, K., Ahtiainen, L., Maunu, H., Jarvela, I., Kyttala, A., and Jalanko, A. (2004). Interconnections of CLN3, Hook1 and Rab proteins link Batten disease to defects in the endocytic pathway. Hum Mol Genet *13*, 3017-3027.

Luo, W.J., Wang, H., Li, H., Kim, B.S., Shah, S., Lee, H.J., Thinakaran, G., Kim, T.W., Yu, G., and Xu, H. (2003). PEN-2 and APH-1 coordinately regulate proteolytic processing of presenilin 1. J Biol Chem *278*, 7850-7854.

Luzio, J.P., Pryor, P.R., and Bright, N.A. (2007). Lysosomes: fusion and function. Nat Rev Mol Cell Biol *8*, 622-632.

Lyly, A., von Schantz, C., Heine, C., Schmiedt, M.L., Sipila, T., Jalanko, A., and Kyttala, A. (2009). Novel interactions of CLN5 support molecular networking between Neuronal Ceroid Lipofuscinosis proteins. BMC Cell Biol *10*, 83.

Ma, G., Li, T., Price, D.L., and Wong, P.C. (2005). APH-1a is the principal mammalian APH-1 isoform present in gamma-secretase complexes during embryonic development. J Neurosci *25*, 192-198.

Mao, Q., Xia, H., and Davidson, B.L. (2003). Intracellular trafficking of CLN3, the protein underlying the childhood neurodegenerative disease, Batten disease. FEBS Letters *555*, 351-357.

Magnuson, B., Ekim, B., and Fingar, D.C. (2012). Regulation and function of ribosomal protein S6 kinase (S6K) within mTOR signalling networks. Biochem J *441*, 1-21.

Mahuran, D.J. (1999). Biochemical consequences of mutations causing the GM2 gangliosidoses..pdf. Biochim Biophys Acta.

Marzban, H., Del Bigio, M.R., Alizadeh, J., Ghavami, S., Zachariah, R.M., and Rastegar, M. (2014). Cellular commitment in the developing cerebellum. Front Cell Neurosci *8*, 450.

Mashiko, D., Fujihara, Y., Satouh, Y., Miyata, H., Isotani, A., and Ikawa, M. (2013). Generation of mutant mice by pronuclear injection of circular plasmid expressing Cas9 and single guided RNA. Sci Rep *3*, 3355.

McBrayer, M., and Nixon, R.A. (2013). Lysosome and calcium dysregulation in Alzheimer's disease: partners in crime. Biochem Soc Trans *41*, 1495-1502.

Meckler, X., and Checler, F. (2016). Presenilin 1 and Presenilin 2 Target gamma-Secretase Complexes to Distinct Cellular Compartments. J Biol Chem *291*, 12821-12837.

Melendez, A., and Levine, B. (2009). Autophagy in C. elegans. WormBook, 1-26.
Mellman, I., and Nelson, W.J. (2008). Coordinated protein sorting, targeting and distribution in polarized cells. Nat Rev Mol Cell Biol *9*, 833-845.

Mindell, J.A. (2012). Lysosomal acidification mechanisms. Annu Rev Physiol *74*, 69-86.

Mizushima, N. (2007). Autophagy: process and function. Genes Dev *21*, 2861-2873.

Mizushima, N., Yoshimori, T., and Levine, B. (2010). Methods in mammalian autophagy research. Cell *140*, 313-326.

Mole, S.E., and Cotman, S.L. (2015). Genetics of the neuronal ceroid lipofuscinoses (Batten disease). Biochim Biophys Acta *1852*, 2237-2241.

Moore, C.B., Guthrie, E.H., Huang, M.T., and Taxman, D.J. (2010). Short hairpin RNA (shRNA): design, delivery, and assessment of gene knockdown. Methods Mol Biol *629*, 141-158.

Muller, U.C., and Zheng, H. (2012). Physiological functions of APP family proteins. Cold Spring Harb Perspect Med *2*, a006288.

Nah, J., Yuan, J., and Jung, Y.K. (2015). Autophagy in neurodegenerative diseases: from mechanism to therapeutic approach. Mol Cells *38*, 381-389.

Neely, K.M., Green, K.N., and LaFerla, F.M. (2011). Presenilin is necessary for efficient proteolysis through the autophagy-lysosome system in a gamma-secretase-independent manner. J Neurosci *31*, 2781-2791.

Nielsen, A.K., and Ostergaard, J.R. (2013). Do females with juvenile ceroid lipofuscinosis (Batten disease) have a more severe disease course? The Danish experience. Eur J Paediatr Neurol *17*, 265-268.

Oddo, S. (2012). The role of mTOR signaling in Alzheimer disease.pdf. Front Biosci.

Oetjen, S., Kuhl, D., and Hermey, G. (2016). Revisiting the neuronal localization and trafficking of CLN3 in juvenile neuronal ceroid lipofuscinosis. J Neurochem *139*, 456-470.

Onyenwoke, R.U., and Brenman, J.E. (2015). Lysosomal Storage Diseases-Regulating Neurodegeneration. J Exp Neurosci *9*, 81-91.

Oot, R.A., Couoh-Cardel, S., Sharma, S., Stam, N.J., and Wilkens, S. (2017). Breaking up and making up: The secret life of the vacuolar H+ -ATPase. Protein Sci *26*, 896-909.

Orr, M.E., and Oddo, S. (2013). Autophagic lysosomal dysfunction in Alzheimer's disease.pdf. Alzheimers Res Ther.

Osorio, N.S., Sampaio-Marques, B., Chan, C.H., Oliveira, P., Pearce, D.A., Sousa, N., and Rodrigues, F. (2009). Neurodevelopmental delay in the Cln3Deltaex7/8 mouse model for Batten disease. Genes Brain Behav *8*, 337-345.

Ostergaard, J.R., Rasmussen, T.B., and Molgaard, H. (2011). Cardiac involvement in juvenile neuronal ceroid lipofuscinosis (Batten disease).pdf.

Pajak, B., Kania, E., and Orzechowski, A. (2016). Killing Me Softly: Connotations to Unfolded Protein Response and Oxidative Stress in Alzheimer's Disease. Oxid Med Cell Longev *2016*, 1805304.

Palmieri, M., Pal, R., Nelvagal, H.R., Lotfi, P., Stinnett, G.R., Seymour, M.L., Chaudhury, A., Bajaj, L., Bondar, V.V., Bremner, L.*, et al.* (2017). mTORC1-independent TFEB activation via Akt inhibition promotes cellular clearance in neurodegenerative storage diseases. Nat Commun *8*, 14338.

Panmontha, W., Rerknimitr, P., Yeetong, P., Srichomthong, C., Suphapeetiporn, K., and Shotelersuk, V. (2015). A Frameshift Mutation in PEN-2 Causes Familial Comedones Syndrome. Dermatology *231*, 77-81.

Parviainen, L., Dihanich, S., Anderson, G.W., Wong, A.M., Brooks, H.R., Abeti, R., Rezaie, P., Lalli, G., Pope, S., Heales, S.J.*, et al.* (2017). Glial cells are functionally impaired in juvenile neuronal ceroid lipofuscinosis and detrimental to neurons. Acta Neuropathol Commun *5*, 74.

Pearce, D.A., Nosel, S.A., and Sherman, F. (1999). Studies of pH regulation by Btn1p, the yeast homolog of human Cln3p.pdf.

Phillips, S.N., Benedict, J.W., Weimer, J.M., and Pearce, D.A. (2005). CLN3, the protein associated with batten disease: structure, function and localization. J Neurosci Res *79*, 573-583.

Podlisny, M.B., Citron, M., Amarante, P., Sherrington, R., Xia, W., Zhang, J., Diehl, T., Levesque, G., Fraser, P., Haass, C.*, et al.* (1997). Presenilin proteins undergo heterogeneous endoproteolysis between Thr291 and Ala299 and occur as stable N- and C-terminal fragments in normal and Alzheimer brain tissue..pdf. Neurobiol Dis.

Pontikis, C.C., Cella, C.V., Parihar, N., Lim, M.J., Chakrabarti, S., Mitchison, H.M., Mobley, W.C., Rezaie, P., Pearce, D.A., and Cooper, J.D. (2004). Late onset neurodegeneration in the Cln3-/- mouse model of juvenile neuronal ceroid lipofuscinosis is preceded by low level glial activation. Brain Res *1023*, 231-242.

Pontikis, C.C., Cotman, S.L., MacDonald, M.E., and Cooper, J.D. (2005). Thalamocortical neuron loss and localized astrocytosis in the Cln3Deltaex7/8 knock-in mouse model of Batten disease. Neurobiol Dis *20*, 823-836.

Prasad, V.V., and Pullarkat, R.K. (1996). Brain Lysosomal Hydrolases in neironal ceroid lipofuscinoses.pdf. Mol Chem Neuropathol.

Proctor, C.J., Pienaar, I.S., Elson, J.L., and Kirkwood, T.B. (2012). Aggregation, impaired degradation and immunization targeting of amyloid-beta dimers in Alzheimer's disease a stochastic modelling approach..pdf. Mol Neurodegener.

Raben, N., Shea, L., Hill, V., and Plotz, P. (2009). Chapter 21 Monitoring Autophagy in Lysosomal Storage Disorders. *453*, 417-449.

Ralser, D.J., Basmanav, F.B., Tafazzoli, A., Wititsuwannakul, J., Delker, S., Danda, S., Thiele, H., Wolf, S., Busch, M., Pulimood, S.A.*, et al.* (2017). Mutations in gamma-secretase subunit-encoding PSENEN underlie Dowling-Degos disease associated with acne inversa. J Clin Invest *127*, 1485-1490.

Ratajczak, E., Petcherski, A., Ramos-Moreno, J., and Ruonala, M.O. (2014). FRET-assisted determination of CLN3 membrane topology. PLoS One *9*, e102593.

Rothberg, P.G., Ramirez-Montealegre, D., Frazier, S.D., and Pearce, D.A. (2004). Homogeneous polymerase chain reaction nucleobase quenching assay to detect the 1-kbp deletion in CLN3 that causes Batten disease.pdf.

Ruivo, R., Anne, C., Sagne, C., and Gasnier, B. (2009). Molecular and cellular basis of lysosomal transmembrane protein dysfunction. Biochim Biophys Acta *1793*, 636-649.

Saftig, P., and Klumperman, J. (2009). Lysosome biogenesis and lysosomal membrane proteins: trafficking meets function. Nat Rev Mol Cell Biol *10*, 623-635.

Sahani, M.H., Itakura, E., and Mizushima, N. (2014). Expression of the autophagy substrate SQSTM1/p62 is restored during prolonged starvation depending on transcriptional upregulation and autophagy-derived amino acids. Autophagy *10*, 431-441.

Sala Frigerio, C., Piscopo, P., Calabrese, E., Crestini, A., Malvezzi Campeggi, L., Civita di Fava, R., Fogliarino, S., Albani, D., Marcon, G., Cherchi, R.*, et al.* (2005). PEN-2 gene mutation in a familial Alzheimer's disease case. J Neurol *252*, 1033-1036.

Sandra, Oetjen. (2014). Ph.D Thesis. Characterization of interactions and trafficking of the Neuronal Ceroid Lipofuscinosis protein CLN3.

Sarkar, S., Davies, J.E., Huang, Z., Tunnacliffe, A., and Rubinsztein, D.C. (2007). Trehalose, a novel mTOR-independent autophagy enhancer, accelerates the clearance of mutant huntingtin and alpha-synuclein. J Biol Chem *282*, 5641-5652.

Schwake, M., Schroder, B., and Saftig, P. (2013). Lysosomal membrane proteins and their central role in physiology. Traffic *14*, 739-748.

Scifo, E., Szwajda, A., Debski, J., Uusi-Rauva, K., Kesti, T., Dadlez, M., Gingras, A.C., Tyynela, J., Baumann, M.H., Jalanko, A.*, et al.* (2013). Drafting the CLN3 protein interactome in SH-SY5Y human neuroblastoma cells: a label-free quantitative proteomics approach. J Proteome Res *12*, 2101-2115.

Shang, L., Chen, S., Du, F., Li, S., Zhao, L., and Wang, X. (2011). Nutrient starvation elicits an acute autophagic response mediated by Ulk1 dephosphorylation and its subsequent dissociation from AMPK. Proc Natl Acad Sci U S A *108*, 4788-4793.

Smith, K.R., Damiano, J., Franceschetti, S., Carpenter, S., Canafoglia, L., Morbin, M., Rossi, G., Pareyson, D., Mole, S.E., Staropoli, J.F.*, et al.* (2012). Strikingly different clinicopathological phenotypes determined by progranulin-mutation dosage. Am J Hum Genet *90*, 1102-1107.

Snapp, E.L., McCaul, N., Quandte, M., Cabartova, Z., Bontjer, I., Kallgren, C., Nilsson, I., Land, A., von Heijne, G., Sanders, R.W.*, et al.* (2017). Structure and topology around the cleavage site regulate post-translational cleavage of the HIV-1 gp160 signal peptide. Elife *6*.

Stanley, P. (2011). Golgi glycosylation. Cold Spring Harb Perspect Biol *3*.

Staudt, C., Puissant, E., and Boonen, M. (2016). Subcellular Trafficking of Mammalian Lysosomal Proteins: An Extended View. Int J Mol Sci *18*.

Steiner, H., and Haass, C. (2000). Intramembrane proteolysis by presenilins.pdf. Nat Rev Mol Cell Biol.

Steiner, H., Winkler, E., Edbauer, D., Prokop, S., Basset, G., Yamasaki, A., Kostka, M., and Haass, C. (2002).PEN-2 is an integral component of the gamma-secretase complex required for coordinated expression of presenilin and nicastrin. J Biol Chem *277*, 39062-39065.

Storch, S., Pohl, S., and Braulke, T. (2004). A dileucine motif and a cluster of acidic amino acids in the second cytoplasmic domain of the batten disease-related CLN3 protein are required for efficient lysosomal targeting. J Biol Chem *279*, 53625-53634.

Stozicka, Z., Zilka, N., and Novak, M. (2007). Risk and protective factors for sporadic Alzheimer's disease. Acta Virol *51*, 205-222.

Takasugi, N., Tomita, T., Hayashi, I., Tsuruoka, M., Niimura, M., Takahashi, Y., Thinakaran, G., and Iwatsubo, T. (2003). The role of presenilin cofactors in the γ-secretase complex.pdf. Nature.

Tanzi, R.E. (2012). The genetics of Alzheimer disease. Cold Spring Harb Perspect Med *2*.

Thinakaran, G., Borchelt, D.R., Lee, M.K., Slunt, H.H., Spitzer, L., Kim, G., Ratovitsky, T., Davenport, F., Nordstedt, C., Seeger, M.*, et al.* (1996). Endoproteolysis of presenilin 1 and accumulation of processed derivatives in vivo..pdf. Neuron.

Thoreen, C.C., Kang, S.A., Chang, J.W., Liu, Q., Zhang, J., Gao, Y., Reichling, L.J., Sim, T., Sabatini, D.M., and Gray, N.S. (2009). An ATP-competitive mammalian target of rapamycin inhibitor reveals rapamycin-resistant functions of mTORC1. J Biol Chem *284*, 8023-8032.

Tien, N.T., Karaca, I., Tamboli, I.Y., and Walter, J. (2016). Trehalose Alters Subcellular Trafficking and the Metabolism of the Alzheimer-associated Amyloid Precursor Protein. J Biol Chem *291*, 10528-10540.

Tokola, A.M., Salli, E.K., Aberg, L.E., and Autti, T.H. (2014). Hippocampal volumes in juvenile neuronal ceroid lipofuscinosis: a longitudinal magnetic resonance imaging study. Pediatr Neurol *50*, 158-163.
Tuxworth, R.I., Vivancos, V., O'Hare, M.B., and Tear, G. (2009). Interactions between the juvenile Batten disease gene, CLN3, and the Notch and JNK signalling pathways. Hum Mol Genet *18*, 667-678.

Uusi-Rauva, K., Luiro, K., Tanhuanpaa, K., Kopra, O., Martin-Vasallo, P., Kyttala, A., and Jalanko, A. (2008). Novel interactions of CLN3 protein link Batten disease to dysregulation of fodrin-Na+, K+ ATPase complex. Exp Cell Res *314*, 2895-2905.

Valdez, C., Wong, Y.C., Schwake, M., Bu, G., Wszolek, Z.K., and Krainc, D. (2017). Progranulin-mediated deficiency of cathepsin D results in FTD and NCL-like phenotypes in neurons derived from FTD patients.pdf. Hum Mol Genet.

van der Ploeg, R., Goudelis, S.T., and den Blaauwen, T. (2015). Validation of FRET Assay for the Screening of Growth Inhibitors of Escherichia coli Reveals Elongasome Assembly Dynamics. Int J Mol Sci *16*, 17637-17654.

Vetrivel, K.S., Zhang, Y.W., Xu, H., and Thinakaran, G. (2006). Pathological and physiological functions of presenilins. Mol Neurodegener *1*, 4.

Vidal-Donet, J.M., Carcel-Trullols, J., Casanova, B., Aguado, C., and Knecht, E. (2013). Alterations in ROS activity and lysosomal pH account for distinct patterns of macroautophagy in LINCL and JNCL fibroblasts. PLoS One *8*, e55526.

Vitiello, S.P., Wolfe, D.M., and Pearce, D.A. (2007). Absence of Btn1p in the yeast model for juvenile Batten disease may cause arginine to become toxic to yeast cells. Hum Mol Genet *16*, 1007-1016.

Volz, C., Mirza, M., Langmann, T., and Jagle, H. (2014). Retinal function in aging homozygous Cln3 (Deltaex7/8) knock-in mice. Adv Exp Med Biol *801*, 495-501.

von Rotz, R.C., Kohli, B.M., Bosset, J., Meier, M., Suzuki, T., Nitsch, R.M., and Konietzko, U. (2004). The APP intracellular domain forms nuclear multiprotein complexes and regulates the transcription of its own precursor..pdf. J Cell Sci.

Wang, H., Luo, W.J., Zhang, Y.W., Li, Y.M., Thinakaran, G., Greengard, P., and Xu, H. (2004). Presenilins and gamma-secretase inhibitors affect intracellular trafficking and cell surface localization of the gamma-secretase complex components. J Biol Chem *279*, 40560-40566.

Ward, M.E., Chen, R., Huang, H.Y., Ludwig, C., Telpoukhovskaia, M., Taubes, A., Boudin, H., Minami, S.S., Reichert, M., Albrecht, P*., et al.* (2017). Individuals with progranulin haploinsufficiency exhibit features of neuronal ceroid lipofuscinosis. Sci Transl Med *9*.

Watanabe, N., Tomita, T., Sato, C., Kitamura, T., Morohashi, Y., and Iwatsubo, T. (2005). Pen-2 is incorporated into the gamma-secretase complex through binding to transmembrane domain 4 of presenilin 1. J Biol Chem *280*, 41967-41975.

Weimer, J.M., Benedict, J.W., Elshatory, Y.M., Short, D.W., Ramirez-Montealegre, D., Ryan, D.A., Alexander, N.A., Federoff, H.J., Cooper, J.D., and Pearce, D.A. (2007). Alterations in striatal dopamine catabolism precede loss of substantia nigra neurons in a mouse model of juvenile neuronal ceroid lipofuscinosis. Brain Res *1162*, 98-112.

Weimer, J.M., Benedict, J.W., Getty, A.L., Pontikis, C.C., Lim, M.J., Cooper, J.D., and Pearce, D.A. (2009). Cerebellar defects in a mouse model of juvenile neuronal ceroid lipofuscinosis. Brain Res *1266*, 93-107.

Weimer, J.M., Custer, A.W., Benedict, J.W., Alexander, N.A., Kingsley, E., Federoff, H.J., Cooper, J.D., and Pearce, D.A. (2006). Visual deficits in a mouse model of Batten disease are the result of optic nerve degeneration and loss of dorsal lateral geniculate thalamic neurons. Neurobiol Dis *22*, 284-293.

Wisniewski, K.E., Kida, E., Gordon-Majszak, W., and Saitoh, T. (1990a). Altered amyloid beta-protein precursor processing in brains of patients with neuronal ceroid lipofuscinosis.pdf. Neurosci Lett.

Wisniewski, K.E., Maslinska, D., Kitaguchi, T., Kim, K.S., Goebel, H.H., and Haltia, M. (1990b). Topographic heterogeneity of amyloid B-protein epitopes in brains with various forms of neuronal ceroid lipofuscinoses suggesting defective processing of amyloid precursor protein..pdf. Acta Neuropathol.

Xie, Z., and Klionsky, D.J. (2007). Autophagosome formation core machinery and adaptations..pdf. Nat Cell Biol.

Xiong, J., and Kielian, T. (2013). Microglia in juvenile neuronal ceroid lipofuscinosis are primed toward a pro-inflammatory phenotype. J Neurochem *127*, 245-258.

Yan, W., Boustany, R.M., Konradi, C., Ozelius, L., Lerner, T., Trofatter, J.A., Julier, C., Breakefield, X.O., Gusella, J.F., and Haines, J.L. (1993). Localization of juvenile but not late infantile neuronal ceroid lipofuscinosis on chromosome 16.pdf.

Yang, D.S., Tandon, A., Chen, F., Yu, G., Yu, H., Arawaka, S., Hasegawa, H., Duthie, M., Schmidt, S.D., Ramabhadran, T.V*., et al.* (2002). Mature glycosylation and trafficking of nicastrin modulate its binding to presenilins. J Biol Chem *277*, 28135-28142.

Ylä-Anttila, P., Vihinen, H., Jokitalo, E., and Eskelinen, E.-L. (2014). 3D tomography reveals connections between the phagophore and endoplasmic reticulum. Autophagy *5*, 1180-1185.

Yoon, Y.S., Cho, E.D., Jung Ahn, W., Won Lee, K., Lee, S.J., and Lee, H.J. (2017). Is trehalose an autophagic inducer? Unraveling the roles of non-reducing disaccharides on autophagic flux and alpha-synuclein aggregation. Cell Death Dis *8*, e3091.

Yu, C., Huang, X., Xu, Y., Li, H., Su, J., Zhong, J., Kang, J., Liu, Y., and Sun, L. (2013). Lysosome dysfunction enhances oxidative stress-induced apoptosis through ubiquitinated protein accumulation in Hela cells. Anat Rec (Hoboken) *296*, 31-39.

Zhang, X., Chen, S., Song, L., Tang, Y., Shen, Y., Jia, L., and Le, W. (2014). MTOR-independent, autophagic enhancer trehalose prolongs motor neuron survival and ameliorates the autophagic flux defect in a mouse model of amyotrophic lateral sclerosis. Autophagy *10*, 588-602.

Zhang, X., Yu, C.J., and Sisodia, S.S. (2015). The topology of pen-2, a gamma-secretase subunit, revisited: evidence for a reentrant loop and a single pass transmembrane domain. Mol Neurodegener *10*, 39.

Zhang, Y.W., Thompson, R., Zhang, H., and Xu, H. (2011). APP processing in Alzheimer's disease. Mol Brain *4*, 3.

Zhang, Y.W., Wang, R., Liu, Q., Zhang, H., Liao, F.F., and Xu, H. (2007). Presenilin/gamma-secretase-dependent processing of beta-amyloid precursor protein regulates EGF receptor expression. Proc Natl Acad Sci U S A *104*, 10613-10618.

Zhou, X., Sun, L., Bastos de Oliveira, F., Qi, X., Brown, W.J., Smolka, M.B., Sun, Y., and Hu, F. (2015). Prosaposin facilitates sortilin-independent lysosomal trafficking of progranulin. J Cell Biol *210*, 991-1002.

Zullo, A.J., Jurcic Smith, K.L., and Lee, S. (2014). Mammalian target of Rapamycin inhibition and mycobacterial survival are uncoupled in murine macrophages.pdf. BMC Biochem.

9 Acknowledgements

First, I would like to express my deep and sincere gratitude to my supervisor PD Dr. Guido Hermey. His wide knowledge and logical way of thinking have helped me to grow professionally and personally. His understanding, encouraging and personal guidance have provided a good basis for my thesis. I am grateful to him for giving me the opportunity to work with him. I have enjoyed my time working under his supervision. Thank you so much for your time, effort and for everything.

I would like to offer my special thanks to Prof. Dr. Dietmar Kuhl for offering to conduct the research work in his Institute.

I would like to thank Prof. Dr. Christian Lohr to be a reviewer of this thesis.

I gratefully acknowledge the funding support received for this project from the NCL-Stiftung Hamburg.

I greatly appreciate the valuable discussions and help received from Dr. Lars Binkle, Dr. Sandra Oetjen, PD Dr. Uwe Borgmeyer, Dr. Ralf Scholz and PD Dr. Sabine Hoffmeister-Ullerich during my research work.

My thanks also go out to Prof. Dr. Meliha Karsak, PD Dr. Stephan Storch and PD Dr. Irm Hermans-Borgmeyer for giving me a valuable advice during my research work and annual progress reports.

My special thanks are extended to all former and current members of the Institute Kuhl for a good working environment, moral support, sharing happy and wonderful moments with me. Barbara Merz, Andrea Zaisser and Ute Süsens are thanked for technical support and their contribution to this project. Special thanks go to other members Dr. Ora Ohana, Dr. Xiaoyan Gao, Dr. Jasper Grendel, Dr. Sergio Castro Gomez and Francesca Xompero, Daks, Joachim, Christina Kroos, Helia Saber, Bendix, Dirk, Alexa-Nicole Sliby and Dominika Wawrzyniak for nice discussions, kind help and for giving me a good time.

Last but not least, I would like to thank my friends and family. This journey would not have been possible without the support of them. I am grateful to my family especially, my parents for their unconditional love, encouraging and motivating me in all of my pursuits, inspiring me to follow my dreams, emotionally and financially supporting me, teaching and guiding me as a person and for their patience throughout my study.

Universitätsklinikum Hamburg-Eppendorf
Zentrum für Molekulare Neurobiologie Hamburg
Forschungsgruppe:
Neuronale Translationskontrolle

Dr. Kent Duncan
Forschungsgruppenleiter
Martinistraße 52
D-20246 Hamburg
Gebäude S50, Raum 3.23
Telefon: +49 (0) 40 7410-56274
Fax: +49 (0) 40 7410-53436
Kent.Duncan@zmnh.uni-hamburg.de
www.uke.de/zmnh
Hausanschrift:
Falkenried 94 / Martinistr. 85
D-20251 Hamburg

Universitätsklinikum Hamburg-Eppendorf | Martinistraße 52 | 20246 Hamburg
Zentrum für Molekulare Neurobiologie | Forschungsgruppe Dr. Kent Duncan

English Language Thesis Certification: Abuzar Kaleem

Hamburg, 20.12.2017

To whom it may concern:

Abuzar Kaleem, who was born on 4th of August 1985 and has matriculation number 6752563, is submitting his doctoral dissertation in English. The title of his thesis is: **'Functional characterization of Ceroid Lipofuscinosis Neuronal 3 (CLN3) interactions'.**

I hereby certify as a native speaker and molecular biologist that the English language used in this thesis is sufficiently correct for submission.

Yours truly,

Kent Duncan, Ph.D.

Universität Hamburg
Universitätsklinikum Hamburg-Eppendorf
Zentrum für Molekulare Neurobiologie
AG Duncan
Falkenried 94 · D-20251 Hamburg